12-2013

Development of Si Device Based Power Converters for High Temperature Operation in HEV Applications

Zhuxian Xu
University of Tennessee - Knoxville, zxu11@utk.edu

To the Graduate Council:

I am submitting herewith a dissertation written by Zhuxian Xu entitled "Development of Si Device Based Power Converters for High Temperature Operation in HEV Applications." I have examined the final electronic copy of this dissertation for form and content and recommend that it be accepted in partial fulfillment of the requirements for the degree of Doctor of Philosophy, with a major in Electrical Engineering.

Fred Wang, Major Professor

We have read this dissertation and recommend its acceptance:

Leon Tolbert, Zhenxian Liang, Rao Arimilli

Accepted for the Council:

Carolyn R. Hodges

Vice Provost and Dean of the Graduate School

(Original signatures are on file with official student records.)

Development of Si Device Based Power Converters for High Temperature Operations in HEV Applications

A Dissertation Presented for the

Doctor of Philosophy

Degree

The University of Tennessee, Knoxville

Zhuxian Xu

December 2013

Acknowledgement

I would like to express my sincere gratitude to my advisor, Dr. Fred Wang, for his support, guidance and encouragement during my study as well as my daily life. On the one hand, he led me in the area of power electronics with his incisive view and profound knowledge. On the other hand, he gave me enough freedom to explore the challenges and opportunities, and encouraged me to dig into the area. His gentle personality and rigorous attitude toward research will benefit my career as well as my whole personal life.

I am also deeply grateful to Dr. Leon Tolbert for his valuable instructions. He is always generous to give me suggestions, encouragement and ideas to help me in my study and research. Special thanks go to Dr. Zhenxian Liang. His advice and experience have contributed significantly to my research and understanding of power semiconductor devices and packaging. I would also like to thank Dr. Rao Arimilli and and Dr. Daniel Costinett for their support and great help.

I would like to thank Ms. Laura D. Marlino and Dr. Puqi Ning in Oak Ridge National Laboratory and Dr. Thomas Jahns in the University of Wisconsin-Madison for their valuable advice and discussions in my research project.

I would like to thank my colleagues in Power Electronics Laboratory at the University of Tennessee, for their help and friendship. They are Dr. Shengnan Li, Dr. Lijun Hang, Dr. Jingxin Wang, Dr. Wenjie Chen, Dr. Xiaoling Yu, Dr. Wanjun Lei, Dr. Faete Filho, Dr. Mithat Can Kisacikoglu, Lakshmi Reddy Gopi Reddy, Bradford Trento, Bailu Xiao, Jing Xue, Jing Wang, Yutian Cui, Yalong Li, Zheyu Zhang, Wenchao Cao, Yiwei Ma, Zhiqiang Wang, Xiaojie Shi, Liu Yang, Yang Xue, Bo Liu, Edward Jones, and Siyao Jiang. In particular, I would like to thank

Dr. Ming Li, Dr. Dong Jiang, Weimin Zhang, and Ben Guo, for their time and help in my research projects.

I would like to thank staff members for offering me a lot of help. They are Mr. Robert B. Martin, Mr. William Rhodes, Ms. Judy Evans, Ms. Dana Bryson, and Ms. Sonja Warwick.

At last but also the most important, I offer my deepest gratitude and love to my parents, Nanping Xu and Xiaoyan Luo, and my boyfriend, Fan Xu, for their unconditional love, support and confidence in me.

Abstract

In this dissertation, the feasibility of operating Si devices at 200 ˚C [degree Celsius] is investigated and the guidelines on the development of a high temperature Si converter for operating with 105 ˚C high temperature liquid coolant in hybrid electrical vehicle (HEV) applications are provided.

First, the characterization of a Si IGBT operating at 200 ˚C junction temperatures is presented. It is shown that the commercial 175 ˚C Si IGBT under test can be successfully switched at an elevated junction temperature of 200 ˚C with increased but acceptable losses.

Second, a comprehensive evaluation of Si IGBT ruggedness at high temperature operation is provided through experiments. The important criteria considering latch-up immunity, short circuit capability, and avalanche capability are given to ensure the safe and reliable operation of Si IGBTs at 200 ˚C.

Third, the feasibility of operating Si devices based converters continuously at the junction temperature of 200 ˚C is demonstrated. A Si IGBT phase-leg module is developed for 200 ˚C operation utilizing high temperature packaging technologies and appropriate thermal management.

Fourth, a method is proposed to measure the junction temperatures of IGBTs during the converter operation using IGBT short circuit current. The calibration experiments show that the short circuit current has good sensitivity, linearity and selectivity, making the method suitable for use as temperature sensitive electrical parameter (TSEP). By connecting a temperature measurement unit to the converter and giving a short circuit pulse during the converter operation, the IGBT junction temperature can be measured.

Fifth, a 30 kW Si IGBT based three-phase converter has been developed for operating at the junction temperature of 200 ˚C with the high temperature coolant in HEV applications. The experimental results demonstrate that the three-phase converter can operate at junction temperature of 200 ˚C with the 105 ˚C high temperature coolant, thus eliminating the need for the additional 65 ˚C coolant in HEV.

Additionally, the emerging 600 V GaN HEMT is investigated as a potential replacement of Si devices for high efficiency and high temperature in future HEV applications.

Keywords: high temperature, Si IGBT, 200 ˚C, reduced cooling, temperature measurement, hybrid electric vehicle

Table of Contents

List of Tables

List of Figures

Chapter 1. Introduction

This chapter introduces the background of high temperature power electronics converter applications. The structure and organization of the dissertation is then given.

1.1 Background

Power electronics are widely used in a variety of industrial applications. During their operations the switches generate relatively large amounts of heat in the order of hundreds of watts (W) per die, leading to their temperature increase. Semiconductor devices and the associated packaging materials ultimately dictate the inherent temperature limitations. The development of high temperature capable power electronics will allow a significant increase in power density or reduced cooling. Applications such as aircraft, vehicles, space exploration, and deep oil and gas wells drilling can benefit much from the high temperature power electronics [1]-[3]. Table 1-1 lists some of the high temperature applications [3].

In the automotive applications, the underhood automotive environment is harsh and pushes the development of high temperature electronic components. The electronics operating above 125 ˚C are defined as high temperature electronics in the automotive industry. The actual temperatures for various electronics mounting locations are listed in Table 1-2 [4].

Table 1-1 High Temperature Electronics Applications [3]

High temperature electronics application	Peak ambient	Chip power	Current Technology	Future Technology
Automotive				
Engine control electronics	150 ˚C	< 1 kW	BS & SOI	BS & SOI
On-cylinder & exhaust pipe	600 ˚C	< 1 kW	NA	WBG
Electric suspension & brakes	250 ˚C	> 10 kW	BS	WBG
Electric/hybrid vehicle	150 ˚C	> 10 kW	BS	WBG
Turbine engine				
Sensors, telemetry, control	300 ˚C	< 1 kW	BS & SOI	SOI & WBG
	600 ˚C	< 1 kW	NA	WBG
Electric actuation	150 ˚C	>10 kW	BS & SOI	WBG
	600 ˚C	>10 kW	NA	WBG
Spacecraft				
Power management	150 ˚C	>1 kW	BS & SOI	WBG
	300 ˚C	>10 kW	NA	WBG
Venus & Mercury exploration	550 ˚C	~1 kW	NA	WBG
Industrial				
High temperature processing	300 ˚C	< 1 kW	SOI	SOI
	600 ˚C	< 1 kW	NA	WBG
Deep-well drilling telemetry				
Oil and gas	300 ˚C	< 1 kW	SOI	SOI & WBG
Geothermal	600 ˚C	< 1 kW	NA	WBG

BS = bulk silicon, SOI = Silicon on insulator, NA = not presently available, WBG = wide bandgap

Table 1-2 Automotive Temperature Extremes (Delphi Delco Electronic Systems) [4]

Location	Typical continuous max temperature	Vibration level
On engine / On transmission	140 ˚C	Up to 10Grms
At the engine (intake manifold)	125 ˚C	Up to 10Grms
Underhood (near engine)	120 ˚C	3-5Grms
Underhood (remote location)	105 ˚C	3-5Grms
Exterior	70 ˚C	3-5Grms
Passenger compartment	70-80 ˚C	3-5Grms

With the more stringent regulations on emissions and fuel economy, global warming, and constraints on energy resources, the electric, hybrid, and fuel cell vehicles have attracted more and more attention by automakers, governments, and customers and will likely increase in

popularity in coming years. Typically, a full hybrid electrical vehicle in city driving can save about 30% to 50% energy, while the cost increases about 30% to 40% [5].

Although HEVs possess many advantages, they also have certain limitations. Today's hybrid electric vehicle (HEV) traction drives cannot meet the aggressive power density and cost targets set by Department of Energy (DOE) for 2015 and 2020 because the electric machine and drive electronics are packaged as separate components [6][7]. Figure 1-1 and Figure 1-2 show the hybrid electric drive system in Ford Fusion HEV and Toyota Prius 2010, respectively. It is shown that the electric machine and drive electronics have their own housings and thermal management systems. The connectors and cables for the interconnections between the machine and drive add to the weight and cost. Also the power electronics are not capable of operating with the 105 ˚C engine coolant. A separate liquid cooling system with coolant temperature at 65 ˚C is used specially to remove the heat from the electric drive system due to the temperature limitations of power electronics.

Figure 1-1. Ford Fusion HEV hybrid electric drive system (Permission is obtained to use the picture) [6].

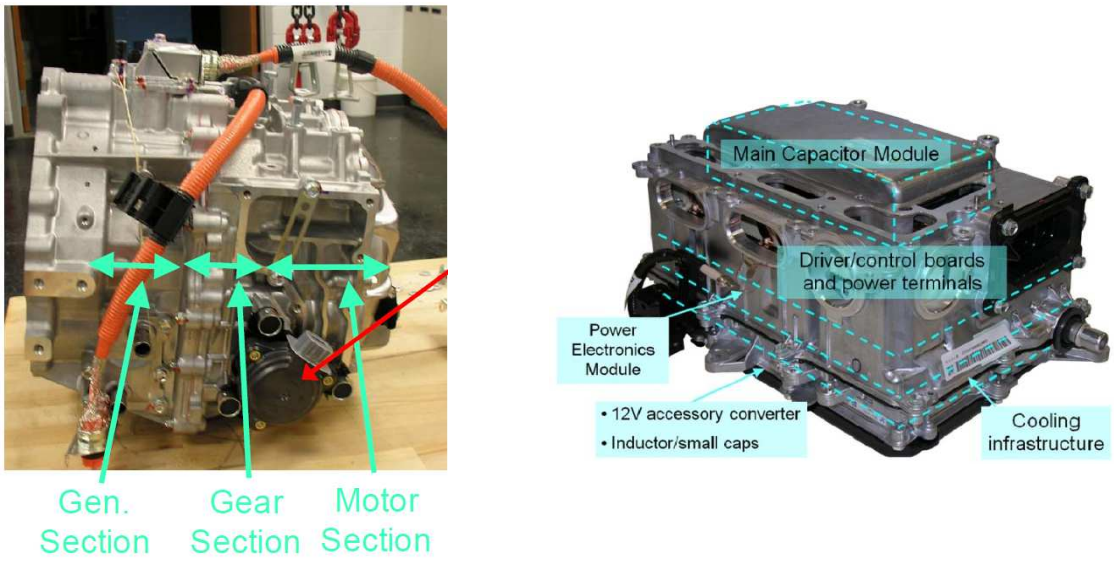

(a) Compartment of motor and generator (b) Compartment of power electronics converter assembly

Figure 1-2. 2010 Toyota Prius hybrid electric drive system [7].

To reduce the cost and complexity, it is advantageous to integrate the machine and power electronics together into a single combined machine-plus-drive structure, as well as eliminate the need for the 65 ˚C cooling loop and cool the power electronics with 105 ˚C engine coolant instead.

The integration of motor and drive offers a number of attractive features such as reduced drive volume and the elimination of power transmission cables. Radiated electromagnetic interference and voltage transients due to power transmission over long cable distances are also reduced. The integrated modular motor drive (IMMD) concept and a demonstrator were introduced in [8], as shown in Figure 1-3 and Figure 1-4.

However, there are still many issues unsolved associated with achieving the physical integration of the motor drive inside the machine housing. Designing power electronics to operate in the hash thermal environment inside an electric motor with the 105 ˚C engine coolant is a challenging task, which drives the demand of high temperature power electronics [9]-[11].

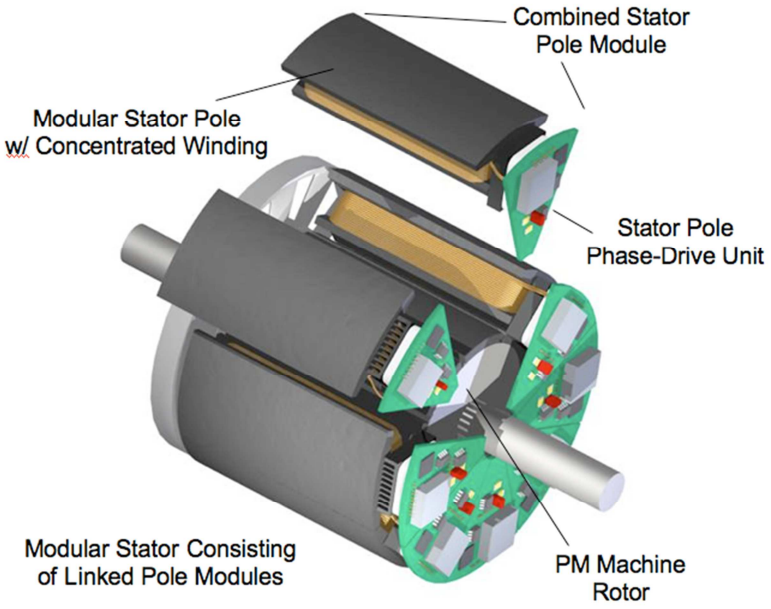

Figure 1-3. Integrated modular motor (IMMD) drive concept (Permission is obtained to use the picture) [8].

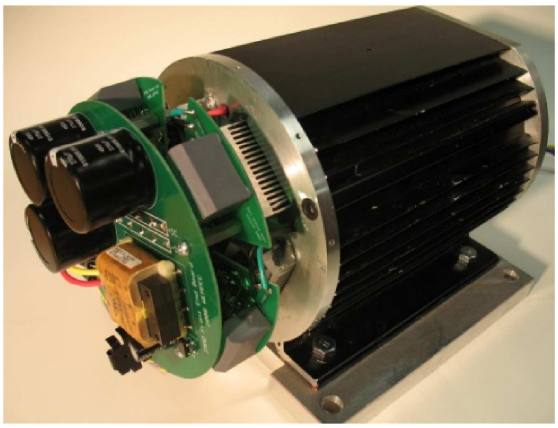

Figure 1-4. Concept demonstrator version of IMMD (< 3 kW) (Permission is obtained to use the picture) [8].

1.2 Dissertation Organization

The dissertation investigates the feasibility of operating Si devices at 200 ˚C and provides the guidelines on the development of a high temperature Si converter for operating with 105 ˚C

high temperature liquid coolant in hybrid electrical vehicle (HEV) applications. The chapters are organized as follows.

Chapter 2 reviews the state-of-the-art research activities in the corresponding areas of high temperature semiconductor devices and power converters. Based on the review, the challenges related to the high temperature operations are then addressed.

Chapter 3 presents the static and switching characterization of Si IGBT operating at 200 ˚C junction temperatures for traction applications. Also the impact of the increased junction temperature on a traction drive converter efficiency and thermal management is analyzed.

Chapter 4 provides a comprehensive evaluation of Si IGBT ruggedness at high temperature operation through experiments. A test circuit is proposed for testing the IGBT safe operating area. The latch-up immunity, short circuit capability and avalanche capability at high temperatures are evaluated through experiments.

Chapter 5 develops a Si IGBT phase-leg module for operating at 200 ˚C utilizing the high temperature packaging technologies and appropriate thermal management. The electrical characteristics and the thermal performance of the module and the cooling system are characterized through experiments. A 10 kW buck converter composed of this module assembly is built and operated at the junction temperature up to 200 ˚C.

Chapter 6 proposes a method to measure the junction temperatures of IGBTs during the converter operation using IGBT short circuit current. The calibration experiments show that the short circuit current has good sensitivity, linearity and selectivity, making the method suitable to be used as TSEP. By connecting a temperature measurement unit to the converter and giving a short circuit pulse during the converter operation, the IGBT junction temperature can be measured.

Chapter 7 develops a 30 kW Si IGBT based three-phase converter for operating at 200 ˚C junction temperature with the 105 ˚C engine coolant in HEVs, leading to lower cost and higher power density. The thermal management system utilizing the integrated pin fin baseplate is adopted to allow improved thermal performance. A 30 kW three-phase converter prototype is designed and tested with the IGBT junction temperature is measured during converter operation using the TSEP introduced in Chapter 6.

Chapter 8 investigates the fast switching characteristics and high temperature performance of the 600 V GaN high-electron-mobility transistor (HEMT). The inherent switching performance of the GaN HEMT is demonstrated in the double pulse test. The limitations of the fast switching capability by the device packaging and application circuit are analyzed. The high temperature static and switching characteristics up to 200 ˚C are also tested and given.

Chapter 9 summarizes the main conclusions of this dissertation and proposes potential future work.

Chapter 2. Literature Review

In this chapter, the state-of-the-art research activities in the corresponding area are reviewed, which helps to identify the importance of this work and its novelty. The challenges related to the high temperature operation are then addressed.

2.1 Si IGBT Development

IGBTs have been developed for many years, with a trend of smaller volumes and increased current densities. Figure 2-1 shows an example of the reduction of the IGBT chip area in the case of the 1200 V/ 75 A IGBT [10]. Figure 2-2 shows the decrease of the chip thickness from the first 1200 V non punch through (NPT) IGBTs to nowadays field-stop (FS) IGBTs in the voltage range of 600 V to 1700 V [12].

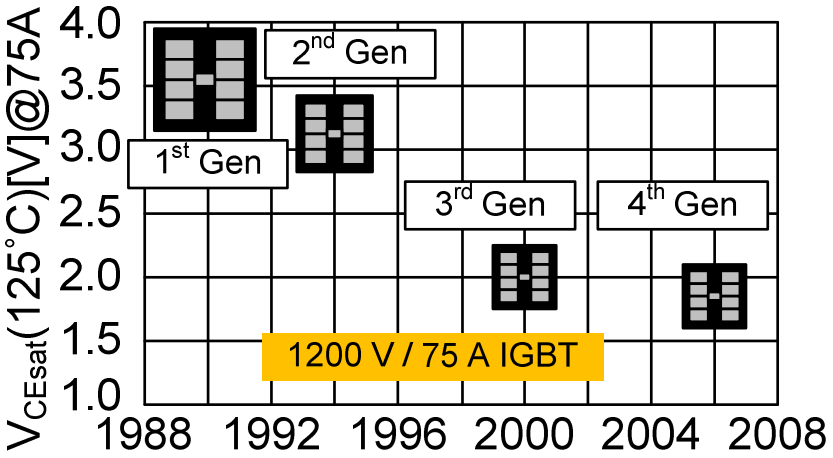

Figure 2-1. IGBT progress for 1200 V / 75 A chip [10].

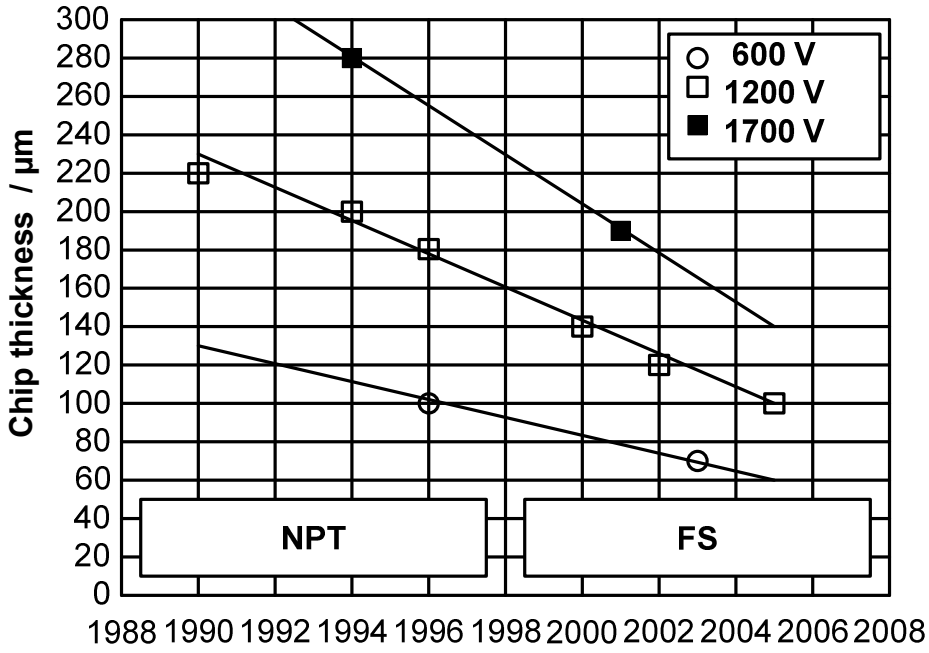

Figure 2-2. Decrease of chip thickness from first 1200 V NPT IGBTs up to nowadays 600-1700 V FS IGBTs [12].

A NPT structure with planar cell is employed in the second generation of IGBT (IGBT^2). Since IGBT^3, the trench-gate field-stop technology has been adopted [13]. Trench-gate field-stop IGBT exhibits good potential for high temperature operation in terms of loss. The trench gate structure shows superior characteristics of low on-state voltage drop due to an increased carrier concentration near the emitter. The lightly doped field stop structure makes it possible to obtain the fast turn-off characteristics, which reduces the switching loss. The maximum ratings in junction temperature T_J is 150 ˚C while the maximum temperature for continuous switching operation $T_{J,op}$ is 125 ˚C.

IGBT^4 has improved the trench gate structure for better V_{CEsat} values. The feature has made the power switches more efficient in combination with the optimized switching characteristics [14]. Furthermore, IGBT^4 allows a 25 ˚C higher maximum operation temperature compared to

IGBT[3]. The maximum ratings in junction temperature T_J is 175 ˚C while the maximum temperature for continuous switching operation $T_{J,op}$ is 150 ˚C. The IGBT maximum temperature for continuous switching operation can be further improved with the advanced assembly and the contact technology, which will be introduced in the next part.

2.2 Si IGBT Power Module Development

The harsh environment in automobiles requires the power modules to meet the high reliability standards. The power module packaging technologies have been improved in packaging materials and assembly technologies to improve the reliability and high temperature capability. The latest technologies for power module packaging and thermal management from different power semiconductor manufactures and automakers will be introduced.

2.2.1 Power Module in 2010 Toyota Prius Hybrid III

The power module in 2010 Toyota Prius Hybrid III has several improvements in packaging compared to 2004 Toyota Prius II [7][15]. Figure 2-3 shows the schematic and the photo of the power module cross section. The chips are soldered to a direct bond aluminum (DBA) substrate with AlN ceramic insulator for electrical isolation. The DBA substrate is brazed to the buffer plate, and the buffer plate is then brazed to the cold plate for liquid cooling. The structure eliminates the need for base plate and thermal grease, and thus achieves a 30% improvement in the thermal performance. The buffer plate with punched holes releases the stress between the cold plate and DBA caused by the coefficient of thermal expansion (CTE) mismatch. Additionally, Al ribbons are used to replace Al bond wires to improve the reliability.

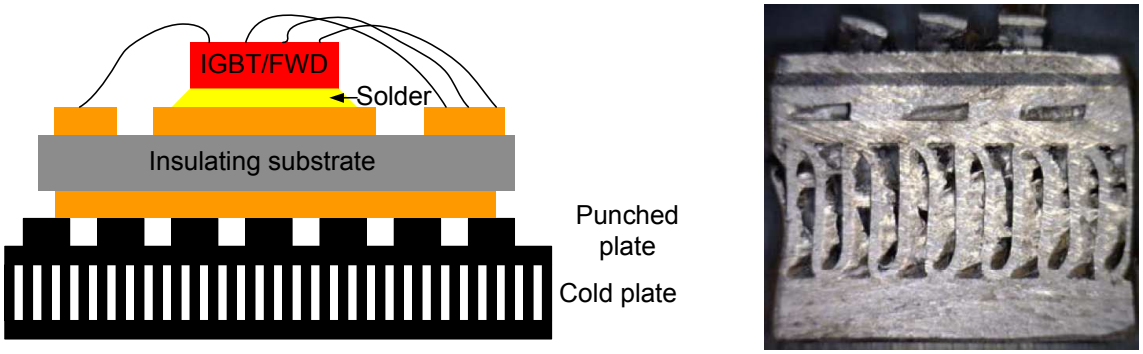

(a) Schematic (b) Photo

Figure 2-3. Cross section of the power module in 2010 Toyota Prius [7][15].

2.2.2 Power Module in 2008 Lexus LS 600H Hybrid

In the 2008 Lexus LS 600H hybrid drive system, the power modules are designed for double sided cooling [15][16]. As shown in Figure 2-4, one IGBT and one diode chip are soldered to two planar Cu plates on both sides for both electrical connection and thermal dissipation. Then the module is encapsulated with transfer molded compound and the Cu plates are exposed to the outside. A ceramic pad is inserted between the power module and cold plate for isolation. Figure 2-5 shows the power module and cooling infrastructure. Twenty four power modules are placed inside the cooling infrastructure with thirteen cooling channels for double side liquid cooling.

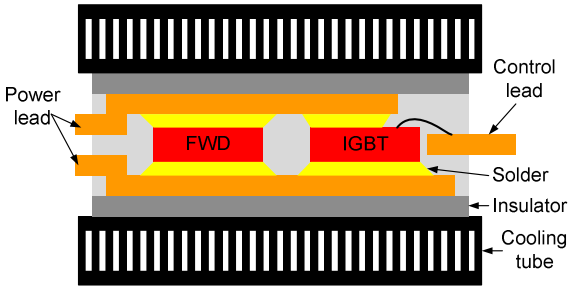

Figure 2-4. Cross section schematic of the power module for double sided cooling [15].

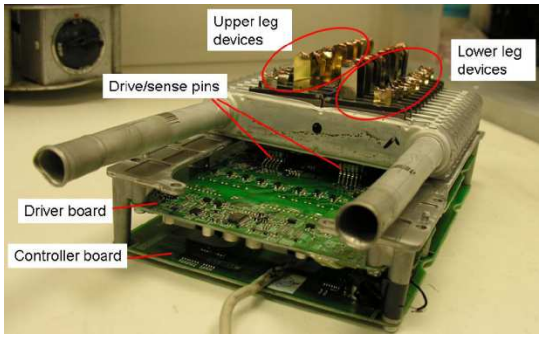

Figure 2-5. Power module and cooling in 2008 Lexus LS 600H Hybrid [16].

2.2.3 Infineon IGBT4 .XT Technology

In 2011, the module PrimePACK^{TM}2 was introduced to the market by Infineon using IGBT^4 and the .XT technology [17]-[18]. The .XT is a set of internal connection technologies that improve all life time limiting areas within an IGBT module, which increases the lifetime by more than a factor of ten and supports the module operating at 175 ˚C continuously.

Figure 2-6 shows the comparison of power cycling capability between IGBT^4 with standard packaging technologies and the .XT technology. IGBT^4 with the .XT technology has a higher power cycling capability and is valid for operation junction temperature up to 175 ˚C.

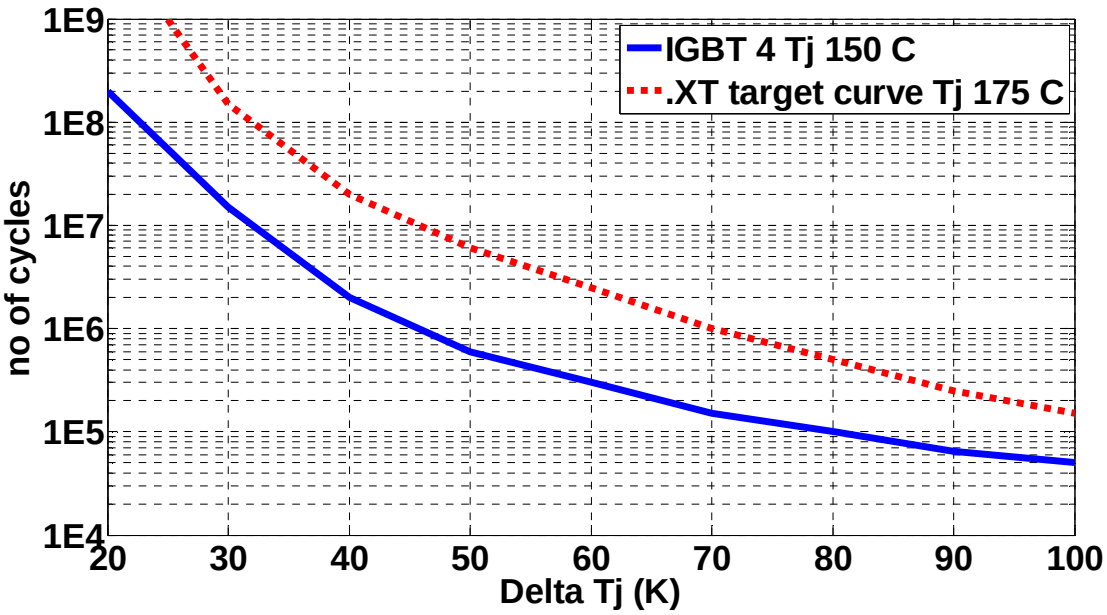

Figure 2-6. Power cycling diagram for standard IGBT^4 and IGBT^4 with .XT for pulses with duration of about 1.5 seconds [17].

The .XT technology improves all life-time limiting areas, including chip front side, chip back side and interconnections between substrate and baseplate.

For the chip front side connection in standard module packaging, the typical lifetime limiting failure mechanism is the bond wire lift-off as a result of the propagation of cracks inside the aluminum wire bond. The large mismatch of CTE between Si and Al and low yield strength of Al is the driving force for the crack propagation. Considering this, copper is used as a replacement material due to its superior mechanical properties. Because the Cu wire could simply sink into the Al metallization and leads to chip damage, the new metallization stack with Cu as the front side metal has been developed for the wire bonding.

For the connection between chip and substrate, in order to overcome the limits of the low melting point of standard tin based soft solders, a diffusion soldering process for power semiconductors to form a high melting bond between chip and substrate has been developed. A high melting chip-to-substrate bond (T_m>400 ˚C) with joint thickness d<10 µm can be realized.

For the connection between substrate and base plate, additional precipitations are implemented in the solder in order to stabilize the solder joint.

2.2.4 Semikron SKiM Technology and SKiN Technology

SKiM was introduced by Semikron in 2007 as the product line for highly reliable IGBT modules made specifically for automotive applications [19]-[21].

Considering that solder fatigue is one of the predominant power module lifetime limitations, the SKiM modules are 100% solder free. The power chips are sintered to a direct bonded copper (DBC) substrate. Under very high pressure of 30 MPa and moderate temperatures of 250 ˚C, the silver paste layer transforms into a solid layer of silver with the melting point at 961 ˚C. The power and auxiliary contacts are pressed to the substrate. The module does not have a base plate, and the substrate is in direct contact with the heat sink. The cross section of SKiM 63 is shown in Figure 2-7.

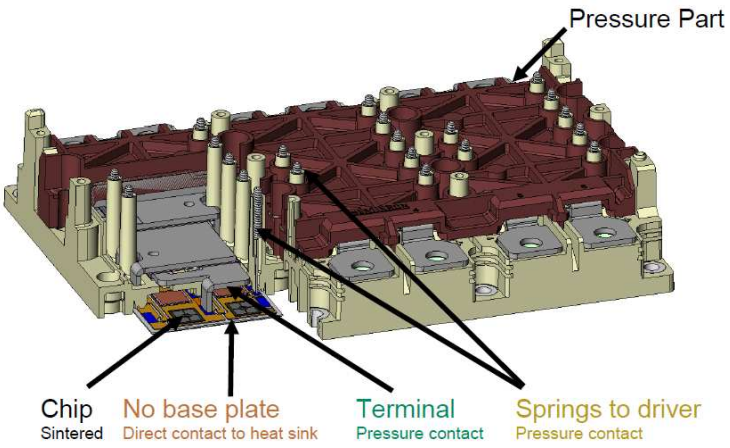

Figure 2-7. Cross section of SKiM 63 [20].

Although silver sintering is used to replace the soldering of chips to DBC substrates in SKiM modules, there are some issues that remain unaddressed corresponding to the wire bonding on the chip top side and the contact between power module and heat sink.

The SKiN technology is revealed by Semikron in 2011 to solve these matters [22]-[23]. A flexible circuit board is designed with polyimide with patterned metal tracks on both sides. The bottom metal carries the load current while the top layer carries gate, auxiliary and sense signals. The chip top surface is sintered on the flexible circuit board and the chip bottom surface is sintered to the DBC substrate. The back of the DBC substrate is sintered to an aluminum pin fin water-cooled heat sink. The power terminals are also sintered to DBC. As a result, all interconnections are made with Ag sinter joints in the module to avoid the use of solder, wire bond, and thermal grease. A schematic cross section and a photo of SKiN module are shown in Figure 2-8 and Figure 2-9 respectively.

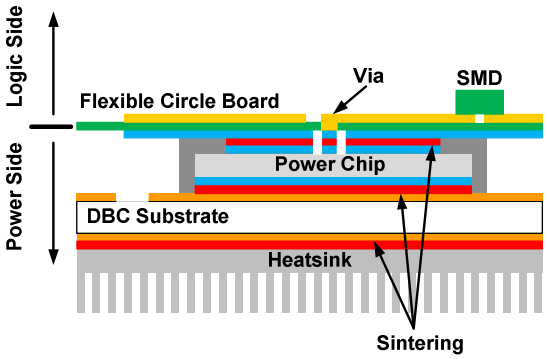

Figure 2-8. Schematic cross section of the SKiN device.

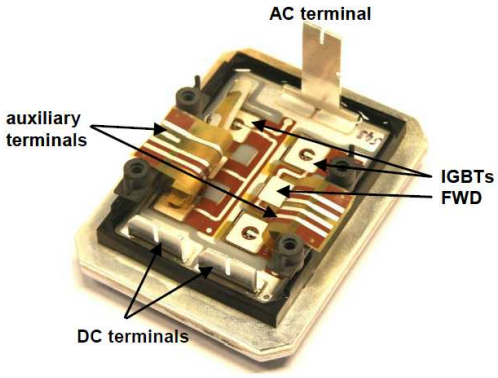

Figure 2-9. Photo of a 400 A, 600 V dual IGBT SKiN device [22].

Figure 2-10 shows the power cycling capability of a SKiN module. The SKiN device holds up to 500k cycles (from 40 ˚C to 150 ˚C within a 10 sec. cycle), while the conventional power module exhibits the fatigue at 20k to 40k cycles.

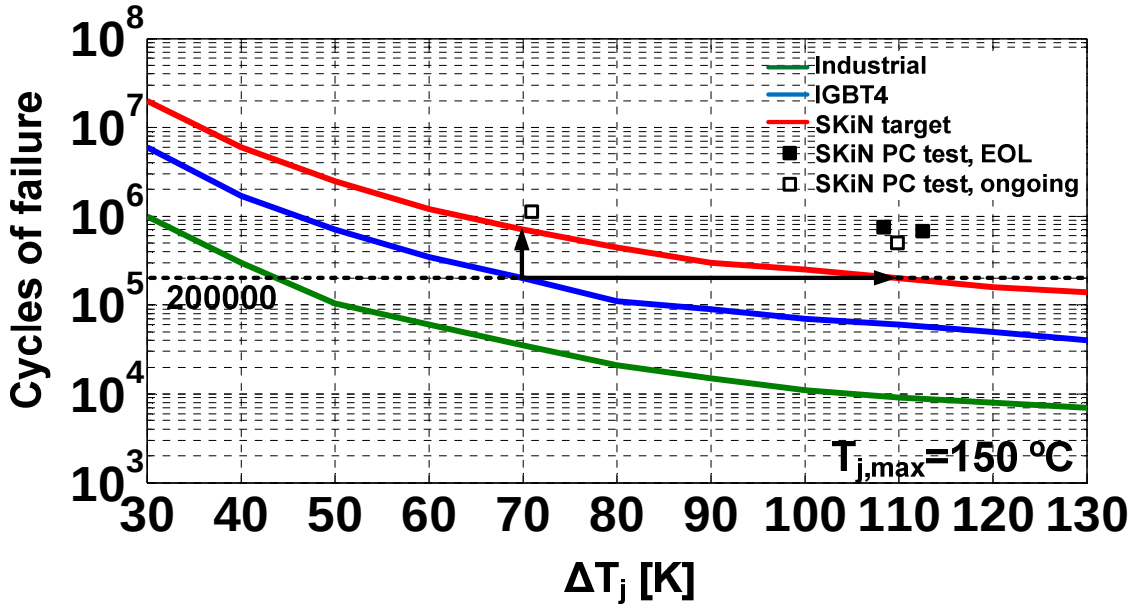

Figure 2-10. Power cycling capability of SKiN as a function of ΔT_j [22].

Passive temperature cycling is a challenge for the integrated SKiN device. The DBC substrate starts to delaminate from the heat sink after several hundred cycles from -50 ˚C to 150 ˚C with a temperature rise and fall time of 3 ˚C/min.

2.2.5 Mitsubishi Transfer Molded Power Module

The J series transfer molded power module (T-PM) is released by Mitsubishi Electric in 2011 for hybrid and electric vehicle applications, as shown in Figure 2-11 [24]. The power chips are bonded to the extended main terminal to eliminate the use of bond wire and reduce the wire resistance and inductance. The traditional DBA structure is replaced by a thick Cu / thermal conductive insulation layer (TCIL) / thin Cu structure. Transfer molding is applied, in which heated and pressurized resin is poured into a metal mold and enclosed. This method enables manufacturers to make multiple molds simultaneously and render power modules highly reliable.

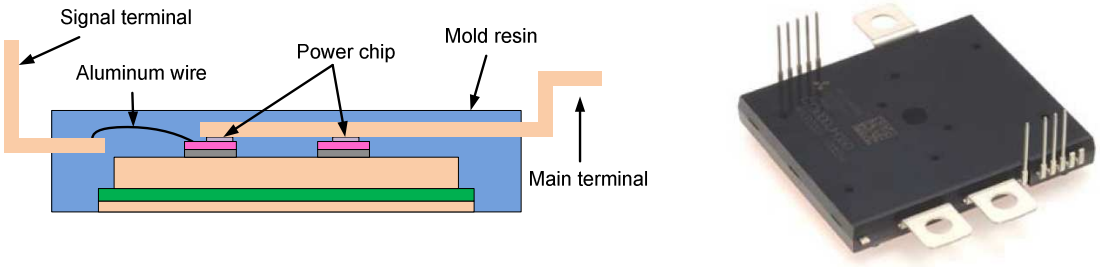

(a) Cross section schematic (b) Photo

Figure 2-11. Transfer molded power module (T-PM) [24].

2.2.6 Summary

Common failures in a packaged power module are often caused by thermal cycling due to the mismatching CTE of different materials. Improvement can be made in the three aspects of die interconnection, die attach, and DBC and baseplate connection.

For die interconnection, traditional Al wire bonding can be replaced by Al ribbon bonding, copper wire bonding or the flexible circuit board. For die attachment, the traditional solder process can be replaced by the diffusion soldering process or Ag sintering technology. For the DBC and baseplate connection, the high reliability soldering process with additional precipitations can be used for improvement. Direct cooling by eliminating the use of baseplate is another option.

2.3 Wide Bandgap Power Devices

Wide bandgap semiconductors have been developed rapidly recently. They have many advantages over Si devices such as high breakdown voltage, fast switching, low on-state resistance, high temperature capability, and high thermal conductivity [25]. The specific on-resistance vs. blocking capability limits for conventional Si devices, SiC devices and GaN devices are compared and shown in Figure 2-12. However, they are still expensive and have limited commercial availability.

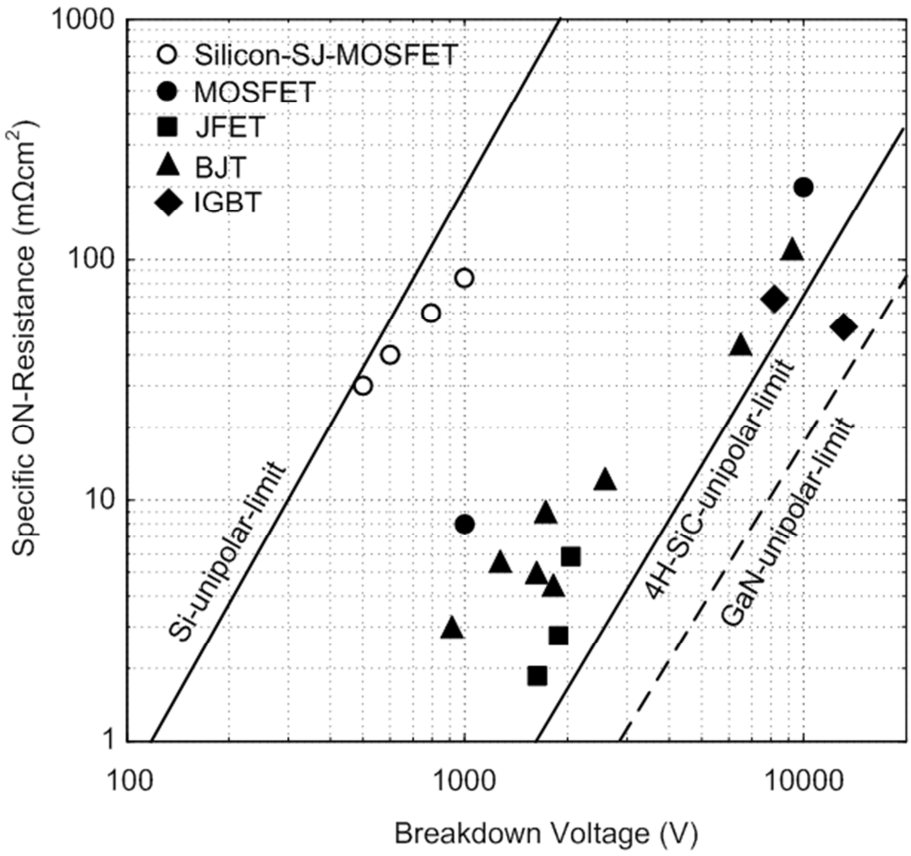

Figure 2-12. Specific on-resistance vs. blocking capability of various devices [25].

SiC diode is the first commercial SiC power semiconductor device. The commercial SiC Schottky diodes at the voltage rating from 600 V to 1200 V are available from Infineon, Cree and Semisouth [26]-[28]. The SiC Schottky diode has negligible reverse recovery and reduces the switching loss.

SiC JFETs have good reliability and provide high temperature capability. However, they are usually normally-on devices, which require special gate drives. The normally-off JFETs have higher on-resistance, limited threshold voltage margin and a limited temperature capability. The SiC JFETs are available from Semisouth and Infineon [29].

SiC power MOSFETs operate normally-off and have less demand on the drive circuits. But its oxide layer has poor reliability under high temperatures [30]-[31]. The commercially available 1200 V SiC MOSFETs are available from Cree.

Theoretically, GaN devices have superior performances over Si and SiC devices, due to their high electron mobility, high breakdown field and high electron velocity. However, today's commercial GaN power electronics devices are still limited to low voltage applications, which usually have a blocking voltage below 200 V [32]-[33]. In the recent years, 600 V GaN devices have emerged, showing the advantages of fast switching and low on-state resistance [34]-[36].

2.4 Converters using High Temperature Coolant in HEV Applications

Currently, hybrid electric vehicles use a separate liquid cooling system with the maximum coolant temperature at 65 ˚C, along with the maximum 105 ˚C engine cooling system. The 65 ˚C cooling system is used specially to remove the heat from the electric drive system due to the temperature limitations of power electronics. To reduce the cost and complexity, it is advantageous to eliminate the need for the 65 ˚C cooling loop and cool the power electronics with 105 ˚C engine coolant instead [1][4][37][38].

Up to date, several researchers have built converters that are capable of operating with high temperature WEG coolant [39]-[43].

In [39], by utilizing the hybrid switch and soft-switching technique for loss reduction, a 55 kW Si devices based three-phase inverter is built for coolant temperatures up to 90 ˚C as an intermediate step. However, this approach requires more usage of semiconductor devices as well as passives, leading to a trade-off between semiconductor cost and cooling system cost in a power module assembly.

In [40], a dc-dc boost converter comprised of SiC DMOSFETs and Schottky diodes is presented with 17 kW output power while using 90 ˚C liquid coolant. In [43], a silicon carbide (SiC) 5 kW dc-dc bidirectional boost converter is introduced for operation with 105 ˚C coolant. Although the wide bandgap devices have a higher junction temperature limit and low losses, they are emerging devices and costly.

2.5 IGBT Junction Temperature Measurement

The power semiconductor devices are required to operate at high junction temperatures due to the challenging thermal environment and the aggressive power density in HEV applications. Therefore the temperature control and thermal management become more of a concern.

An accurate junction temperature measurement is an effective tool for converter prototype evaluation, which helps to determine the safe operating region and avoid the unnecessary safety margin regarding device operating temperatures, thus, increasing the power density or reducing the cooling requirement.

Traditional method to estimate the junction temperature by adhering the thermocouple to the heat sink is not accurate. Thermistor or sensing diode in contact with the case cannot indicate the device temperature accurately either due to the distance to the chip [44]-[45]. In [46]-[48], IGBT on-state voltage drop or gate threshold voltage are employed as TSEP for junction temperature estimation. However these methods are suitable for thermal impedance characterization, but not applicable for temperature measurement during converter operation. Some papers introduce the TSEPs that are adapted for on-line temperature measurement. In [49], the IGBT switching behavior as a function of temperature is investigated, with the conclusions that turn-on delay time and turn-off time are suitable to be used as TSEP for temperature measurement. However, the switching time can be easily affected by other parameters (voltage,

current, gate drive and circuit parasitics) than temperature, as explained in chapter 5. Also the temperature sensitivity of switching time is very limited, usually less than 2 ns/˚C. In [50], a method is proposed using the saturation current under the gate voltage, which is just higher than the threshold voltage. However, the temperature sensitivity is very low and it is nonlinear. In [51], the voltage with a high current injection is measured for temperature indication. But the voltage drop on the electrical connection can cause larger measurement errors. Therefore, it is important to find a TSEP which is suitable as an indicator of the junction temperature.

2.6 Research Challenges and Objectives

According to the literature survey, there are many unsolved issues and challenges in the development of the high temperature converter for hybrid electrical vehicles to meet the power density and cost target application.

The main challenges include:

(1) The characteristics and ruggedness of Si devices when operating at the elevated temperature of 200 ˚C are not clear.

(2) The criteria for operating a Si device at 200 ˚C safely need to be defined in terms of safe operating area and thermal requirement.

(3) The packaging technology and thermal management to support Si devices operating continuously at temperatures as high as 200 ˚C need investigation.

(4) There are no effective methods to measure the device junction temperature during converter operation for the prototype evaluation.

(5) The implementation of the converter using Si devices for operating with the 105 ˚C high temperature coolant in HEV has not been previously demonstrated.

(6) The advantages and feasibility of emerging 600 V GaN devices are not fully explored. The high temperature characteristics of the device remain unclear.

Corresponding to the challenges discussed above, the objective of this work is to understand the potential and possible threats of Si devices operating at 200 ˚C and develop the guidelines for the development of a high temperature Si converter for operating with 105 ˚C high temperature coolant in HEV applications. Additionally, the emerging 600 V GaN HEMT is investigated as a potential candidate for future HEV applications. The work in this dissertation includes six parts:

(1) Investigate the characteristics of operating Si IGBTs at the elevated temperature of 200 ˚C through experiments.

(2) Evaluate Si IGBT ruggedness under high temperature operation conditions, including latch-up immunity, short circuit capability and avalanche capability.

(3) Develop a Si IGBT phase-leg module for operating at 200 ˚C utilizing high temperature packaging technologies and appropriate thermal management.

(4) Propose a method to measure the junction temperatures of IGBTs during the converter operation using temperature sensitive parameters for prototype evaluation.

(5) Develop a 30 kW Si devices based converter for operating at the junction temperature of 200 ˚C with 105 ˚C coolant.

(6) Investigate the emerging 600 V GaN HEMT as a potential replacement of Si devices for high efficiency and high temperature in future HEV applications.

Chapter 3. Si IGBT Characterization at High Temperatures

In this chapter, the feasibility of operating Si device at elevated temperatures as high as 200 ˚C is studied by device characterization and thermal analysis. The chapter is organized as follows: Section 3.2 discusses the selection of device for high temperature investigation. Section 3.3 and 3.4 show the IGBT static and switching characteristics up to 200 ˚C respectively. Based on these characteristics, the impact of the increased junction temperature on converter loss and thermal management is presented in 3.5. Conclusions are drawn in 3.6.

3.1 Introduction

Power semiconductor switches play a critical role in the automotive electric traction drive systems. During their operation the switches generate relatively large amounts of heat in the order of hundreds of watts (W) per die, leading to their temperature increase. Semiconductor devices and the associated packaging materials ultimately dictate the inherent temperature limitations.

Currently, hybrid electric vehicles use a separate liquid cooling system with the maximum coolant temperature at 65 ˚C, along with the maximum 105 ˚C engine cooling system. The 65 ˚C cooling system is used specially to remove the heat from the electric drive system due to the temperature limitations of power electronics. To reduce the cost and complexity, it is advantageous to eliminate the need for the 65 ˚C cooling loop and cool the power electronics with 105 ˚C engine coolant instead [1][4][37][38].

The challenging thermal environment as well as the aggressive power density and cost targets established by industry and government makes the high temperature operation of power electronics devices desirable [1]. Wide band gap semiconductor devices like SiC and GaN have

intrinsic high temperature capability and can theoretically operate at 500 ˚C. Some papers have developed the power converters for operating above the junction temperature of 200 ˚C, all with SiC devices [44]-[60]. However, they are emerging devices and costly. Considering the rising cost imposed by these newly developed techniques, it is meaningful to investigate the prospects for extending Si device junction temperatures to 200 ˚C as a lower-cost solution.

State-of-the-art commercial silicon (Si) devices usually have a maximum junction temperature rated at 150 ˚C, with some devices rated at 175 ˚C. As an alternative, it is desirable to extend the Si device junction temperatures higher, e.g. to 200 ˚C for continuous operation as a lower-cost approach for meeting the thermal management challenges. Several researchers took the first steps by investigating the operation of Si devices at high temperatures up to 200 ˚C and drew initial conclusions [61]-[62]. In [61], the Si MOSFETs operating at 200 ˚C is investigated from the standpoint of thermal stability, and a closed loop thermal system and stability criteria is developed considering the higher leakage current loss. In [62], the 1200 V soft-punch-through (SPT) Si insulated gate bipolar transistor (IGBT) is characterized in terms of leakage current, avalanche capability and short circuit performance with experiments. It is found that thermal runaway sets the upper limit for the operating temperature, and the blocking condition cannot be maintained at 200 ˚C due to the high leakage current.

Furthering the past work, this chapter evaluates the feasibility and issues of Si IGBT operating at 200 ˚C junction temperatures through device characterization and thermal analysis. Specifically, based on the specifications of HEVs, the 1200 V trench-gate field-stop Si IGBT rated at 175 ˚C is selected for study. The static and switching characteristics are tested at various temperatures. Based on these characteristics, the thermal requirement is given to allow the blocking condition at 200 ˚C without failure due to thermal runaway. Also the impact of the

increased device junction temperature on a traction drive converter loss and its thermal management is analyzed.

3.2 Device Selection

Trench-gate field-stop IGBT exhibits good potential for high temperature operation in terms of loss. Figure 3-1 shows the structure of the trench-gate field-stop IGBT. The trench gate structure shows superior characteristics of low on-state voltage drop due to an increased carrier concentration near the emitter [12][13]. The lightly doped field stop structure makes it possible to obtain the fast turn-off characteristics, which reduces the switching loss. Enabled by the structure, the commercial IGBTs rated at the temperature as high as 175 ˚C are available from Infineon, Fairchild, Microsemi, and etc.

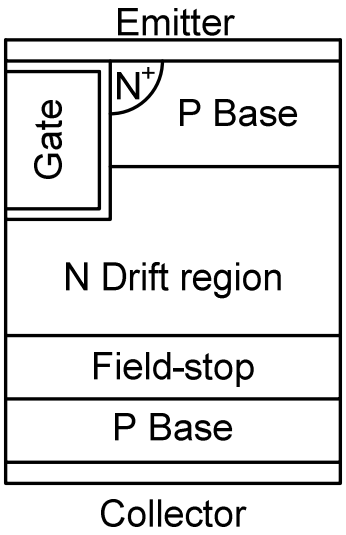

Figure 3-1. Structure of trench-gate filed-stop IGBT.

The specifications of the three-phase converter under study are selected considering both Department of Energy (DOE) FreedomCAR targets [37] and the commercial HEVs [16],[63]-

[65]. In DOE FreedomCAR targets, the continuous output power is 30 kW, and the peak output power for 18 seconds is 55 kW. The operating dc voltage rating is 200 V to 450 V and the nominal voltage is 325 V. However, there is a trend to increase the dc bus voltage to improve the system efficiency. In 2007 Toyota Camry hybrid electric drive system, the dc voltage rating is from 250 V to 650 V [65].

In the design in this dissertation, the dc link voltage is 650 V. The power rating for each phase-leg is 10 kW. Six phase-leg modules can be used for a six phase converter to achieve the 55 kW output power and fault tolerance. Three phase-leg modules can be used for a three phase converter to achieve 30 kW output power. Assuming the modulation index of 1 is used for the rated voltage and the load power factor is 0.95, then the rms phase current and voltage is 46 A and 217 V respectively.

So a 1200 V / 40 A trench-gate field-stop Si IGBT with soft, fast-recovery anti-parallel diode rated at 175 ˚C (IKW40N120H3) from Infineon is selected for study at higher temperature operation up to 200 ˚C.

3.3 Si IGBT Static Characteristics

The static characteristics are measured with Tektronix 371B high power curve tracer. The device is heated by a hot plate with its temperature monitored by the thermal couple as shown in Figure 3-2.

Figure 3-2. Test setup for static characterization at high temperatures.

3.3.1 Output Characteristics

Temperature effects on forward conduction characteristics and leakage current are characterized. Figure 3-3 shows the output characteristics of the IGBT and its anti-parallel diode at 200 ˚C. Since the relationship between the on-state current and voltage is fairly linear, a linear approximation in (2-1) can be applied to the curves,

$$V_{CE} = I_C \cdot R_{CE} + V_t, \qquad V_F = I_F \cdot R_{AK} + V_f \tag{2-1}$$

where R_{CE} and R_{AK} represent the on-state resistances, while V_t and V_f represent the built-in voltages of the IGBT and diode respectively. The four parameters together determine the on-state voltage drop and thus conduction loss. Table 3-1 shows V_t, R_{CE}, V_f and R_{AK} measured at various temperatures. As the temperature rises, the on-state resistance increases because of carrier mobility reduction while the built-in voltage decreases due to a sharp increase in intrinsic carrier concentration. The parameters measured at 25 ˚C and 175 ˚C agree well with datasheet. Figure 3-4 shows the on-state voltage drop as a function of junction temperature. The experiments are based on limited number of devices.

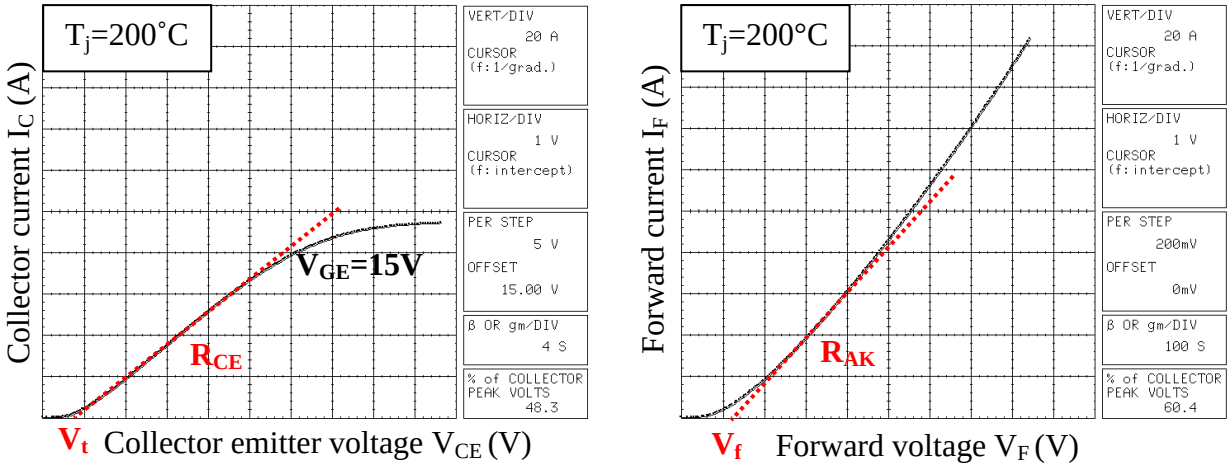

(a) IGBT (b) Anti-parallel diode

Figure 3-3. Output characteristics of IGBT and the anti-parallel diode at 200 ˚C and their linear approximation.

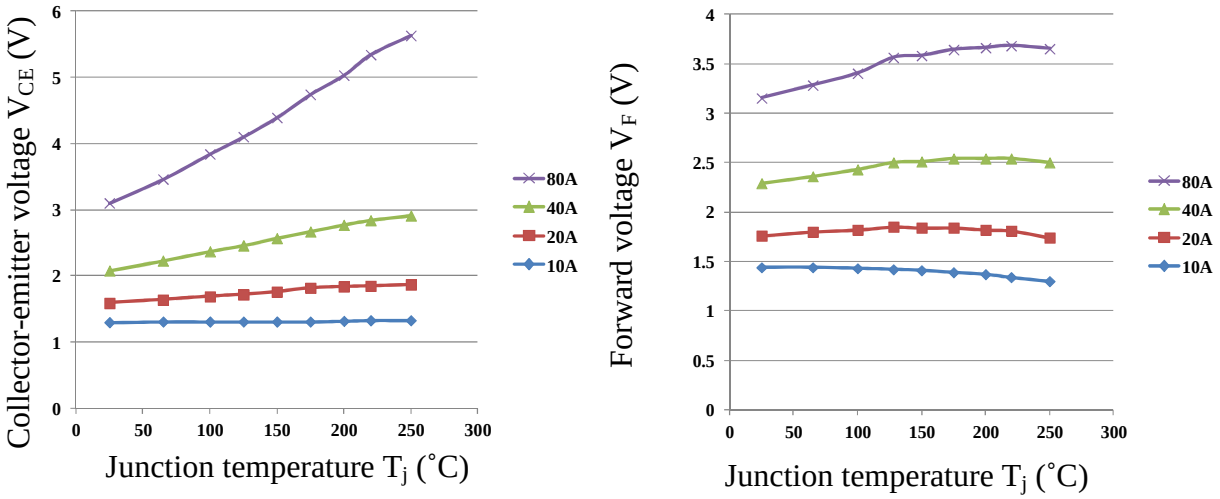

(a) IGBT (b) Anti-parallel diode

Figure 3-4. On-state voltage drop of the IGBT and the anti-parallel diode as a function of junction temperature.

Table 3-1 Parameters of IGBT Output Characteristics at Various Temperatures

	25 ˚C	**100 ˚C**	**175 ˚C**	**200 ˚C**
V_t	1 V	0.9 V	0.8 V	0.7 V
R_{CE}	26 mΩ	37 mΩ	49 mΩ	52 mΩ
V_f	1.3 V	1.2 V	1.1 V	1.1 V
R_{AK}	23 mΩ	30 mΩ	35 mΩ	35 mΩ

3.3.2 DC Blocking Characteristics

Leakage current is the sum of diffusion components in the neutral region and generation current in the depletion region. As the temperature goes up, the diffusion leakage current grows rapidly and becomes dominant. Figure 3-5 shows the leakage current of the IGBT with the anti-paralleled diode at 650 V as a function of the junction temperature. At high temperatures, especially above 175 ˚C, the leakage current doubles every 5.2 degrees and reaches 16.6 mA at 200 ˚C. From the curve fitting, the relationship between the junction temperature and the leakage current at 650 V can be expressed in (2-2).

$$I_{leakage} = 0.581 \cdot 10^{-3} \cdot 2^{\frac{T_j - 175}{5.196}} \text{ (A)} \qquad (2\text{-}2)$$

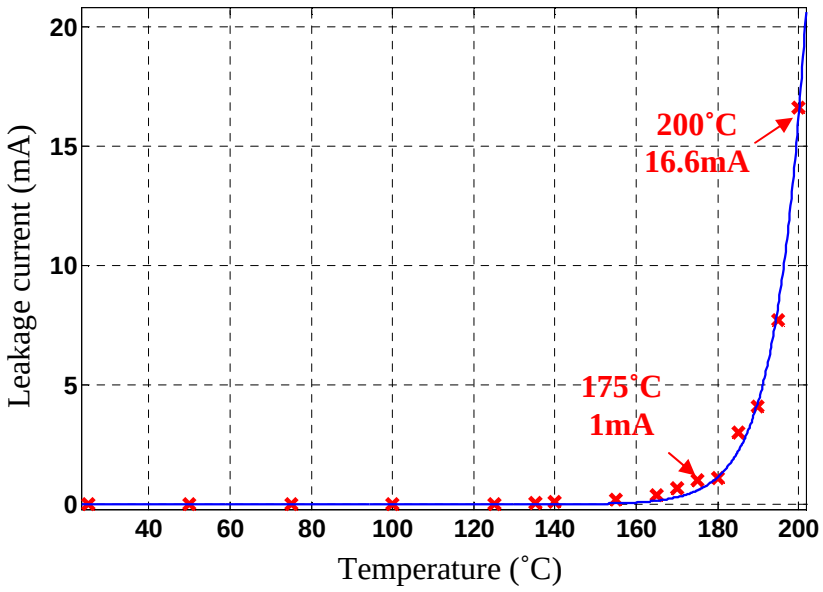

Figure 3-5. IGBT and diode leakage current at 650 V as a function of junction temperature.

The increased leakage current at high temperatures will cause additional power loss and possible thermal instability, which should be considered in the thermal design to prevent thermal runaway.

The leakage current caused power loss for one IGBT in a phase leg is half of the product of the dc bus voltage and the leakage current considering the current commutation, as is given in (2-3). The critical thermal resistance allowing stable operation at 200 ˚C is the slope of the leakage current loss curve at 200 ˚C [61]. From the calculation in (2-4), the IGBT thermal resistance from junction to ambient should be less than 1.41 ˚C/W to prevent thermal runaway. This provides an important criterion in terms of thermal stability. In HEV applications, the semiconductors are cooled by liquid, which usually has smaller thermal resistance than air cooling and provides the benefit for satisfying the thermal stability requirement.

$$P_{leakage} = \frac{1}{2} I_{leakage} \cdot V_{dc} = 0.189 \cdot 2^{\frac{T_j - 175}{5.196}} \tag{2-3}$$

$$R_{th-crit} = 1 \Big/ \frac{d(P_{leakage})}{d(T_j)}\Big|_{T_j=200} = 1.41 \ ^{\circ}\text{C/W} \tag{2-4}$$

Besides, high temperature operation can give rise to thermal instabilities due to the easier current filament formation at higher temperatures even if the thermal performance stays within the limit. Thus the reliability of the device should be further studied under the harsh environmental conditions using a combination of standard tests including high temperature reverse bias (HTRB), high temperature gate bias (HTGB), temperature humidity bias (THB) and so on, which are not covered in this work.

3.4 Si IGBT Switching Characteristics

The switching performance of the Si IGBT is evaluated with an inductive load double-pulse tester. Figure 3-6 shows the circuit schematic of double pulse test (DPT) with over-current protection. The double pulse is generated by Agilent 33220 arbitrary waveform generator. The device under test (DUT) is driven by a high-speed, high-current gate driver IXDN409 from

IXYS, with gate voltage from 0 V to 15 V. A 0.1 Ω shunt resistor with the bandwidth of 2 GHz is connected in series with the device emitter terminal to measure the collector current. V_{GE} and V_{CE} are measured using the Tektronix voltage probes P6139 and P5100 respectively. The protection board is comprised of an IGBT with low on-state resistance and the gate driver IR2127 with de-saturation protection. When the protection board detects an over-current fault, the IGBT is turned off and limits the current. Figure 3-7 shows the hardware testbed for high temperature switching experiments. DUTs are connected to the hot plate through the copper connector with the case temperature monitored by thermocouples. The glass wool and fans are used to keep the PCB board (especially for shunt resistors and gate drivers) under 50˚C. Since the switching loss caused by two pulses is negligible, the DUT junction temperature can be regarded as the same as the case temperature.

With the DPT hardware testbed, the IGBT switching characteristics are tested at 25 ˚C, 100 ˚C, 175 ˚C and 200 ˚C. The test conditions are: dc bus voltage V_{CC}=650 V, collector current I_C=40 A, gate-emitter voltage V_{GE}=0.0 V/15.0 V, and gate resistance R_G=12.0 Ω.

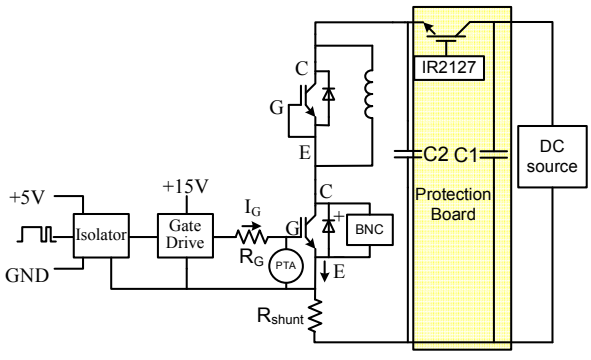

Figure 3-6. High temperature experiment setup for switching characteristics test.

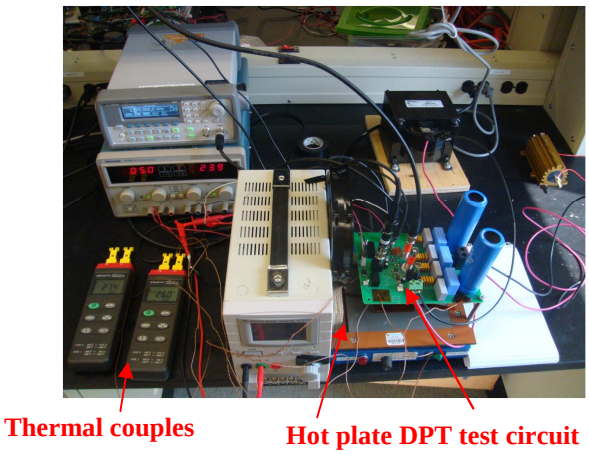

Figure 3-7. Hardware testbed for high temperature switching experiments.

Figure 3-8 shows the IGBT switching characteristics during turn-on and turn-off transients at 200 ˚C. The device's switching transients are captured at the end of the first pulse and beginning of the second pulse respectively under the pre-set collector-emitter voltage and collector current conditions. The switching time as well as switching energy at 25 ˚C, 100 ˚C, 175 ˚C and 200 ˚C is summarized in Table 3-2 with the comparisons shown in Figure 3-9 and Figure 3-10. The definition of switching time and energy follow that used in the datasheet.

The diode reverse recovery current as well as reverse recovery energy increases at high temperature due to an increase in the lifetime and number of minority carriers stored in the drift layer. In addition, diode reverse recovery causes current overshoot and extra turn-on losses of the complementary IGBTs. The IGBT turn-on energy is increased at high temperature mainly due to the increased diode reverse recovery current, while the prolonged minority carrier lifetime slows down the IGBT turn-off speed and increases the turn-off energy. One alternative option is to use the combination of Si IGBT and SiC Schottky diode to reduce the switching loss, considering that SiC Schottky diode has very small reverse-recovery energy, which shows no significant increase with temperature [66]-[67].

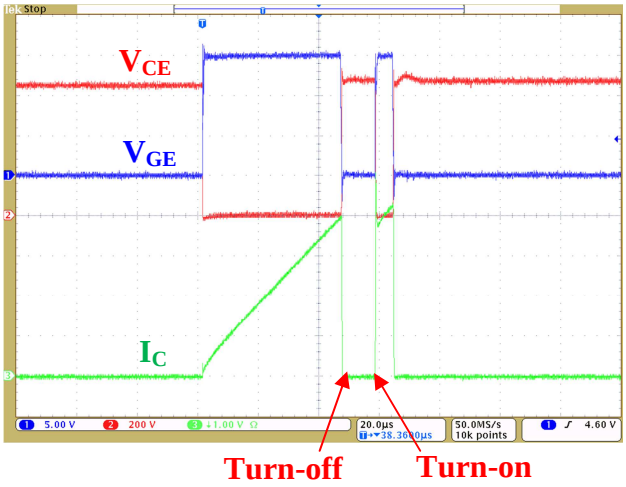

(a) Double pulse waveforms

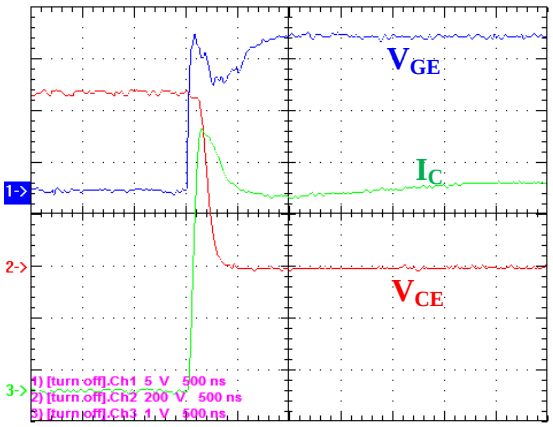

(b) Turn-on transient

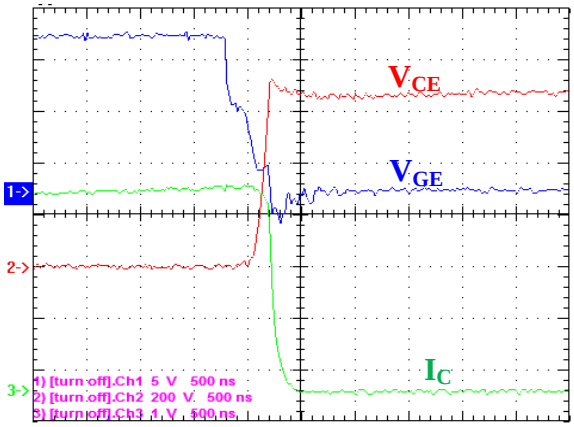

(c) Turn-off transient

Figure 3-8. Waveforms of IGBT switching characteristics at 200˚C.

Table 3-2 IGBT Switching Characteristic Values at Various Temperatures

Parameter	25 ˚C	100 ˚C	175 ˚C	200 ˚C
Turn on delay time $t_{d(on)}$	24.4 ns	21 ns	23.6 ns	20 ns
Rise time t_r	60.4 ns	62.6 ns	78.4 ns	80 ns
Turn off delay time $t_{d(off)}$	278 ns	311.2 ns	380 ns	400 ns
Fall time t_f	38.8 ns	79.2 ns	120 ns	140 ns
Turn-on energy E_{on}	3.19 mJ	3.99 mJ	4.50 mJ	4.61 mJ
Turn-off energy E_{off}	1.31 mJ	2.05 mJ	2.83 mJ	3.02 mJ
Total switching energy E_{ts}	4.50 mJ	6.04 mJ	7.33 mJ	7.63 mJ
Diode reverse recovery energy E_{rr}	109.1 µJ	227.8 µJ	416.6 µJ	639.8 µJ

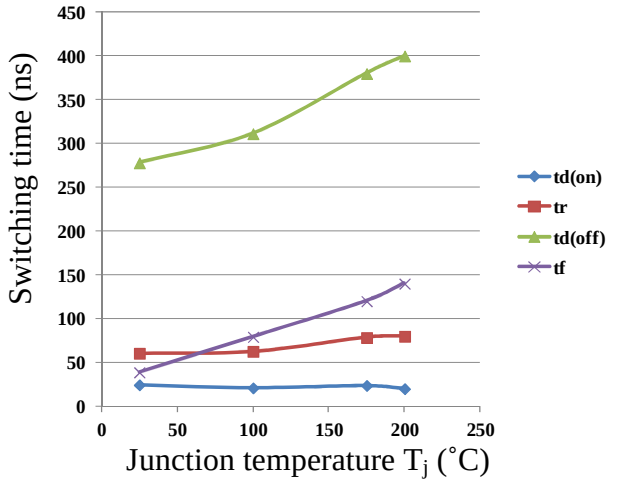

Figure 3-9. Switching time as a function of junction temperature.

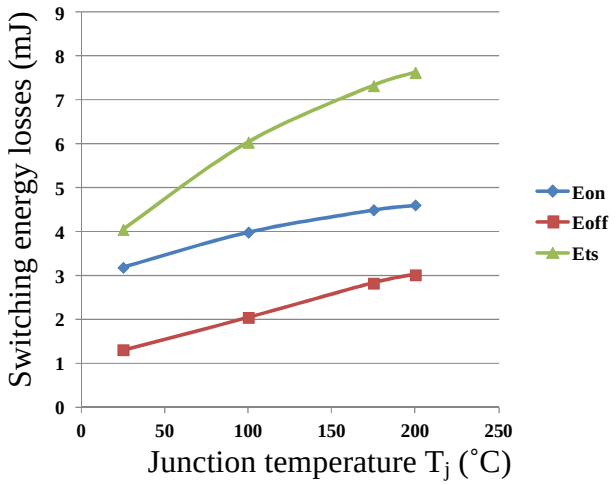

Figure 3-10. Switching energy losses as a function of junction temperature.

From the high temperature characterization, it is shown that the commercial 175 ˚C Si IGBT under test can be successfully switched at an elevated junction temperature of 200 ˚C with increased switching energy by 4.09 % compared with that at the rated temperature of 175 ˚C.

3.5 Impact on Converter Power Loss and Thermal Management

High temperature operation of Si devices causes more losses, as indicated in the device characterization. In this section, the impact of the increased device loss and junction temperature on a traction drive converter loss and converter thermal management is analyzed. As mentioned before, the power rating for each phase-leg of the three phase drive is 10 kW and the dc link voltage is 650 V. A minimum-loss space vector modulation (SVM) [68] is used for the three-phase converter switching control. The total loss generated from power devices consists of conduction loss, switching loss and leakage current loss. For simplicity, the conduction loss and switching loss for one IGBT and diode cell are calculated based on a linear loss model [69].

The switching loss is given by

$$P_{sw} = \frac{1}{4}(E_{on} + E_{off} + E_{rr})\frac{V_{dc} I}{V_{rated} I_{rated}} f_s \tag{2-5}$$

In (2-5), E_{on} and E_{off} are the rated IGBT turn-on loss, turn-off loss given for the reference commutation voltage and current V_{rated} and I_{rated}. They are obtained from switching characterization. V_{dc} and I indicate the actual voltage and the averaging absolute value of current respectively. f_s is the switching frequency.

The conduction loss of the IGBT and diode is calculated with the closed-form equations, which is given by [69]

$$P_{con\_IGBT} = \frac{1}{2} \cdot I \cdot V_t \left(\frac{1}{\pi} + \frac{M}{2\sqrt{3}} \cos\phi\right) + I^2 R_{ce} \left(\frac{1}{8} + \frac{2M}{3\sqrt{3}\pi} \cos\phi\right) \tag{2-6}$$

$$P_{con\_diode} = \frac{1}{2} \cdot I \cdot V_f \left(\frac{1}{\pi} - \frac{M}{2\sqrt{3}} \cos\phi\right) + I^2 R_{ak} \left(\frac{1}{8} - \frac{2M}{3\sqrt{3}\pi} \cos\phi\right) \tag{2-7}$$

In (2-6) and (2-7), V_t and V_f are the threshold voltages of the IGBT and diode respectively, while R_{ce} and R_{ak} are the differential on-state resistances of the IGBT and diode respectively. These four parameters are obtained from the output characteristics evaluation. M is the modulation index defined as peak value of the phase voltage divided by half of the dc bus voltage. ϕ is the displacement angle between the fundamental ac phase voltage and current.

The leakage current loss given by

$$P_{leakage} = \frac{1}{2} I_{leakage} \cdot V_{dc} \tag{2-8}$$

Figure 3-11 shows the power losses in one phase-leg, which increase with temperature. The total loss is increased by 7.40 % when the junction temperature increases from 175 ˚C to 200 ˚C.

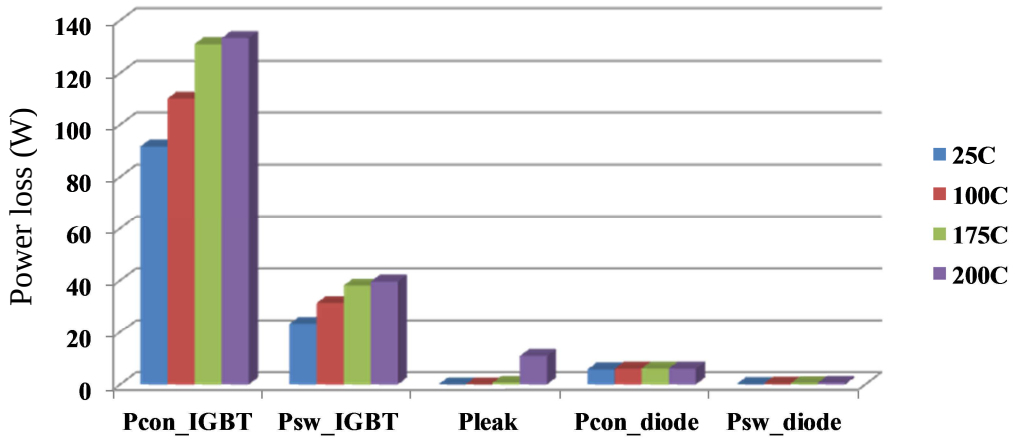

Figure 3-11. Power losses in one phase-leg at various temperatures (f_s=10 kHz).

To keep the device junction temperature below allowable maximum junction temperature and prevent thermal runaway, certain thermal transfer capability is required, which is represented by thermal resistance and depends on the semiconductor packaging and cooling system.

The relationship between junction temperature, ambient (coolant) temperature, power losses and thermal resistance can be expressed in equation (2-9).

$$T_J - T_{amb} = P_{loss} \cdot R_{THj-amb} \tag{2-9}$$

Where T_J is device junction temperature, T_{amb} is inlet coolant temperature, P_{loss} is power losses of semiconductor devices, and $R_{THj\text{-}amb}$ is thermal resistance from device junction to inlet coolant.

From the losses obtained above, the IGBT thermal resistances required corresponding to various phase-leg power ratings are calculated for operation at 175 ˚C and 200 ˚C respectively with the 105 ˚C engine coolant, as shown in Figure 3-12.

Figure 3-12 reveals the potential to increase the power density or reduce the cooling requirement by extending the junction temperature from 175 ˚C to 200 ˚C despite the higher losses. On the one hand, for a fixed thermal resistance of 1.03 ˚C/W, the power rating of the phase-leg can be enhanced by 15% from 8.7 kW to 10 kW. On the other hand, if the power rating

is fixed at 10 kW, the thermal resistance from junction to ambient can be increased from 0.825 ˚C/W to 1.03 ˚C/W. Considering that the thermal resistance from junction to case can be as high as 0.5 ˚C/W, the cooling requirement is greatly reduced and much easier to achieve for the 200˚C case.

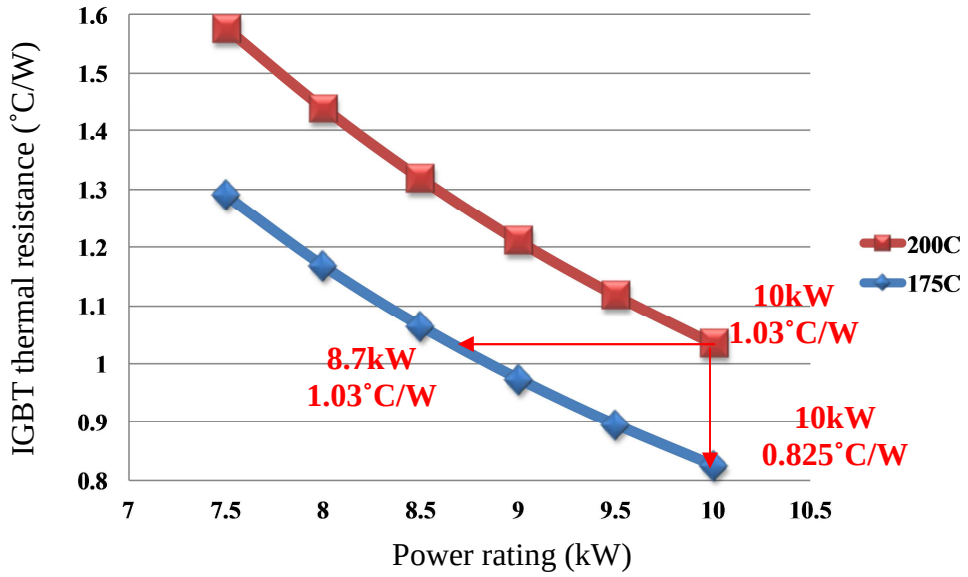

Figure 3-12. Thermal resistance required for various rated power at 175 ˚C and 200 ˚C.

To further evaluate the feasibility of operating IGBTs at 200 ˚C with 105 ˚C coolant, the 200 ˚C semiconductor operation is compared with the lower temperature operation in today's HEVs in terms of power density, thermal management, efficiency and cost. The power semiconductors in today's HEVs usually have a maximum junction temperature of 150 ˚C with 65 ˚C coolant. Thus a 1200 V/40 A trench-gate field-stop IGBT rated at 150 ˚C from Infineon (IGW40T120) is selected for loss calculation in the commercial case. The losses for the device are calculated based on its datasheet under the same operation conditions. The IGBT thermal resistance required for a 10 kW phase leg is calculated in two cases. The IGBT thermal resistance in the commercial case is 1.044 ˚C/W, which is only 0.014 ˚C/W larger than that in the proposed

commercial case. As a result, by extending the junction temperature to 200 ˚C and keeping the same power density and thermal resistance, the additional 65 ˚C coolant can be eliminated, which leads to lower cost, weight and volume. The trade-off is that the efficiency is decreased by 0.2 percent from 98.3 % to 98.1 %.

3.6 Summary

The chapter presents the characterization of Si IGBT operating at 200 ˚C junction temperatures for traction applications. The 1200 V trench-gate field-stop IGBT rated at 175 ˚C is selected for the study. Through device characterization, it is shown that the commercial 175 ˚C Si IGBT under test can be successfully switched at an elevated junction temperature of 200 ˚C with increased but acceptable losses. The thermal requirement is given to allow the reverse blocking condition at 200 ˚C without thermal runaway. Also the impact of the increased junction temperature on a traction drive converter loss and thermal management is analyzed, showing an enhancement of power density or the decrease of the cooling requirement. Comparing with the power semiconductor operation in commercial HEVs, by extending the junction temperature to 200 ˚C without compromising power density and thermal management design, the additional 65 ˚C coolant can be eliminated with the trade-off of the decreased efficiency by 0.2 percent.

Chapter 4. Si IGBT Ruggedness Evaluation at High Temperatures

This chapter investigates Si IGBT ruggedness under high temperature operation conditions by evaluating latch-up immunity, short circuit capability and avalanche capability through experiments. The chapter is organized as follows: The short circuit capability evaluation is shown in 4.2. The latch-up immunity evaluation is given in 4.3. The avalanche capability of several kinds of Si IGBT is given in 4.4. Conclusions are drawn in 4.5.

4.1 Introduction

IGBTs are widely employed in hard-switching applications, where they are required to turn on or turn off rated current with full bus voltage across the terminals, and also survive during malfunctions of systems like short circuit conditions.

In order to withstand the high-stress conditions, these power devices are required to have robust SOA. The SOA is generally referred as the current-voltage boundary within which a power device can operate without destructive failure. The SOA of an IGBT can be divided into three boundaries. Maximum current is typically limited by latch-up of the parasitic thyristor. Usually the de-saturation current is set far below the latch-up current level to prevent such kind of failure. Maximum voltage is limited by breakdown voltage. Maximum power dissipation corresponding to maximum allowed temperature rise is also a limitation.

When temperature increases, the latch-up current is decreased because the current gains of the NPN and PNP transistors within IGBT increase. The static avalanche breakdown voltage increases with the temperature due to the decrease in impact ionization coefficient with temperature. However, the avalanche capability to suppress the turn-off voltage spike is reduced.

Besides, the short circuit capability is also an important issue related to device ruggedness in high temperature operation, especially in practical motor drive applications. To ensure the safe and reliable operation of IGBT at 200 ˚C, it is necessary to evaluate the high temperature ruggedness of IGBT by testing the SOA limits.

Some literatures discussed the temperature dependence of device ruggedness. Various short circuit failure mechanisms are discussed in [70]-[76]. In [70], destruction is observed during turn-off period caused by overvoltage. These are the transition failures during turn-on or turn-off. In [71]-[74], short circuit destruction is observed several hundred microseconds after turning off the gate. The failure is described as thermal runaway caused by leakage current. These failures belong to the excessive power loss during the steady state. The IGBT latch-up mechanisms are discussed in [77]-[79]. In [77], it is shown that destruction due to the latch-up can occur resulting from turning the gate off before the device voltage rises to dc bus voltage. In [80]-[85], the device ruggedness corresponding to the turn-off capability and failure dynamics are discussed. However, these references do not have experimental results on Si devices operation at temperatures as high as 200 ˚C. A systematic and comprehensive assessment of IGBT ruggedness operating at 200 ˚C is needed for traction applications.

This chapter provides a comprehensive evaluation of Si IGBT ruggedness at high temperature operation through experiments. The test circuits are proposed for ruggedness evaluation and the hardware is setup accordingly. The possible failure mechanisms including latching, short circuit fault, and avalanche capability are tested at elevated temperatures. The criteria considering latch-up immunity, short circuit capability and avalanche capability are given at 200 ˚C to ensure the safe and reliable operation of Si IGBTs.

4.2 Short Circuit Capability

4.2.1 Short Circuit Conditions and Test Circuits

In a typical motor drive system, the short circuit can happen in various conditions [86], as shown in Figure 4-1. Arm short circuit is caused by the destruction of IGBT or diode. Series arm short circuit usually results from fault control signals. Short circuit can also happen between phase to phase, phase to dc bus +/- terminals, or across the motor terminals.

The four short circuit modes listed above result in different fault current profiles. In arm short circuit, IGBT turn on into a short circuit, which is called hard switching fault (HSF). In series arm short circuit, initially an IGBT is in normal conduction; then the complementary IGBT is turned on by fault signal, causing a shoot-through. Since in this case, the short circuit is applied to an IGBT already on, it is called fault under load (FUL). When short circuit takes place in output circuit, depending on where it happens, the short circuit current goes through certain amount of inductance.

Figure 4-2 shows the waveforms of three short circuit conditions. In HSF, initially IGBT is off and dc bus voltage is supported across the device. At t_1, the device is turned on to short circuit. A notch on the V_{CE} is observed when the voltage drops on the resistive and inductive parasitic elements of the circuit. At t_2, the device is turned off. The fault current falls quickly and causes an overshoot of V_{CE}. The voltage spike is determined by both the turn-off speed and loop inductance. In FUL, at t_1, IGBT is turned on and the voltage across the device V_{CE} is low. At t_2, a short circuit is applied to the device. The current increases quickly and enters active region. The rise of V_{CE} charges the miller capacitor and thus pumps the gate voltage V_{GE}. The collector current shows a peak due to the increase of the gate voltage. In short circuit through large

inductance, the di/dt at turn on is low and it delays the IGBT saturation. Under this condition, the device can survive a longer short circuit time.

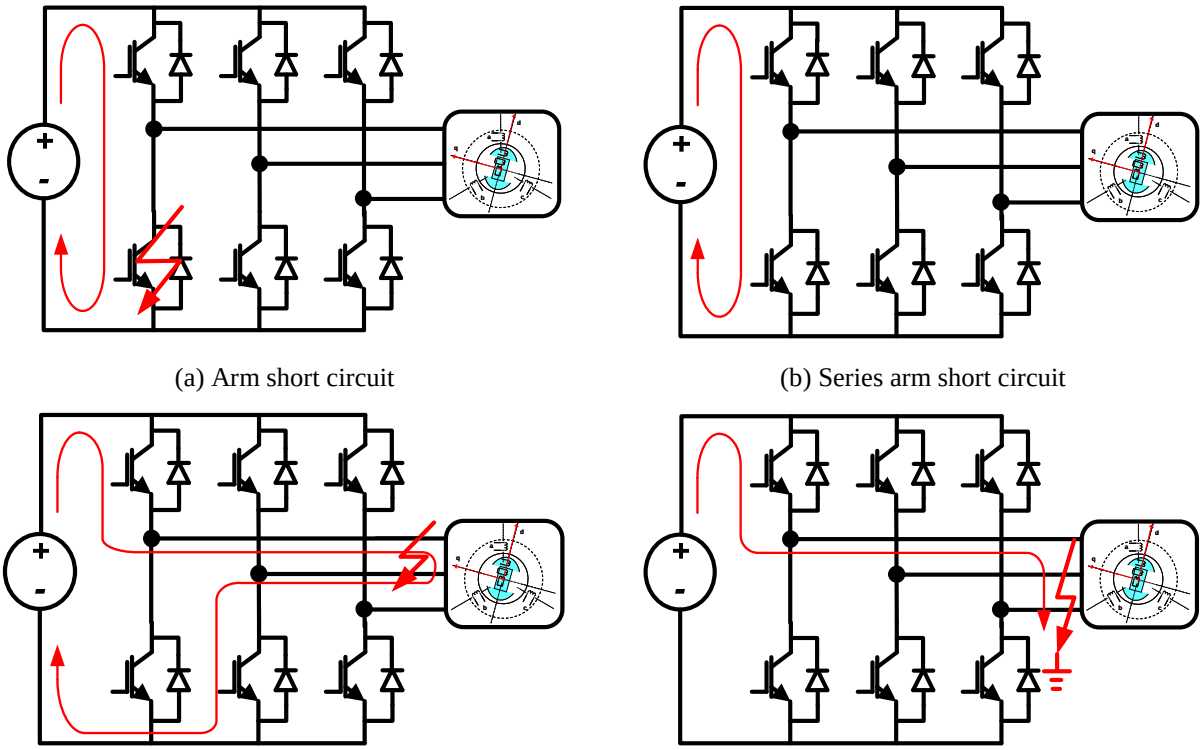

(a) Arm short circuit

(b) Series arm short circuit

(c) Short in output circuit

(d) Ground fault

Figure 4-1. Short circuit modes.

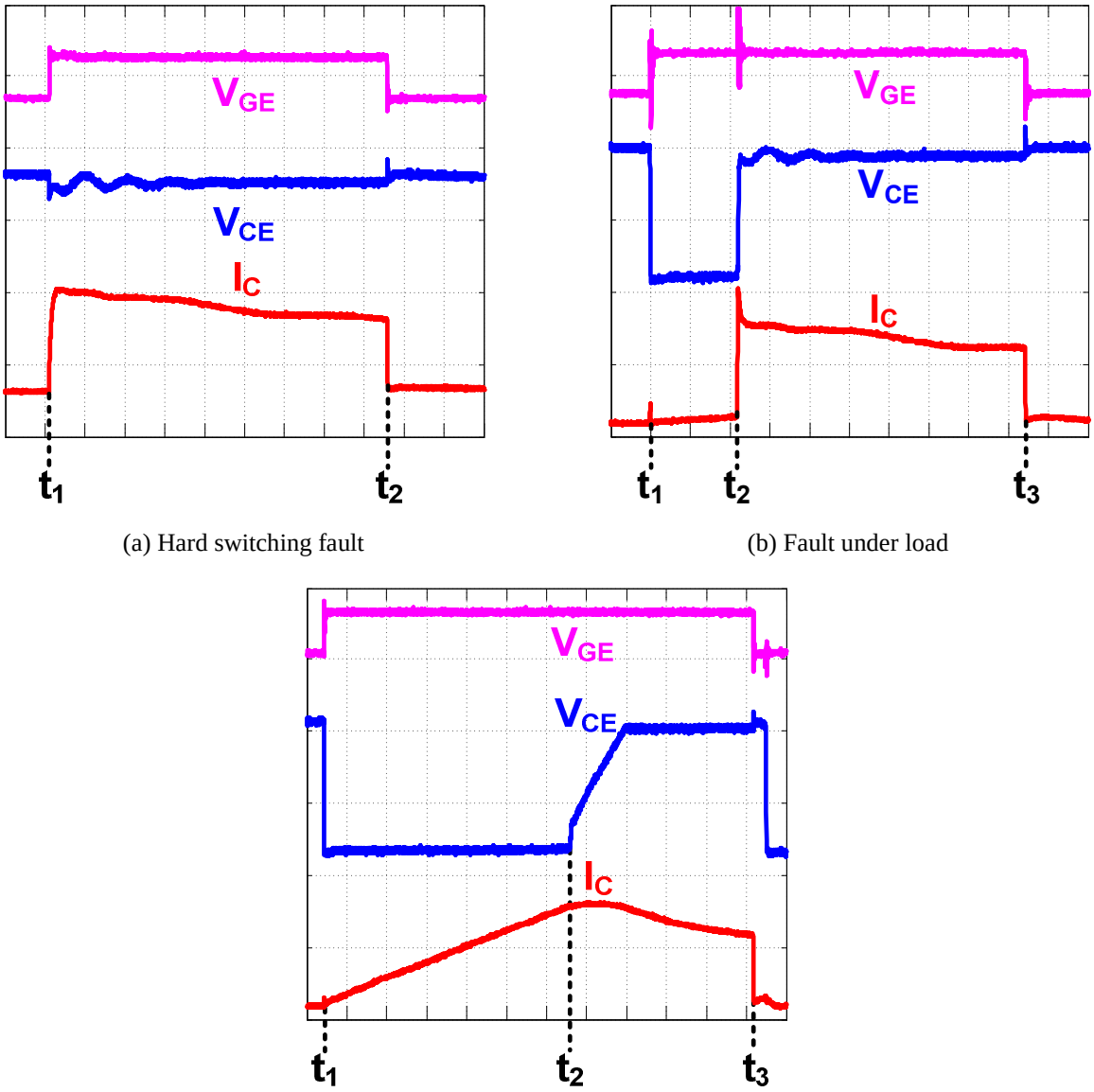

(a) Hard switching fault

(b) Fault under load

(c) Short circuit through large inductance

Figure 4-2. Types of short circuit fault conditions.

To evaluate the short circuit properties of IGBT, test circuits corresponding to three different types of short circuit conditions are proposed and shown in Figure 4-3. In Figure 4-3 (a), the test circuit is composed of dc power supply, DUT, protection IGBT and series IGBTs. The series IGBTs control whether the dc bus voltage is applied to DUT. The protection IGBT is driven by IR2127, a gate drive with de-saturation protection. The protection IGBT is activated at the

occurrence of DUT destruction and disconnects the dc bus with DUT in a few microseconds. In Figure 4-3 (b), the inductive load is used to limit the current after DUT is turned on. An additional control IGBT is connected in parallel with the inductor. By turning on the control IGBT, the short circuit is applied to DUT that is already conducting. In Figure 4-3 (c), an inductor in connected in the loop. After DUT is turned on, the current rises linearly and then enters the active region.

Figure 4-4 shows the hardware testbed for short circuit evaluation experiments under different short circuit conditions. The gate signal generation board provides the gate signals for DUT, series and control switches. DUT is driven by a high-speed, high-current gate driver IXDN409 from IXYS. Bulk capacitor should be placed close to DUT to minimize ringing during short circuit transients. The collector current is monitored with a shunt resistor of 0.015 Ω with high bandwidth.

DUT is connected to the hot plate through the copper connector with the case temperature monitored by thermal couples. In real applications, IGBTs are attached to the heat-sink with air or liquid cooling. However, these cooling conditions can be ignored for the short circuit analysis which happens within sub-milliseconds. It is because low thermal conductivity of the thick solder is reported to take at least 500 μs until the heat sink fin works effectively to cool the silicon die. Some glass wools fill the gap between circuit board and hot plate to keep the board temperature below 50 ˚C.

With the proposed circuit and hardware setup, the high temperature short circuit capability of Si IGBT is fully evaluated under different conditions with respect to different failure mechanisms.

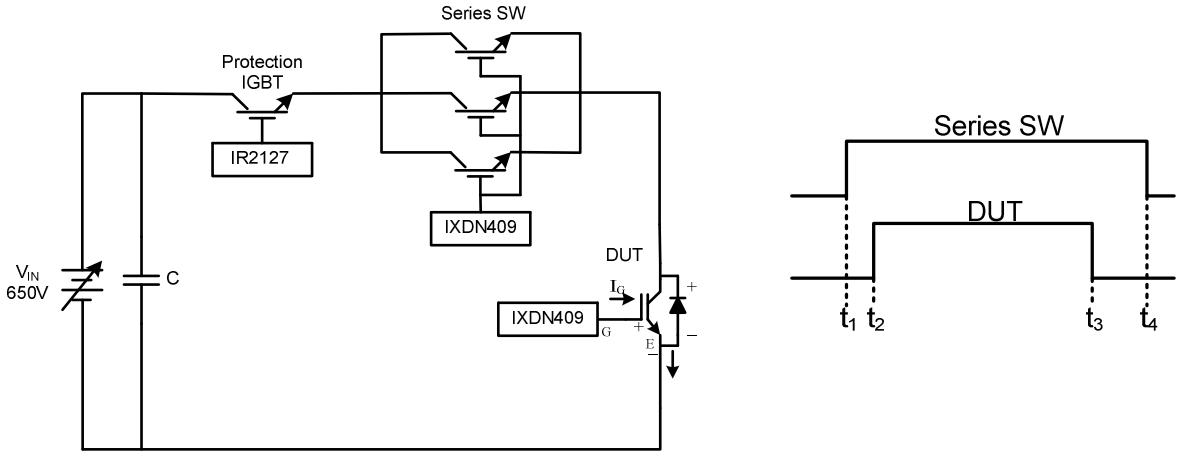

(a) Circuit schematic and gate signal for short circuit evaluation in hard switching fault condition

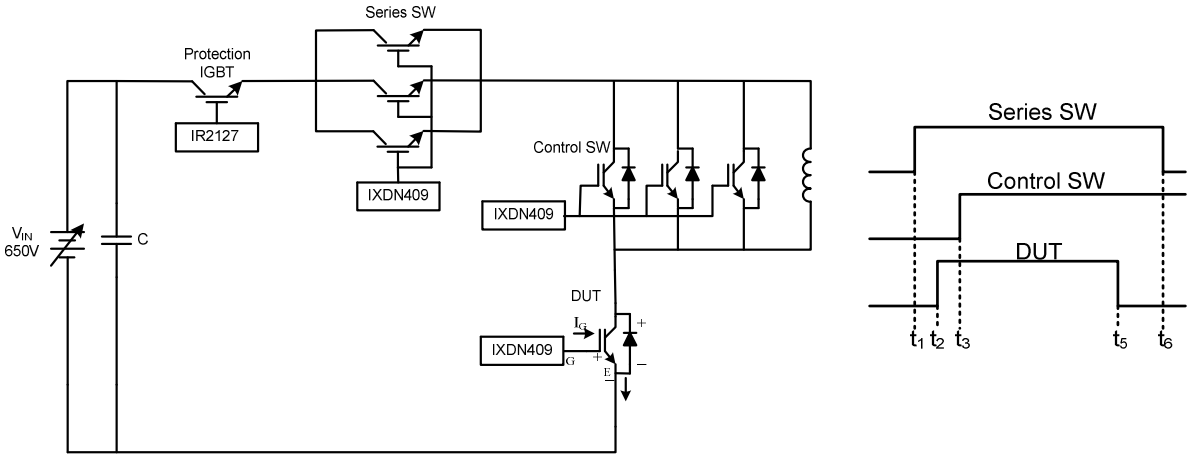

(b) Circuit schematic and gate signal for short circuit evaluation in fault under load condition

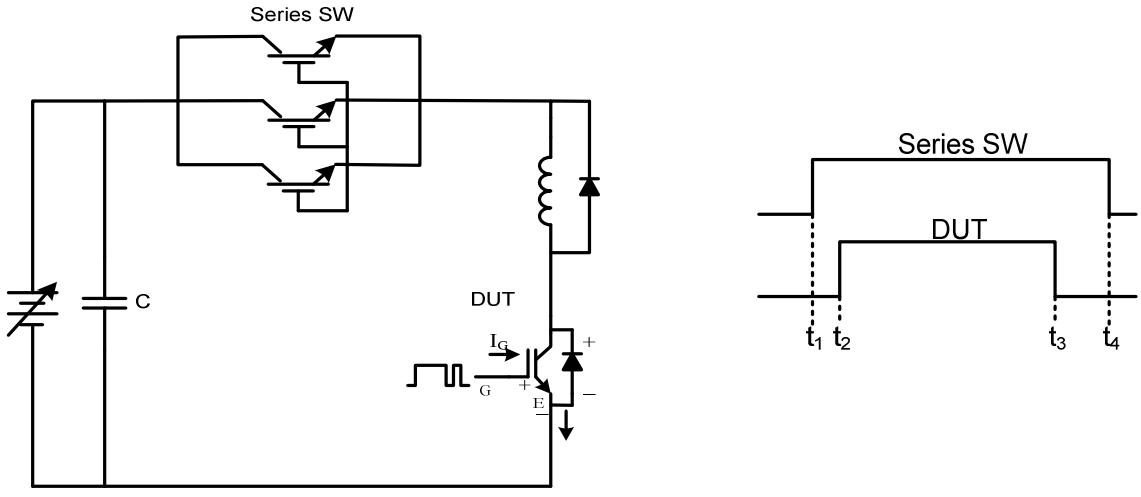

(c) Circuit schematic and gate signal for testing short circuit through large inductance

Figure 4-3. Circuit schematic and gate signal for evaluation of different types of short circuit conditions.

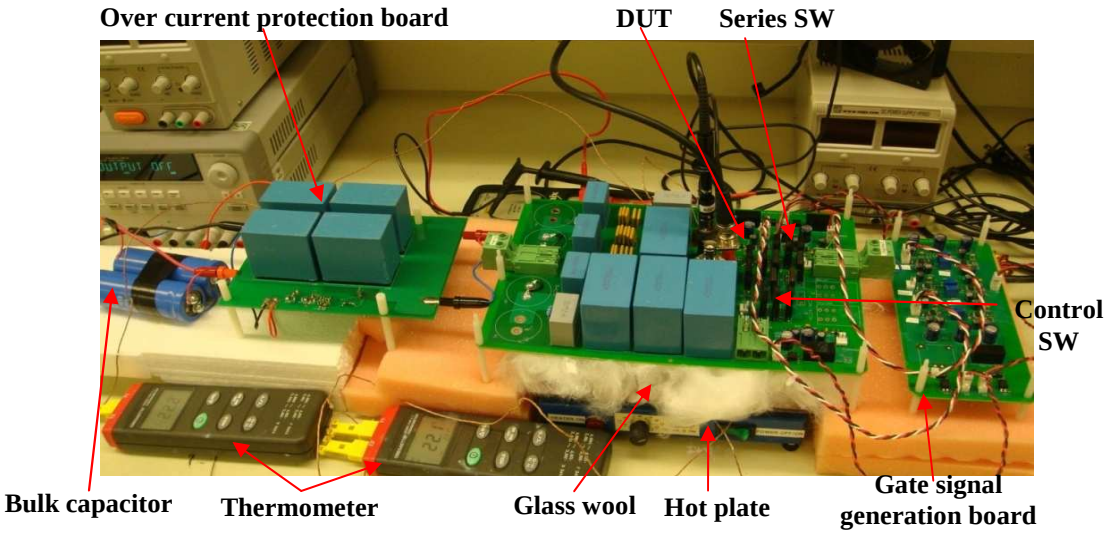

Figure 4-4. Hardware testbed for short circuit capability evaluation.

4.2.2 Short Circuit Failure by Thermal Destruction

During a short circuit, IGBT has to sustain both high voltage and high current at the same time, which can cause a significant increase in the localized device temperature from the high power dissipation. High localized temperature beyond a critical value abates the devices' capability to sustain the collector-emitter voltage and can cause the destruction of the device.

When operating at high temperatures, the short circuit energy as well as short circuit withstand time are reduced due to the higher initial temperature. IGBT manufacturers generally guarantee 10 μs of the short circuit withstand time below the maximum junction temperature. For operation of IGBT at the elevated temperature of 200 ˚C, short circuit ruggedness needs experimental evaluation.

In the experiment, DUT is under short circuit condition until thermal destruction. The measuring conditions are: gate-emitter voltage V_{GE}=15 V/0 V, gate resistance R_G=12 Ω, dc voltage V_{DC}=650 V, junction temperature T_j=25 ˚C /200 ˚C.

Figure 4-5 shows the short circuit failure by thermal destruction at 25 ˚C under short circuit through inductance, HSF and FUL conditions respectively. In Figure 4-5 (a), at t_1, dc bus voltage is applied to DUT by turning on series IGBTs. After DUT is turned on at t_2, the collector current ramps up at a rate of V_{dc}/L until the device reaches the active region at t_3, when the current reaches a peak of 162 A, which is about four times of its rated current. After t_3, the current gradually decreases with time. This is because the short-circuit energy consumption in the device increases the device temperature as well as the MOS-channel resistance. At t_4, the device is thermally damaged and can no longer sustain the voltage. The current continue to rises up as the inductor is charged by dc bus voltage. The series IGBTs are turned off after 40 μs to disconnect the dc bus voltage. Here the short circuit withstand time (SCWT) is calculated from t_3 to t_4 in a conservative way.

In Figure 4-5 (b), a hard switching short circuit fault occurs at t_2 and DUT enters active region quickly. The current reaches a peak of 162 A and then gradually decreases with time until it is thermally damaged at t_3. After that, since the current is only limited by stray inductance in the loop, it goes up very quickly. The high current activates the protection IGBT, which is then turned off and disconnects dc power supply at t_4.

In Figure 4-5 (c), at t_2, DUT is turned on and goes into normal conduction. At t_3, the control IGBT is turned on and shorts the inductor, which makes a fault under load to DUT. The collector to emitter voltage of DUT increases quickly, which boost the gate voltage through miller capacitance and further increase the short circuit current. The peak current reaches 175 A. Then DUT is destructed by thermal at t_4 and dc bus voltage is removed at t_5.

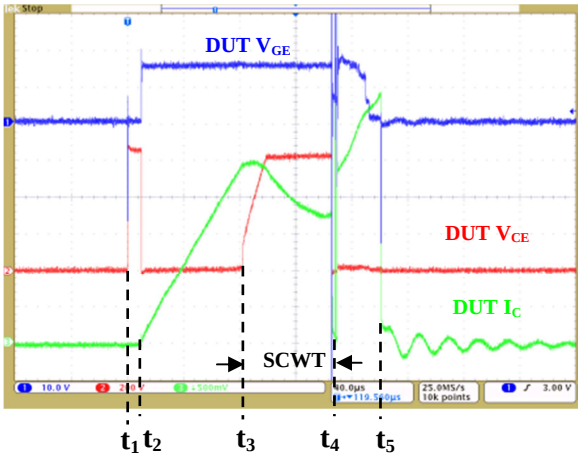

(a) Short circuit through large inductance

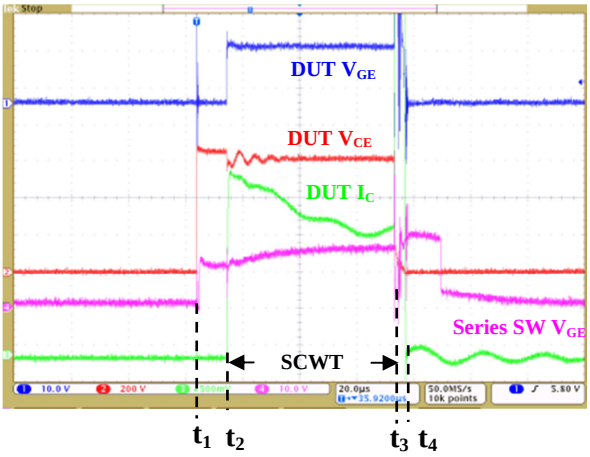

(b) HSF

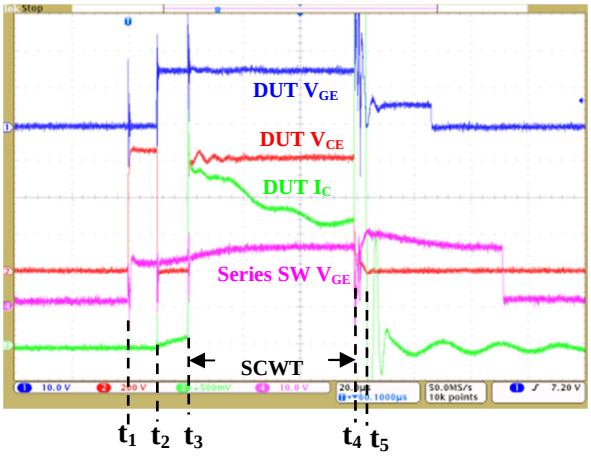

(c) FUL

Figure 4-5. Short circuit failure by thermal destruction at 25 ˚C.

When operating at high temperatures, it has smaller short circuit peak current. However, due to the higher initial temperature, the short circuit energy as well as short circuit withstand time are reduced. Figure 4-6 shows the short circuit failure by thermal destruction at 200 ˚C in different short circuit conditions. Take HSF for example, the peak current is 125 A at 200 ˚C compared with 162 A at 25 ˚C. The SCWT is reduced to 54 μs at 200 ˚C compared with 58 μs at 25 ˚C. The short circuit withstand time in different conditions at both 25 ˚C and 200 ˚C are listed in Table 4-1.

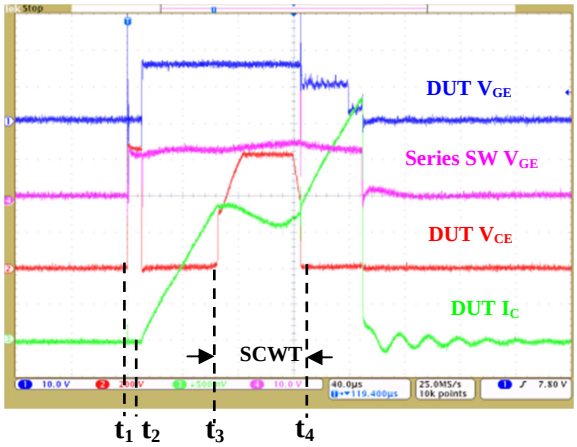

(a) Short circuit through large inductance

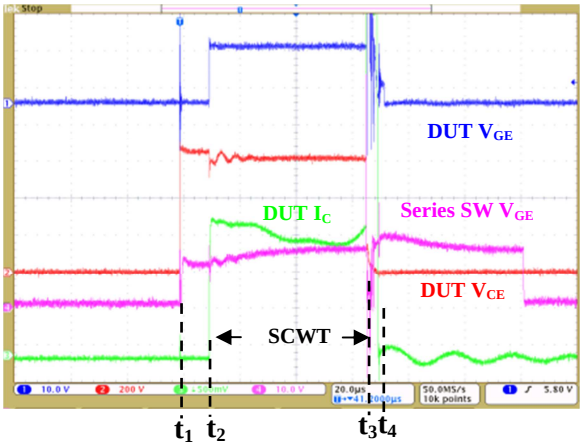

(b) HSF

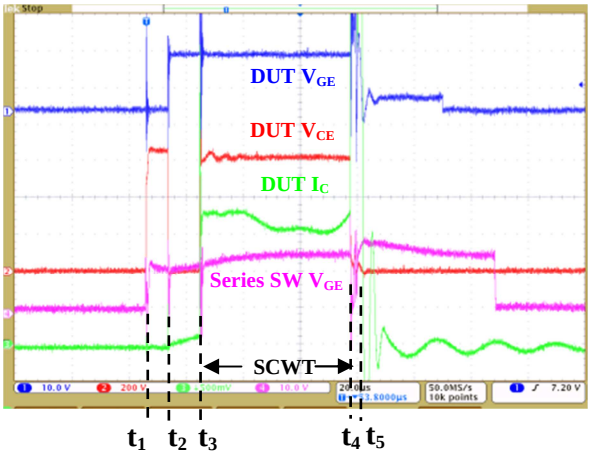

(c) FUL

Figure 4-6. Short circuit failure by thermal destruction at 200 ˚C.

Table 4-1 Short Circuit Withstand Time in Different Conditions at 25 ˚C / 200 ˚C

Short circuit withstand time (μs)		Temperature	
		25 ºC	200 ºC
Types of short circuit fault	Short circuit through large inductance	62 μs	54 μs
	Hard switching fault	58 μs	54 μs
	Fault under load	58 μs	52 μs

After the destructive tests, each time the impedance between the DUT pins after destruction are measured. The typical value is shown below: R_{GE}=7.5 Ω, R_{GC}=7.5 Ω and R_{CE}=0.3 Ω. It shows that device failure is not caused from the wire lifting-off from over conduction current.

4.2.3 Short Circuit Failure by Thermal Runaway

Besides the destruction due to over energy consumption, it is reported that field-stop IGBTs exhibit a peculiar failure mechanism, further limiting the critical short circuit energy and withstand time. The destruction of IGBT is observed during the blocking state after a few hundred microseconds of the short-circuit turn-off condition.

During the short circuit, the p-well/n-drift junction has the hottest region, where it has the highest electric field as well as the largest local current density. The backside region has less electric heat generation because of the lower electric field. After short circuit turn-off, however, the heat flow from the device surface is propagated through the bulk and causes the temperature rise as well as large leakage current in the backside layers, as shown in Figure 4-7. When the heat generation produced by high temperature leakage current exceeds a critical value, the device is destroyed by thermal runaway even though it is turned off.

Since field-stop IGBT has smaller silicon volume as well as heat capacity compared to other structures, it has a higher device temperature after the turn-off with the same short circuit energy and tends to have such kind of short circuit failure more easily.

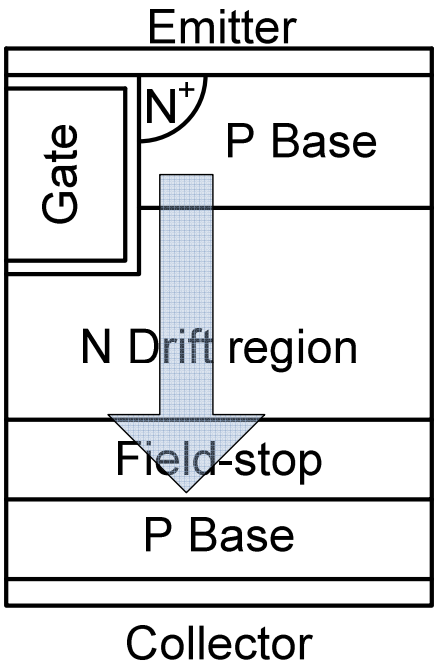

Figure 4-7. Heat spreading in FS-IGBT after short circuit turn-off.

Experiments are conducted with the proposed test circuits. The test conditions are: gate-emitter voltage V_{GE}=15 V/0 V, gate resistance R_G=12 Ω, dc bus voltage V_{DC}=650 V, junction temperature T_j=25 ˚C / 200 ˚C. Figure 4-8 shows the measured results of the short circuit waveforms in hard switching fault condition at 25 ˚C. In Figure 4-8 (a), the short circuit pulse is 32 μs. The device is turned off safely without any destruction. In Figure 4-8 (b), the short circuit pulse is extended to 38 μs. The device looks as if it has safely turned-off but destruction happens at 86 μs after turn-off. The device cannot sustain the dc bus voltage and current increases quickly. The large current activates the protection IGBT, which opens the short circuit loop soon to prevent the test circuit from being damaged.

The critical short circuit time can be defined by conditions where the maximum pulse width is applied under a dc bus voltage of 650 V, with a gate-driving voltage of 15 V until device failure occurs. The critical short circuit time is reduced when operating at high temperatures.

Figure 4-9 shows the measured results of the short circuit waveforms in hard switching fault condition at 200 ˚C. The critical short circuit time is reduced to 22 μs. When short circuit happens through high inductance or in fault under load condition, similar failures due to thermal runaway are observed once the applied short circuit pulse time exceeds the critical time, as shown in Figure 4-10.

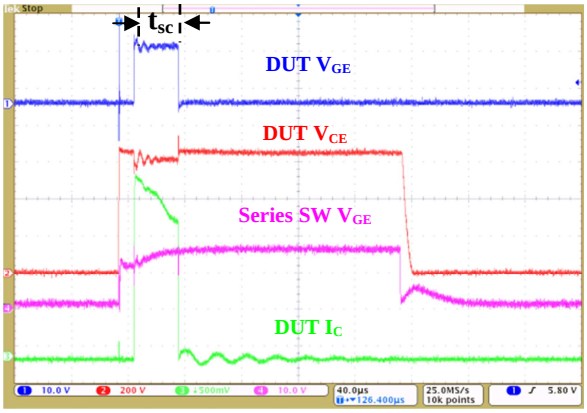

(a) IGBT is turned off safely when short circuit pulse of 32 μs is applied at 25 ˚C.

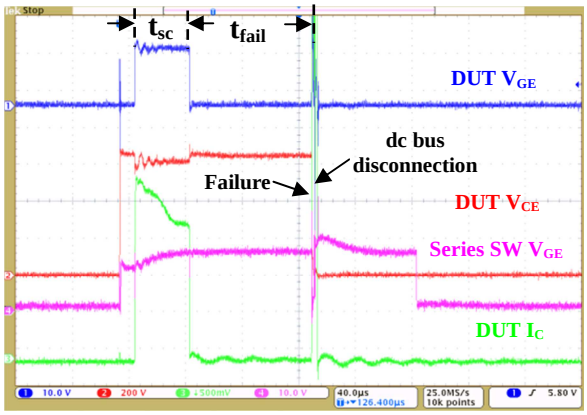

(b) IGBT is destructed at 86 μs after turn-off. The short circuit pulse of 38 μs is destructed at 25 ˚C.

Figure 4-8. Short circuit failure by thermal runaway in HSF condition at 25 ˚C.

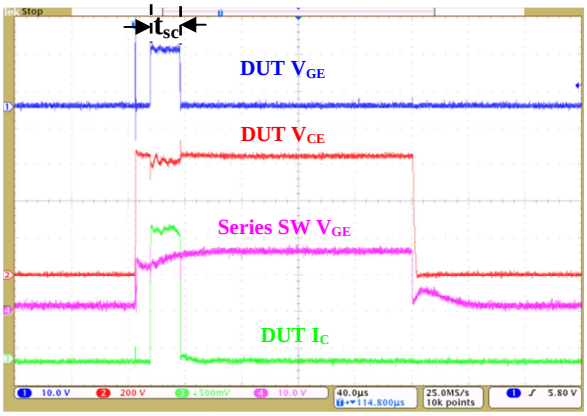

(a) IGBT is turned off safely when short circuit pulse of 22 μs is applied at 200 ˚C.

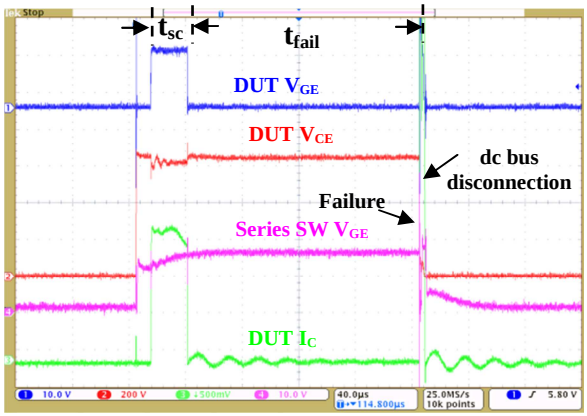

(b) IGBT is destructed at 164 μs after turn-off. The short circuit pulse of 25 μs is destructed at 200 ˚C.

Figure 4-9. Short circuit failure by thermal runaway in HSF condition at 200 ˚C.

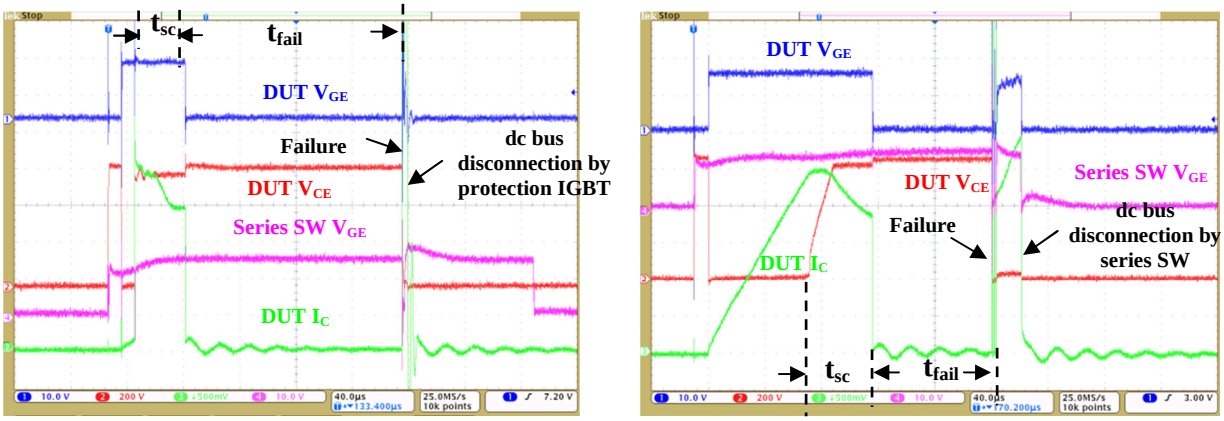

(a) Short circuit failure in FUL condition. IGBT is destructed at 152 μs after turn-off. The short circuit pulse of 36 μs is destructed at 25 ˚C.

(b) Short circuit failure through large inductance. IGBT is destructed at 84 μs after turn-off. The short circuit pulse of 44 μs is destructed at 25 ˚C.

Figure 4-10. Short circuit failure by thermal runaway through large inductance and in FUL condition at 25˚C.

Experimental results show that the 1200 V / 40 A field-stop IGBT has the short circuit failure by the thermal run-away during the off state due to the high temperature leakage current caused by heat spreading after short circuit turn-off. IGBT should be turned off within the critical short circuit time in order to prevent it from destruction. Table 4-2 lists the critical short circuit time in different short circuit conditions at various temperatures. The experimental results show that FUL is the worst case, the critical short circuit time of which at 200 ˚C is about 65 % of that at 25 ˚C. However, it is still adequate for protection.

Table 4-2 Critical Short Circuit Time in Different Conditions at 25 ˚C /200 ˚C

Critical short circuit time (μs)		Temperature	
		25 ˚C	200 ˚C
Types of short circuit fault	Short circuit through large inductance	36 μs	28 μs
	Hard switching fault	32 μs	22 μs
	Fault under load	32 μs	21 μs

4.3 Latch-up Immunity

Latch-up means IGBT is tied to a state of continuous current conduction and gate voltage has no influence on output collector current. It is reported that turning the gate off before the device voltage rises completely to the clamped value could lead to the destruction of IGBT due to latch-up [77]. After the device is turned on, the current through the device ramps up. Once the gate is turned off, flow of electrons through the channel is cut off. Holes continue to inject from IGBT collector. This process stops when electrons in IGBT N-base are depleted. At this point IGBT current is almost all hole current. Large number of holes flow under the N-base region. If the IGBT does not reach the clamp voltage, the IGBT can latch up and fail.

At high temperature operation, the latch-up current is decreased because the current gains of the NPN and PNP transistors increase. The effect is further aggravated by an increase in the resistance of the P base region due to the mobility reduction. Also, the turn-off speeds have influence on the latching phenomenon. If the turn-off process is slowed down, a major fraction of inrushing holes will recombine in the drift zone and reduce the chance of latching.

For today's commercial IGBTs, they have good latch-up immunity with latch-up suppressed designs, which employ the heavily doped P-base region underneath the N-emitter structure, sufficient emitter ballast resistance, or optimized bipolar current gain. The trench-gate IGBT structure further improves the latching current capability in comparison with the conventional IGBT [78]. In conventional structure, the hole current mainly flow horizontally underneath the N-emitter, which causes a potential voltage drop and latch-up. In trench-gate IGBT, the hole current flows vertically. By using a shallow P+ region with proper ratios of the trench and diffusion regions, the device becomes more latchup-resistant.

The test circuit for latch-up immunity evaluation is similar to that of short circuit capability evaluation under large inductance, as shown in Figure 4-3 (c). The experiment is conducted to evaluate the latch-up immunity of the IGBT at various temperatures. The test conditions are: gate-emitter voltage V_{GE}=15 V / 0 V, gate resistance R_G=12 Ω, junction temperature T_j=25 ˚C / 200 ˚C. In Figure 4-11, after the IGBT is turned on at t_2, the current increases. At t_3, the IGBT has just entered the active region and collector current is 165 A at 25 ˚C and 122 A at 200 ˚C. At the time the gate signal is brought down to zero abruptly right before the voltage reaches the clamped value. The IGBT is turned off safely without latch-up either at 25 ˚C and 200 ˚C.

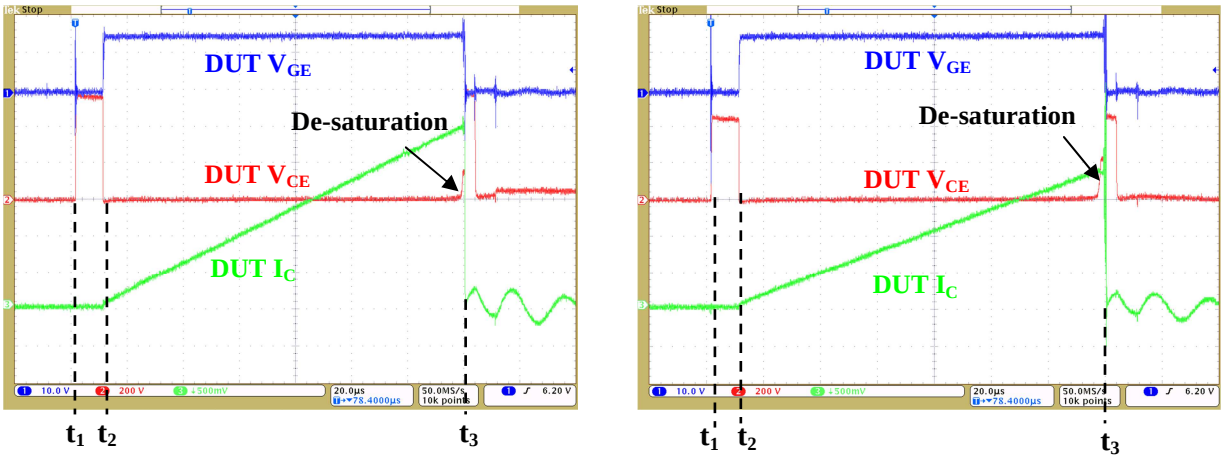

(a) Latch-up immunity evaluation at 25 ˚C (b) Latch-up immunity evaluation at 200 ˚C

Figure 4-11. Latch-up immunity evaluation at 25 ˚C and 200 ˚C.

The evaluation is then conducted in extreme conditions: The gate voltage V_{GE} is increased to from 15 V to 30 V to prevent the IGBT from de-saturation at a low current level. The gate resistance is reduced from 12 Ω to 3 Ω to increase the turn-off speed. Also the ambient temperature is increased to 250 ˚C. In Figure 4-12 (a), it is shown that IGBT turned off the current of 300A with a small gate resistance (3 Ω) at 250 ˚C. The turn off transients is zoomed in and shown in Figure 4-12 (b). Figure 4-12 (c) shows the corresponding switching locus of the

turn-off transients compared with the SOA defined in the datasheet. From the experimental results, it is demonstrated that the IGBT shows very good latch-up immunity even at very high temperatures.

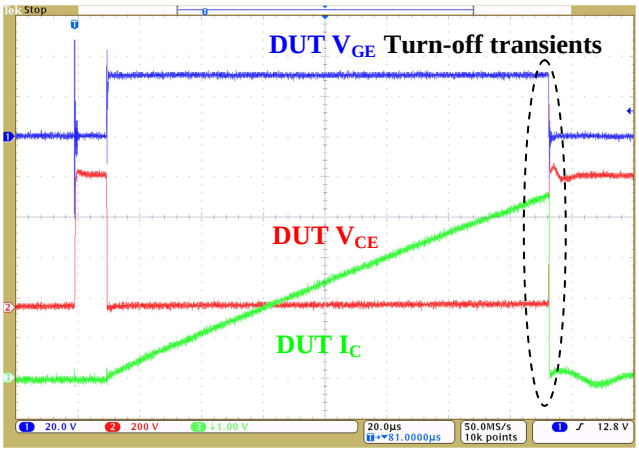

(a) Switching waveforms of V_{GE}, V_{CE} and I_C in latch-up evaluation

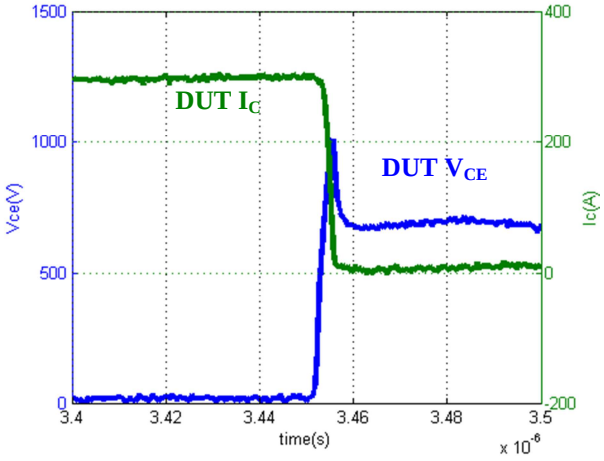

(b) Waveforms of V_{CE} and I_C in turn-off transients in latch-up evaluation

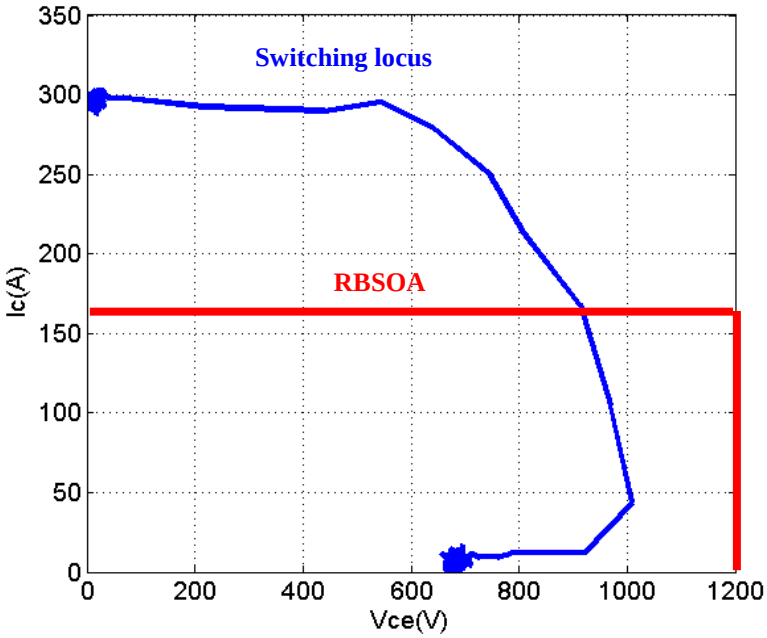

(c) Switching locus of turn-off transient in latch-up evaluation

Figure 4-12. Latch-up immunity evaluation in extreme conditions: gate voltage V_{GE}=30V, gate resistance R_G=3 Ω, ambient temperature T=250 ˚C.

4.4 Avalanche Capability

During turn-off transients of IGBT, the high di/dt causes the voltage spike resulting from the parasitic inductance, which could subject the IGBT to overvoltage stress. In this section, the IGBT turn-off capability is evaluated at various temperatures up to 200 ˚C as the guidance for practical applications.

A large stray inductance of 1.25 μH is employed in the circuit. When the gate voltage of the DUT is turned off, the current begins to commutate from the DUT to the upper diode. The decreasing current in the stray inductance causes a voltage spike. Figure 4-13 shows the turn-off transients of the DUT with various dc bus voltages. The dc bus voltage V_{DC} is increased from 600 V to 850 V in the increment of 50 V while the current I_C is kept at 40 A. In normal conditions, the voltage spike increases with higher dc bus voltage. In Figure 4-13, however, it is observed that the voltage spike of V_{CE} is suppressed to 1350 V when various dc bus voltages are applied, which means DUT enters the avalanche sustaining mode. With V_{DC} increasing, the avalanche sustaining time increases until DUT fails.

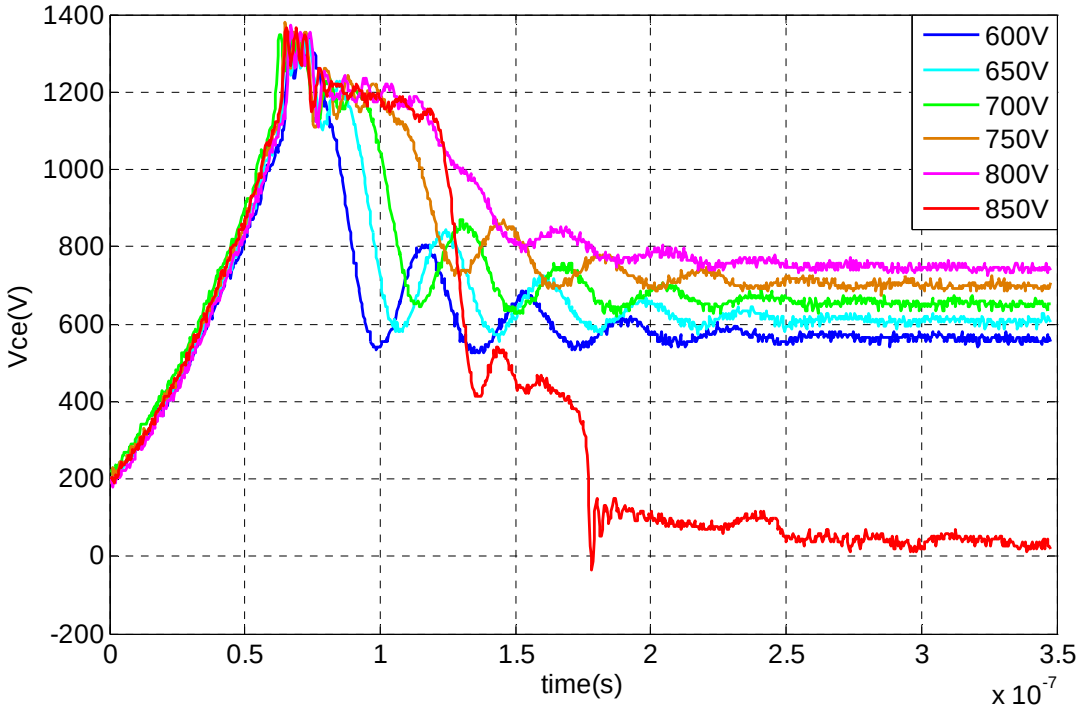

Figure 4-13. V_{CE} voltage at turn-off with various V_{DC} applied when IGBT enters the dynamic avalanche mode at 25 ˚C.

Figure 4-14 shows the safe and failed turn-off transition at 25 ˚C with the dc bus voltage at 800V and 850V respectively. In Figure 4-14 (a), after the turn-off gate voltage is applied, V_{CE} starts rising up and then enters the avalanche sustaining mode. The stressful condition finishes when I_C decreases to zero and all the energy stored in the stray inductance is transferred to DUT. Then V_{CE} falls to the dc bus voltage and DUT is turned off safely. In Figure 4-14 (b), V_{CE} is not sustained at V_{DC} after the voltage spike and collapses to zero. DUT is damaged and loses its dc blocking capability. The avalanche sustaining time is 70 ns at 25 ˚C, which is defined as the period from the time when the avalanche starts to the time when voltage collapses.

The avalanche capability of DUT is further evaluated at 200 ˚C, as shown in Figure 4-15. The avalanche sustaining time is reduced to 35 ns. The shortened failure time occurs due to the elevated temperature before self-heating begins. However, it is also observed that the turn-off

speed is slowed down at high temperature and delays the avalanche. As a result, the IGBT can still be turned off with V_{DC} at 800V at 200 ˚C.

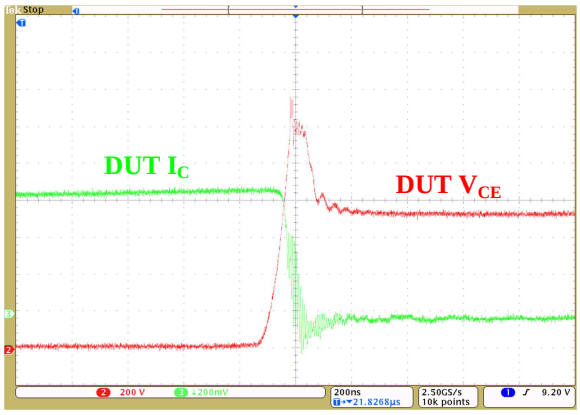

(a) Safe turn-off transition when V_{DC}=800 V, I_C=40 A

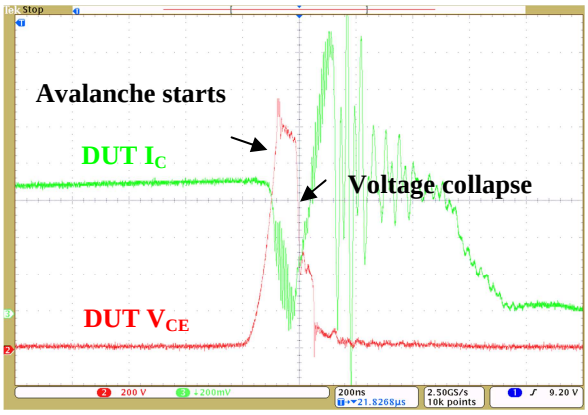

(b) Failed turn-off transition when V_{DC}=850 V, I_C=40 A

Figure 4-14. Safe and failed turn-off transition at 25 ˚C in clamping inductive test.

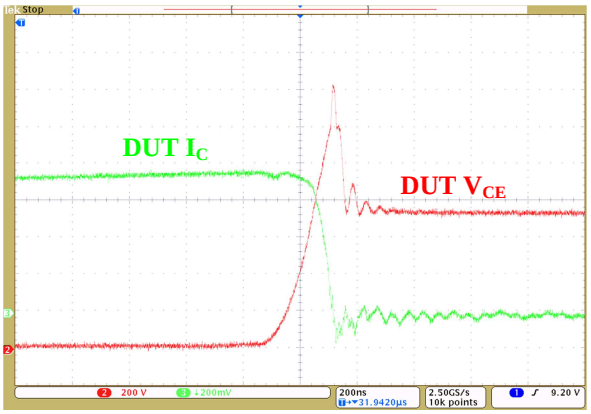

(a) Safe turn-off transition when V_{DC}=800 V, I_C=40 A

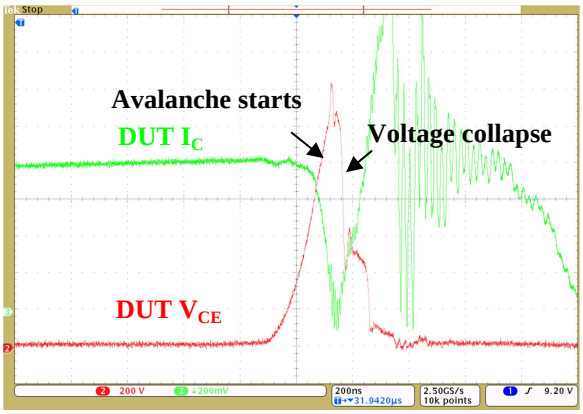

(b) Failed turn-off transition when V_{DC}=850 V, I_C=40 A

Figure 4-15. Safe and failed turn-off transition at 200 ˚C in clamping inductive test.

The experimental results show that the 1200 V IGBT can be turned off safely in the wide temperature range from 25˚C to 200 ˚C as long as it is not operated exceeding the rated voltage. However, it has limited avalanche capability and cannot be subjected to the over voltage stress.

Some IGBTs, mostly low-voltage IGBTs, have improved avalanche capability and offer certain circuit design advantages. The ruggedness of a 600 V/6.3 A IGBT from IXYS

(IRG4IBC20KDPbF) is evaluated in the unclamped inductive switching (UIS) test with an inductive load of 500 μH. The test conditions are: gate-emitter voltage V_{GE}=15 V/0 V, gate resistance R_G=12 Ω, dc bus voltage V_{DC}=300V, collector current I_C=10A, junction temperature T_j=25 ˚C /200 ˚C.

The experimental waveforms are shown in Figure 4-16. When IGBT is turned off, the collector to emitter voltage VCE of DUT is driven to a high value by the inductor. DUT enters the avalanche-sustaining mode until it fails. At 25 ˚C, the voltage is clamped at 720 V and IGBT sustains in the avalanche mode for 7 μs. At 200 ˚C, the voltage is clamped at 600 V and IGBT sustains in the avalanche mode for 1.5 μs. The avalanche sustaining time as well as the energy dissipated during the sustaining time is considerably reduced at 200 ˚C.

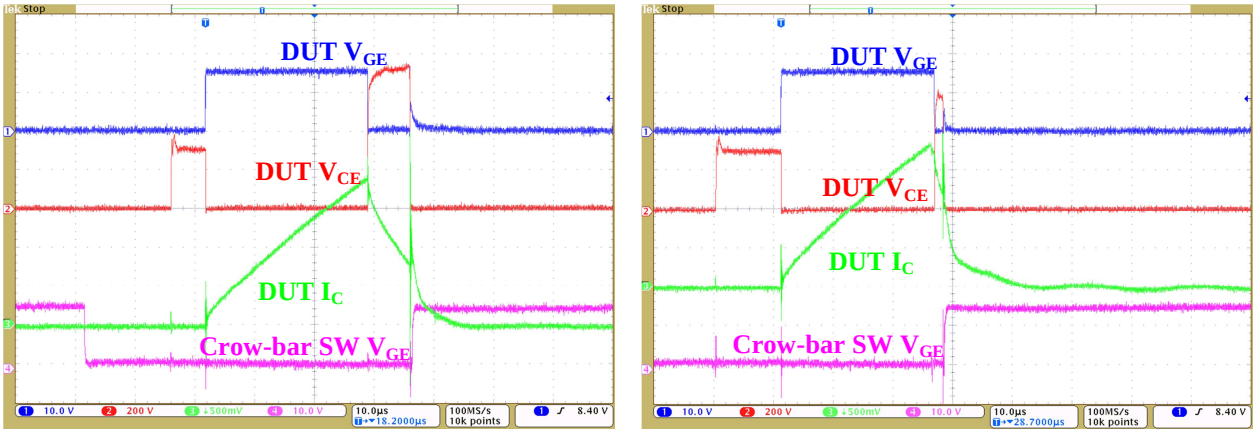

(a) UIS test at 25 ˚C (b) UIS test at 200 ˚C

Figure 4-16. Unclamped inductive switching tests of 600V IXYS IGBT at 25 ˚C and 200 ˚C.

In conclusion, the 1200 V IGBTs under test have very limited avalanche capability. It is critical that the turn-off spike voltage is below the rated voltage, especially for severe conditions such as the turn-off after the short circuit occurs. If necessary, some external overvoltage protections are needed such as voltage clamps, snubbers and gate-controlled soft turn-off. For those IGBTs with avalanche capability, they give the users the freedom in designing the systems

without external voltage clampers or leaving less voltage margin. However, it should be noted in the design that the avalanche capability is considerably reduced at high temperatures.

4.5 Summary

This chapter provides a comprehensive evaluation of Si IGBT ruggedness at high temperature operation through experiments. The IGBT shows very good latch-up immunity even at very high temperatures. The short circuit capability is decreased at high temperatures, but it is still adequate for protection. The critical short circuit time is given at 200 ˚C within which the IGBT should be turned off in order to prevent it from destruction. The IGBT can be turned off safely in the wide temperature range from 25˚C to 200 ˚C as long as it is not operated exceeding the rated voltage. However, it has limited avalanche capability and cannot be subjected to the over voltage stress. The important criteria considering latch-up immunity, short circuit capability and avalanche capability are given to ensure the safe and reliable operation of Si IGBTs at 200˚C.

Chapter 5. Si IGBT High Temperature Phase-leg Module Development

In this chapter, a Si IGBT phase-leg module is developed for operating at 200 ˚C in HEV applications utilizing the high temperature packaging technologies and appropriate thermal management. A 10 kW buck converter composed of this module assembly is built and operated at the junction temperature up to 200 ˚C. The experimental results demonstrate the feasibility of operating Si devices based converters continuously at 200 ˚C. The chapter is organized as follows: Section 5.2 presents the design and electrical characterization of the high temperature power module. Section 5.3 shows the thermal management design and thermal performance evaluation with experiments. Section 5.4 provides the experimental results of the module operating continuously at 200 ˚C. Conclusions are drawn in Section 5.5.

5.1 Introduction

The challenging thermal environment in HEVs as well as the aggressive power density and cost targets established by industry and government makes the high temperature operation of power electronics devices desirable.

Up to date, some papers have developed the power converters for operating above the junction temperature of 200 ˚C, all with SiC devices [44]-[58]. The design of 250 ˚C phase-leg power modules utilizing paralleled SiC power JFET devices is reported in [44]-[53]. In [54]-[56], a power module that integrates SiC power JFETs with silicon-on-insulator (SOI) control electronics is developed. The SiC three-phase inverter is tested to 4 kW with the estimated junction temperature of 300 ˚C. However, these converters are operated without the measurement of junction temperatures. Most of them are operated with the case temperature

monitored by the integrated thermocouples, while a few of them obtain the junction temperature estimated by case temperature and thermal simulation [53]. The missing or inaccurate information of junction temperatures limit the pushing of power rating of the converters because more safety margin is needed.

Considering the rising cost imposed by these newly developed techniques, it is meaningful to investigate the prospects for extending Si device junction temperatures to 200 ˚C as a lower-cost solution.

In chapter 3 and 4, it is demonstrated that Si trench-gate field-stop IGBT can successfully operate in the pulse test at the extended temperature of 200 ˚C with elevated but acceptable losses and adequate ruggedness. The continuous operation of Si device based converters at the junction temperature of 200 ˚C need to be evaluated through experiments to further investigate the feasibility of Si IGBT operating at high temperatures.

Further the past work, the objective of this chapter is to determine the feasibility of operating Si devices based converters continuously at 200 ˚C and to take full advantage of the converter high temperature operation through measurement of the device junction temperature. Specifically, a 200 ˚C Si IGBT phase-leg module has been developed utilizing the high temperature packaging technologies and appropriate thermal management. Both electrical and thermal performance is characterized through experiments. The switching time is employed as the TSEP for junction temperature measurement. A 10 kW buck converter composed of the phase-leg module is operated successfully with the device junction temperature heated up to 200 ˚C, which demonstrates the high temperature capability of the designed package module. The design approach as well as the test procedure presented in this paper can be used as the guideline for the high-temperature operation of Si converters.

5.2 Phase-leg Module Design and Characterization

5.2.1 Module Design and Fabrication

The presented high temperature phase-leg power module utilizes Si IGBTs and diodes, and is designed for multi-kilowatts and 200 ˚C operation. Two Si IGBT and two Si diode dies from Infineon Technologies with maximum ratings of 1200 V, 50 A, 175 ˚C are employed for power switches. The conventional wire-bonding technology is adopted. The materials for each part of the package are selected for high temperature operation and listed in Table I with the corresponding dimensions. The Al_2O_3 direct bonded copper (DBC) is used as the substrate, and the finishing metallization of electroplated Ag is added to prevent the oxidation of the bare copper. The die attachment material is Au80Sn20 solder with the preferred thickness of 200 μm and a melting temperature of 280 ˚C. Aluminum wires of 10 mils are selected for wire-bonding with a maximum current rating of 22 A for each wire [87]. To enhance reliability, copper lead frame is used as connection terminal instead of pole connection. The encapsulant of the whole module is Nusil R-2188. Figs. 1 (a) and (b) show the schematic of the phase-leg module and its layout design. The fabricated power module is shown in Fig. 1 (c).

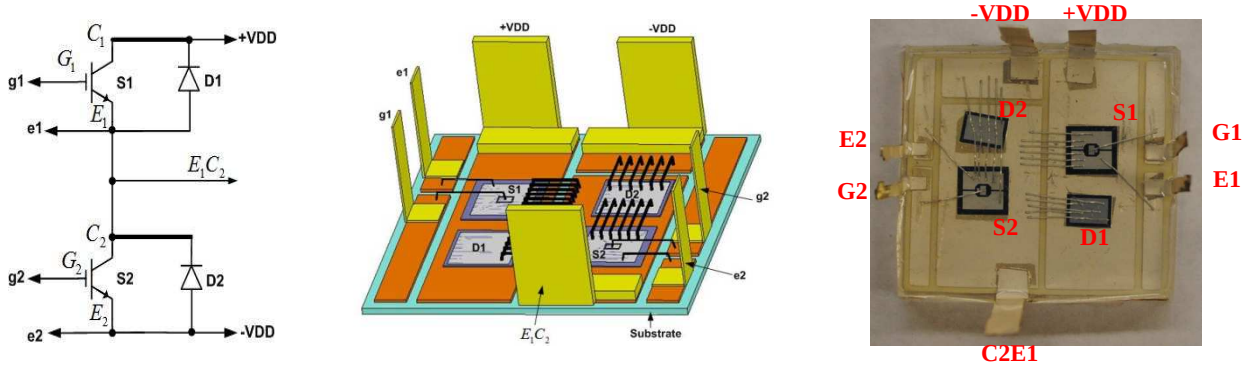

(a) Phase-leg schematic (b) Layout design (c) Fabricated power module

Figure 5-1. Design and fabrication of the high temperature phase-leg power module.

Table 5-1 Materials Selection

Component	Dimension (mm)
IGBT chip (IGC50T120T6RL)	7.25 × 6.84 × 0.115
Emitter pad	5.37 × 5.74 × 0.004
Gate pad	1.31 × 0.81 × 0.004
Diode chip (IDC28D120T6M)	6.3 × 4.5 × 0.11
Anode pad	5.35×3.55×0.004
Substrate	30.6×30× (Cu: 0.203, Al_2O_3: 0.381)
Die attachment	Solder Au80Sn20, thickness: 0.2
Aluminum wires	10 mils × 6
Encapsulant	Silicone gel (Nusil R-2188)

5.2.2 Static Characterization

The static characterization of the fabricated power module is conducted with Tektronix 371B high power curve tracer. Figure 5-2 (a) and (b) show the I-V curves of the IGBT with the typical gate voltage of 15 V and the diode at various temperatures, respectively. These I-V curves can be approximated by a linear relationship.

$$V_{CE} = I_C \cdot R_{CE} + V_t \tag{5-1}$$

$$V_F = I_F \cdot R_{AK} + V_f \tag{5-2}$$

Respectively, where R_{CE} and R_{AK} represent the on-state resistance, while V_t and V_f represent the built-in voltage drop of the IGBT and diode. Table 5-2 lists V_t, R_{CE}, V_f and R_{AK} measured at various temperatures, which determine the on-state voltage drop and thus conduction loss. As the temperature rises, the on-state resistance increases.

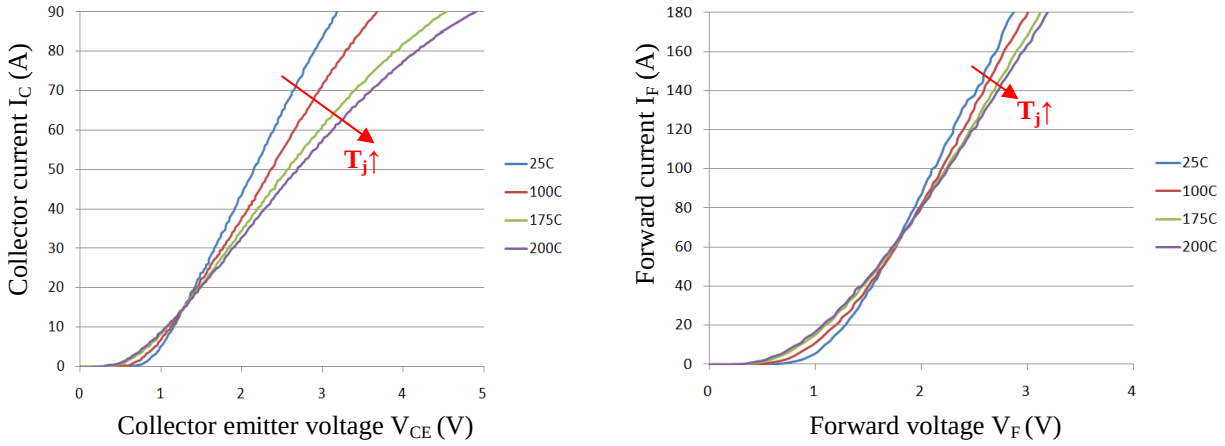

(a) Static characterization of Si IGBT in fabricated power module (V_{GE}=15V)

(b) Static characterization of Si FWD in fabricated power module

Figure 5-2. Static characterization of the fabricated power module at various temperatures.

Table 5-2 Parameters of IGBT Output Characteristics at Various Temperatures

	25 ˚C	**100 ˚C**	**175 ˚C**	**200 ˚C**
V_t	0.9 V	0.8 V	0.7 V	0.6 V
R_{CE}	33.5 mΩ	41 mΩ	53.5 mΩ	57.3 mΩ
V_f	1 V	0.9 V	0.8 V	0.7 V
R_{AK}	31 mΩ	43.5 mΩ	48.5 mΩ	53.5 mΩ

Figure 5-3 shows the leakage current of the IGBT and the anti-parallel diode at 650 V as a function of junction temperature. The leakage current increases with temperature exponentially and reaches 3.98 mA at 200 ˚C, which can be expressed in (4-3) from the curve fitting.

$$I_{leakage} = 0.912 \cdot 10^{-3} \cdot 2^{\frac{T_j - 175}{11.71}} \text{ (A)} \quad (5\text{-}3)$$

The increased leakage current at high temperature will cause loss increase and possible thermal runaway. To prevent thermal runaway up to 200 ˚C, the thermal resistance must be less than a critical one, which is the slope of the leakage current power loss curve at 200 ˚C [61]. Such curve of the IGBT in the module can be expressed in (4-4). Its critical thermal resistance is 6.5 ˚C/W, by calculation as in (4-5). This provides an important criterion in terms of thermal stability. Additionally, the critical thermal resistances versus junction temperatures are shown in

Figure 5-4. Higher operation temperature requires much smaller thermal resistance. For example the safe operation of Si devices at 225 ˚C needs thermal resistance to be less than 1.47 ˚C/W.

$$P_{leakage} = I_{leakage} \cdot V_{dc} = 0.593 \cdot 2^{\frac{T_j - 175}{11.71}} \ (\text{W}) \tag{5-4}$$

$$R_{th-crit} = 1 \Big/ \frac{d(P_{leakage})}{d(T_j)}\Big|_{T_j=200} = 6.5 \ (^{\circ}\text{C/W}) \tag{5-5}$$

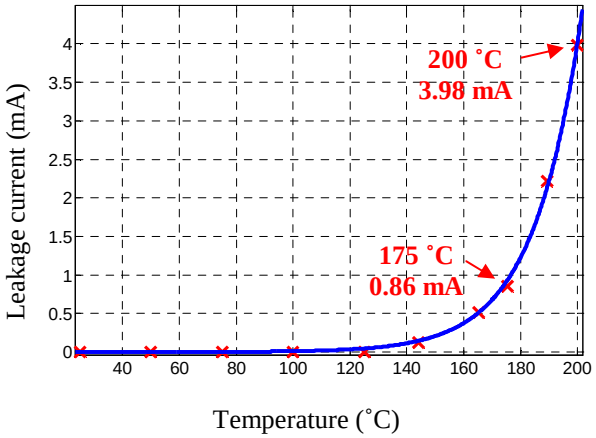

Figure 5-3. Leakage current at 650V as a function of junction temperature.

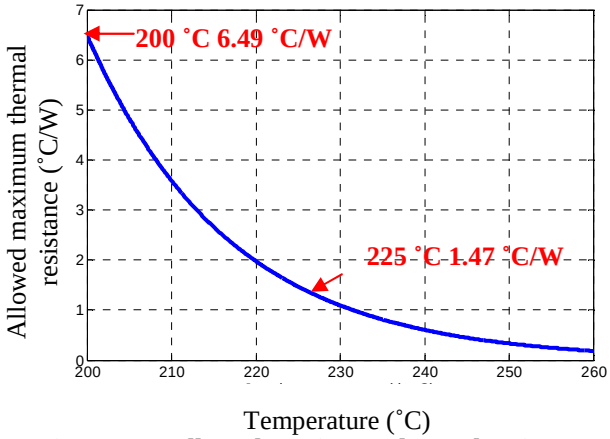

Figure 5-4. Allowed maximum thermal resistance for operation at certain temperatures.

5.2.3 Switching Characterization

The turn-on and turn-off waveforms of IGBT in module with 650 V dc voltage and 70 A load current with various temperatures are shown in Figure 5-5.

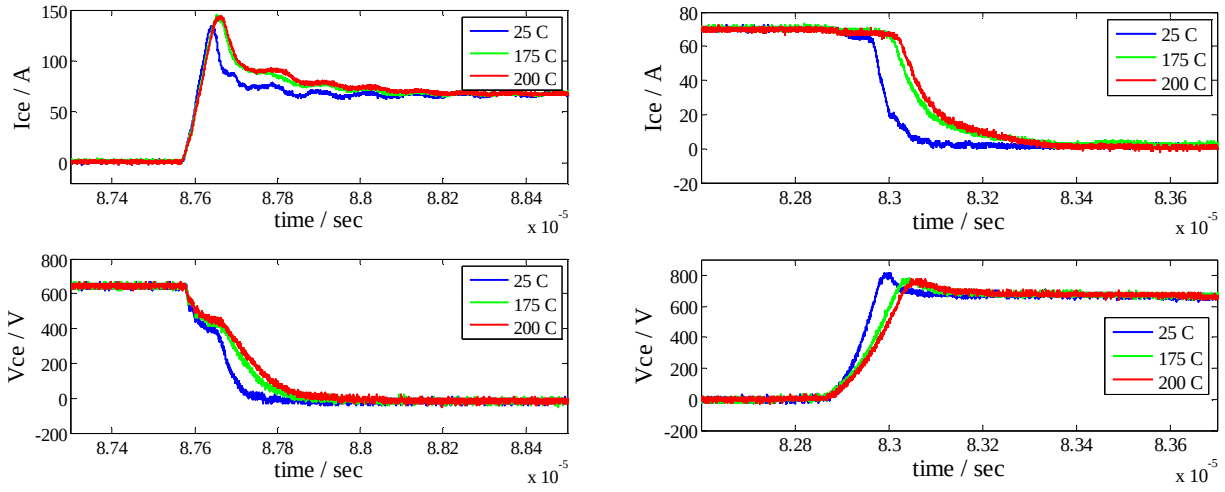

(a) turn on transients (b) turn off transients

Figure 5-5. Switching waveform comparison for designed IGBT phase-leg module.

As shown in Figure 5-5, the turn-on and the turn-off time of the designed IGBT module increase with temperature, causing more switching loss for the IGBT module at higher temperature. What is more, the reverse recovery current is also worse with higher temperature, which introduces extra losses. The loss comparison is listed in Table 5-3. The total switching loss is increased by 8.3 % at 200 ˚C compared to the rated temperature of 175 ˚C. The experimental results show that the Si devices based power module can operate successfully at 200 ˚C with increased but acceptable losses in the pulse test.

Table 5-3 Switching Loss Comparison (650 V/70 A)

Junction temperature (˚C)	IGBT turn-on loss (mJ)	IGBT turn-off loss (mJ)	Diode reverse recovery loss (mJ)
25	3.9	3.2	1.2
175	6.7	6.1	2.8
200	7.2	6.5	3.2

5.3 Thermal Management System Design and Evaluation

5.3.1 Thermal Management System Design

To keep the device junction temperature maximum to 200 ˚C and prevent thermal runaway at high temperatures, the thermal management of the module is designed. An aluminum cold plate from Aavid Thermalloy is used as the baseline design. Duralco 132 with high thermal conductivity of 69 W / (m·˚C) is selected as the thermal interface material (TIM) between the substrate of the fabricated module and the cold plate, as shown in Figure 5-6 (a). The water ethylene glycol (WEG) coolant is pumped to the cold plate with its inlet temperature regulated by the liquid chiller, as shown in Figure 5-6 (b). The coolant flow rate is 2.5 gallons per minute (GPM), which is the maximum value according to DOE specifications released in 2006.

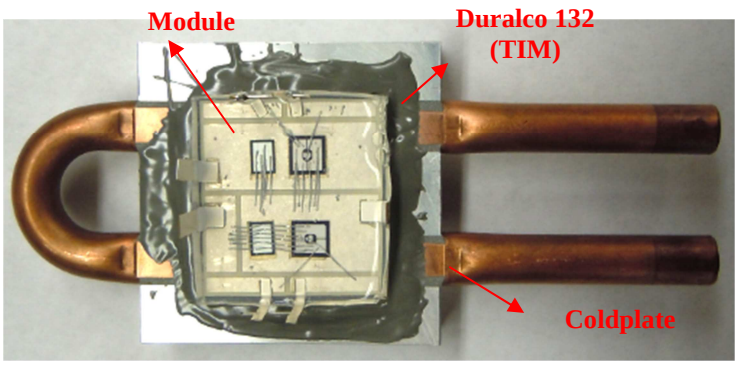

(a) Module attached to cold plate with TIM

(b) Chiller for liquid circulation and temperature regulation

Figure 5-6. Hardware setup for the thermal management system.

5.3.2 Thermal Performance Evaluation through Experiments

An electro-thermal method has been employed to measure the thermal resistance, in which the device is heated by the electric power dissipation and then its junction temperature is monitored as it cools down with power cutoff. The junction temperature is measured using

forward voltage drop $V_{CE(on)}$ as a temperature sensitive parameter, which has high temperature sensitivity, good linearity as well as the easy calibration [88].

The calibration is first conducted to determine the relationship between $V_{CE(on)}$ and the device temperature. The power module together with the cold plate is heated to various temperatures in the thermal chamber with the corresponding V_{CE} measured by the oscilloscope. Figure 5-7 shows the calibration curve representing the relationship between V_{CE} and temperatures with a current injection of 30 mA and gate to emitter voltage V_{GE} of 8 V. The curve shows a temperature sensitivity of about -2.3 mV/˚C and a good linearity at a forward current of 30 mA. The selection of the injected current value is critical, because a too low current level could results a nonlinear relationship at high temperatures and a high current level could introduce non-negligible self-heating.

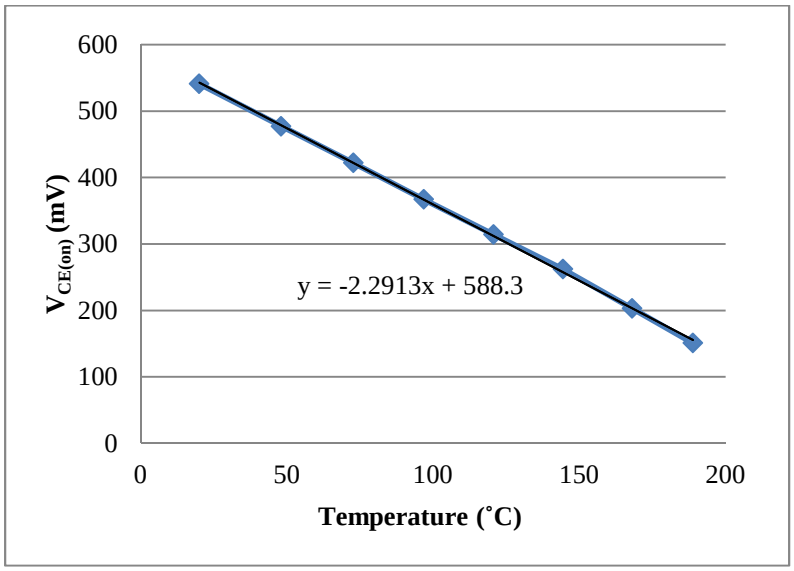

Figure 5-7. V_{CE} and T_j calibration curve (V_{GE}=8 V, I_C=30 mA).

The circuit diagram of thermal resistance measurement system is shown in Figure 5-8. First, the switch is closed so that the heating pulse is applied to the device. A few amperes source

current flows through the DUT with fixed V_{GE}, which drives the IGBT into the active region and generates the loss dissipation around 100 W in the steady state. Equilibrium has been reached when $V_{CE(on)}$ has stabilized. Then the switch is opened, and the main current I_p drops to zero. Only 30 mA measurement current is continued going through the DUT. $V_{CE(on)}$ transient is recorded. The junction temperature as well as thermal impedance can be calculated from $V_{CE(on)}$, injected power and calibration curve.

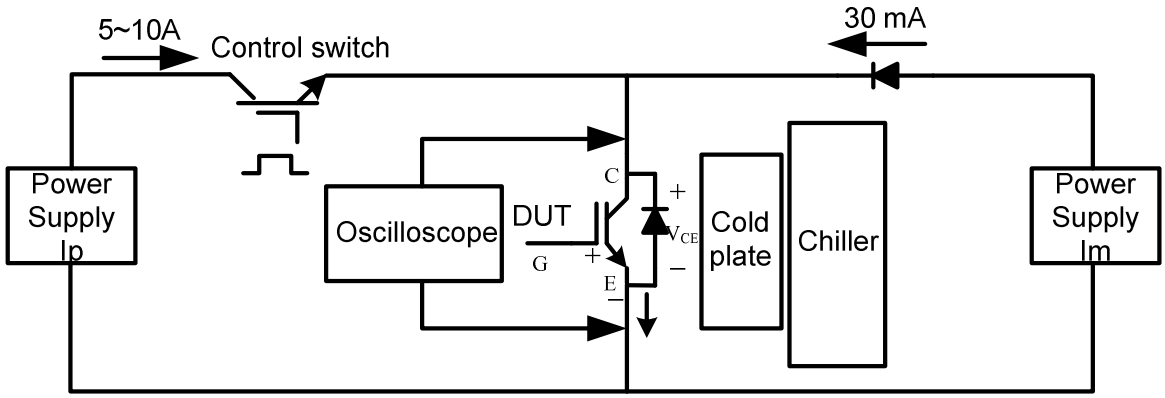

Figure 5-8. Circuit diagram for thermal performance evaluation.

Figure 5-9 shows the hardware setup for the thermal evaluation. The 10 A current source for heating is provided by TDK-Lamda power supply. The 30 mA current source comes from a current source circuit board composed of two BJTs. The cold plate is connected to the chiller for the liquid circulation.

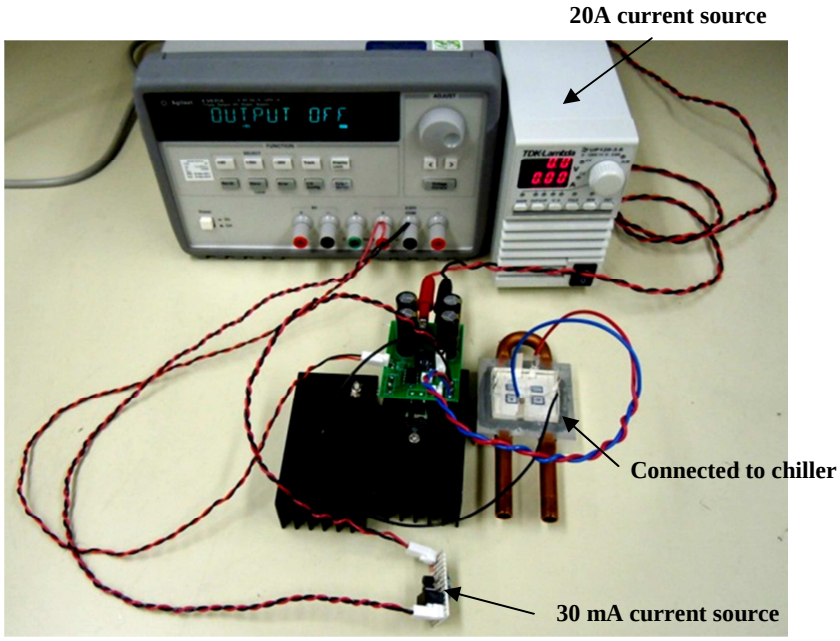

Figure 5-9. Hardware setup for thermal performance evaluation.

In the thermal evaluation experiment, the coolant temperature of 25 ˚C is used instead of 105 ˚C due to the limitations of the chiller in the lab. The heating pulse of 9.7 A is applied to the IGBT. V_{CE} of the IGBT is measured to be 11.92 V with the gate voltage of 8 V. The power loss generated by the dc current source is then calculated to be 115.6 W. Then the 9.7 A current source is disconnected and the IGBT is forward biased by a 30 mA current source. At the moment, $V_{CE(on)}$ is monitored and shown in Figure 5-10. $V_{CE(on)}$ is measured to be 125 mV at the moment the heating pulse is removed, which means the junction temperature is 193.6 ˚C based on the calibration curve. The thermal resistance from IGBT junction to ambient is 1.46 ˚C/W, which is smaller than the critical one calculated above. The designed thermal management system can support the Si power module operating at 200 ˚C without thermal runaway.

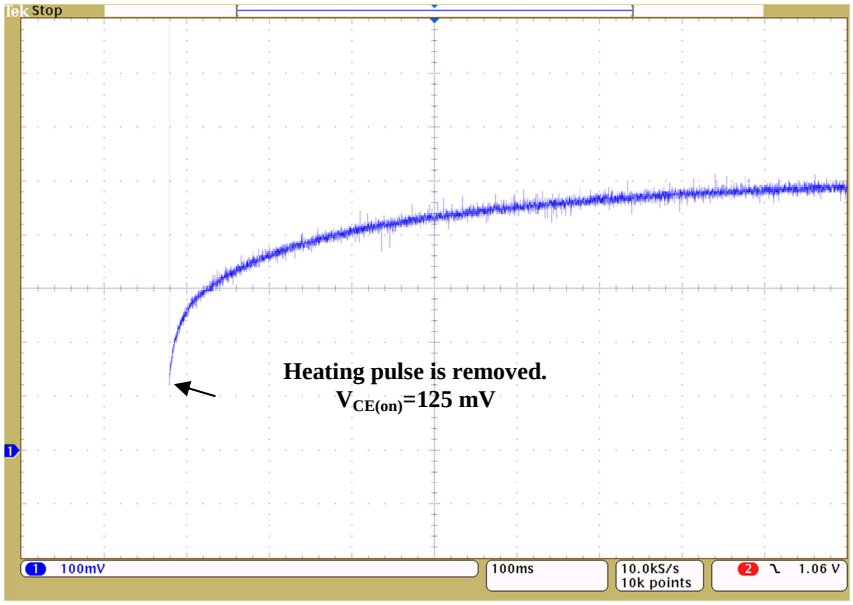

Figure 5-10. Waveform of $V_{CE(on)}$ during cooling down period.

It is noted that the thermal management system is not specially designed and optimized, because the design target is to support the power module operating at 200 ˚C safely. The advanced cooling technologies such as pin-fin baseplate with direct liquid cooling [89], microchannel cold plate [90], and integrated vapor chamber [91] can be utilized to further increase the power density.

5.4 Continuous Operation of a 10 kW Buck Converter at 200 ˚C

In order to evaluate the high temperature capability of the designed package and cooling system, a buck converter composed of the fabricated phase-leg module is built and operated continuously with the device junction heated up to 200 ˚C by controlling the loss dissipation.

5.4.1 Junction Temperature Measurement during Converter Operation

As mentioned before and shown in Figure 5-5, the waveforms of the switching transients vary with temperature. Thus the junction temperature of the power module can be derived by monitoring the temperature sensitive switching parameters.

In our study, the turn-off delay time $T_{d(off)}$ is selected for temperature measurement during converter operation, which is defined as the time between the falling edge of the gate-emitter voltage V_{GE} and the rising edge of the collector-emitter voltage V_{CE}. $T_{d(off)}$ has a higher the temperature sensitivity, compared to other switching parameters such as turn-on delay time $T_{d(on)}$, rising time T_r and falling time T_f. Moreover, the $T_{d(off)}$ measurement is only based on the voltage waveforms, simplifying the test procedure and maintain high accuracy.

A calibration curve representing the relationship between turn-off delay time $T_{d(off)}$ and the junction temperature T_j is needed before the junction temperature is measured for continuous operation. However, the switching transients are influenced by many factors besides temperature, including gate drivers, gate resistance, circuit parasitics, and measurement probes, etc. Thus the test circuit for calibration and continuous operation were kept the same for the accuracy of the measurement. Figure 5-11 shows the test circuit setup for calibration and continuous operation respectively. Comparing the two, the same gate drive boards, power boards and probes are used. The loads and heating methods are different, which influence $T_{d(off)}$ little. For calibration, a hot plate is installed underneath the module, heating it to desired temperature with the case temperature monitored by thermocouples. Since only a pulse is applied to the module in the calibration, it is assumed that the junction temperature is the same with the case temperature. The inductive load is applied.

In the continuous test, the module is heated by the device losses while a cold plate with liquid cooling is attached to keep the junction temperature not exceeding 200 ˚C. The resistive load with the L-C low pass filter is applied.

Besides the parameters of the test circuits, the dc bus voltage V_{DC} and load current I_C can also influence the turn off delay time $T_{d(off)}$. Figure 5-12 show the influence of V_{DC} and I_C on

$T_{d(off)}$ at 20 ˚C. The turn-off delay time increases with V_{DC} and decreases with I_C, with the sensitivity of 0.19 ns/V and 2.02 ns/A respectively. To prevent the temperature measurement error due to different voltages and currents, the voltage and current in calibration should be kept the same with those of the measured points in the continuous operation.

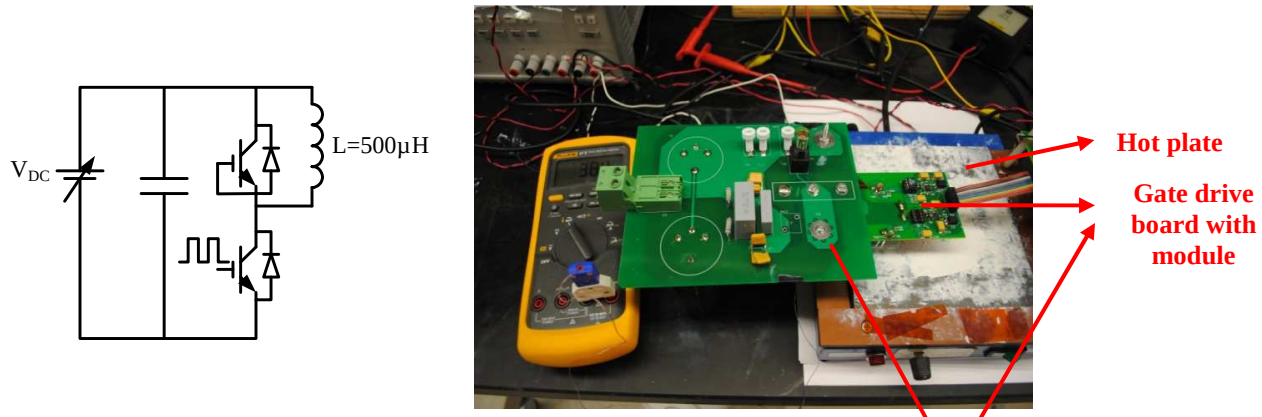

(a) Circuit schematic and test setup for temperature and turn-off delay time calibration

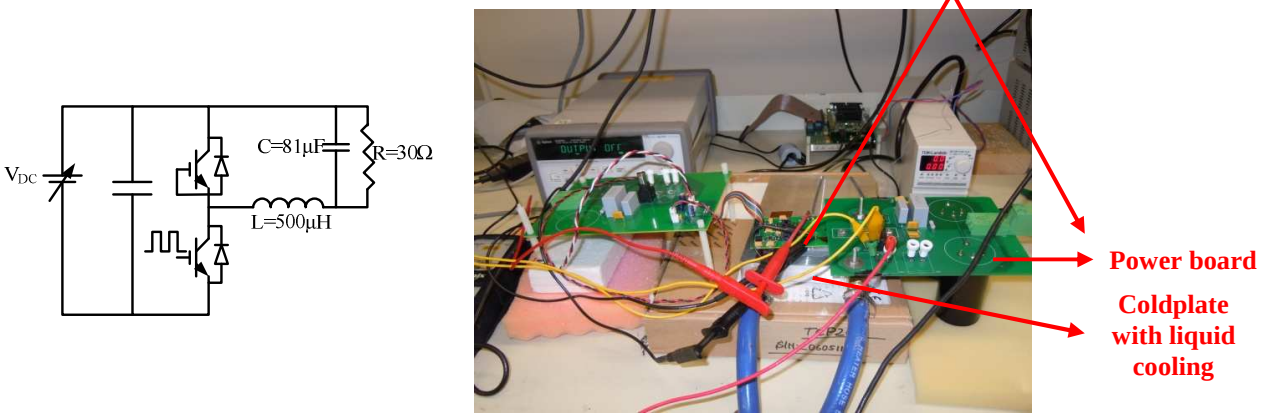

(b) Circuit schematic and test setup for continuous operation

Figure 5-11. Comparison of test circuits for calibration and continuous operation.

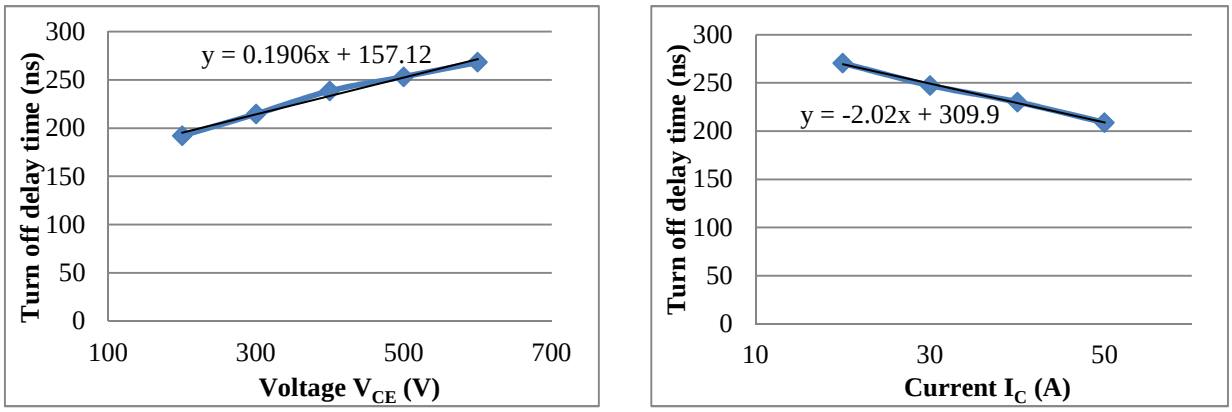

(a) $T_{d(off)}$ vs. V_{DC} (I_C=20A T_j=20˚C)

(b) $T_{d(off)}$ vs. I_C (V_{DC}=650V T_j=20˚C)

Figure 5-12. Influence of dc bus voltage V_{DC} and load current I_C on the turn-off delay time $T_{d(off)}$.

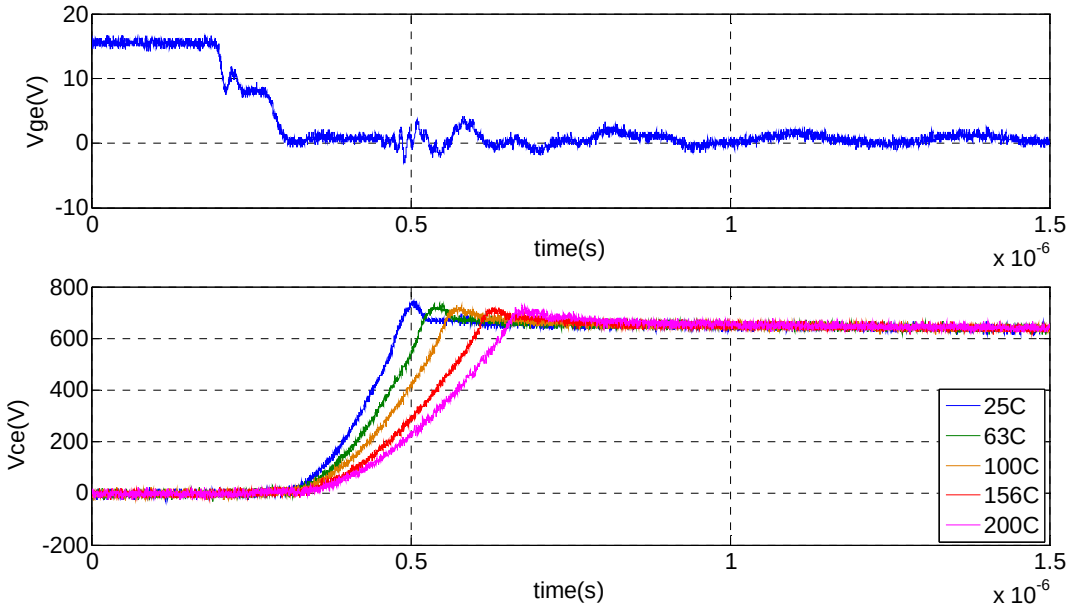

Figure 5-13. Turn-off transients at various temperatures during calibration (T_j=25 ˚C, 63 ˚C, 100 ˚C, 156 ˚C, and 200 ˚C.).

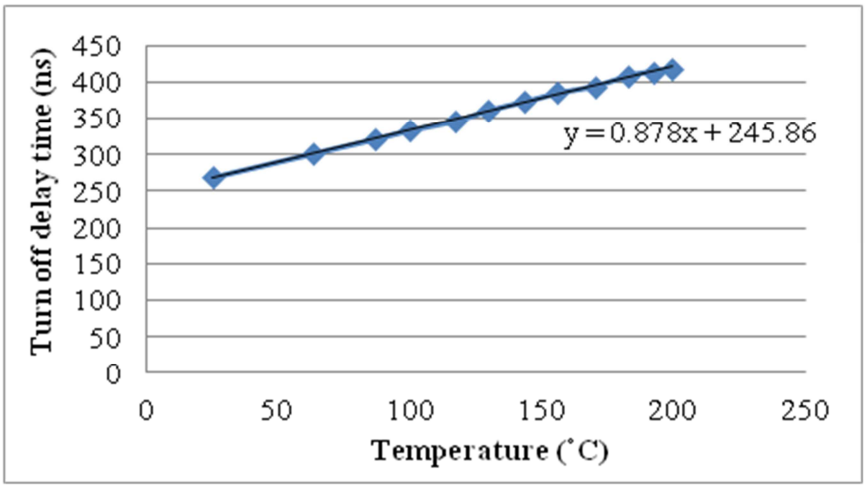

Figure 5-14. Calibration curve representing the relationship between $T_{d(off)}$ and T_j (V_{DC}=650V I_C=23A).

With test circuit built up, the turn-off transients of the fabricated power module are measured at certain voltage and current level and various temperatures, as shown in Figure 5-13. Figure 5-14 shows the calibration curve of turn-off delay time $T_{d(off)}$ and junction temperature T_j with the dc bus voltage V_{DC} at 650 V and load current I_C at 23 A. The turn off delay time increases with temperature, and its temperature sensitivity is 0.878 ns/˚C. With the calibration curve, the junction temperature of the power module during continuous operation can be derived from the switching transients.

5.4.2 Buck Converter Operation at the Junction Temperature of 200 ˚C

The power module is operated with 650 V input voltage, duty cycle of 0.85 and the power rating of 10 kW. The L-C filter is composed of an inductor of 500 µH and a capacitor of 81 µF. The resistive load is 30 Ω. The switching frequency is increased from 10 kHz to 20 kHz to increase the power loss in IGBT to elevate its device junction temperature. Liquid cooling is applied to the converter with the flow rate of 2.5 GPM, coolant temperature of 25 ˚C.

Experimental results at 12 kHz and 20 kHz are shown in Figure 5-15 and Figure 5-16 respectively with the V_{CE} and V_{GE} of bottom IGBT, and inductor current. When the switching frequency is 12 kHz, the turn-off delay time is 337 ns, indicating a junction temperature of 136 ˚C based on the calibration curve. When the switching frequency is 20 kHz, the turn-off delay time is 424 ns, which represents a junction temperature of 203 ˚C. After 60 minutes continuous operation in the steady state, a primary conclusion can be drawn that the designed package and cooling system can support the Si devices operating at 200 ˚C junction temperature.

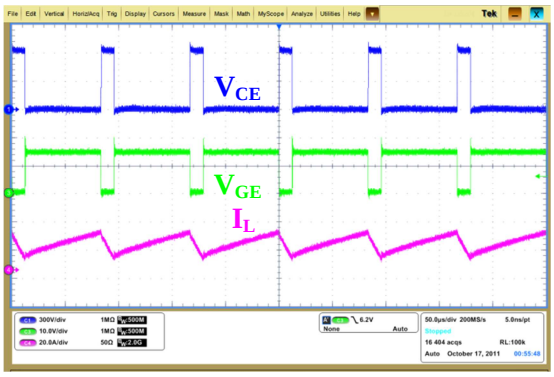

(a) Experimental waveforms

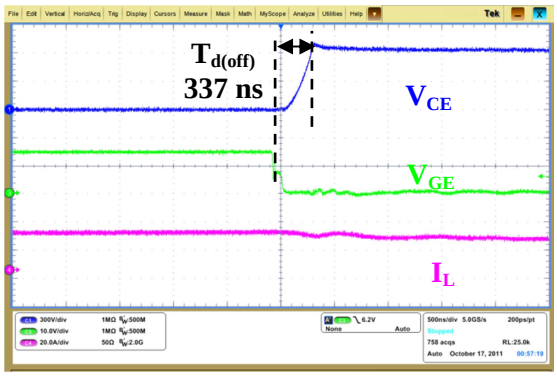

(b) Switching transients

Figure 5-15. Experimental waveforms of a 10 kW buck converter continuous operation at the switching frequency of 12 kHz.

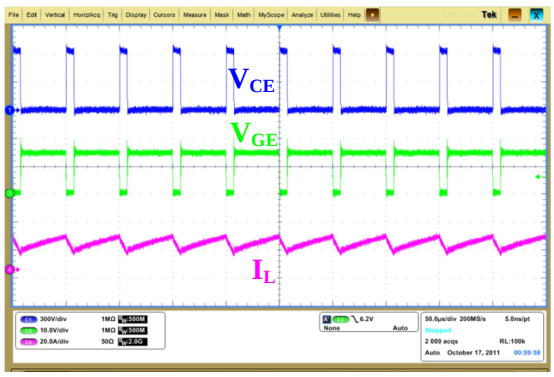

(a) Experimental waveforms

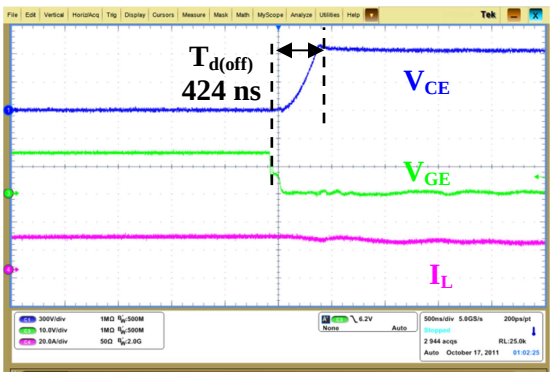

(b) Switching transients

Figure 5-16. Experimental waveforms of a 10 kW buck converter continuous operation at the switching frequency of 20 kHz.

5.5 Summary

The chapter demonstrates the feasibility of operating Si devices based converters continuously at the junction temperature of 200 ˚C for HEV applications. A Si IGBT phase-leg module is developed for 200 ˚C operation utilizing high temperature packaging technologies and appropriate thermal management. The electrical characterization shows the module can operate at 200 ˚C with increased but acceptable losses in the pulse test. The thermal performance of the module and cooling system is evaluated and shows the designed thermal management system can support the Si power module operating at 200 ˚C without thermal runaway. Two temperature sensitive electrical parameters, on state voltage $V_{CE(on)}$ with low current injection and turn-off delay time $T_{d(off)}$, are employed for thermal resistance measurement and junction temperature measurement during converter operation respectively. Finally, a 10 kW buck converter composed of the phase-leg module is operated successfully with the device junction temperature heated up to 200 ˚C, which demonstrates the high temperature capability of the designed package module.

Chapter 6. Junction Temperature Measurement Method Using Short Circuit Current

In this chapter, a method is proposed to measure the junction temperatures of IGBT discrete devices and modules during the converter operation. The chapter is organized as follows: Section 6.2 introduces the calibration circuit schematic and hardware setup, based on which the calibration curve between the short circuit current and temperature is presented. In Section 6.3, the short circuit current is evaluated and compared with the other TSEPs in various aspects to determine its advantages and applicability. The proposed temperature measurement method is demonstrated in a three phase converter for prototype evaluation as an example and the circuits for the other converter topologies are given in Section 6.4. Conclusions are drawn in Section 6.5.

The proposed junction temperature method will be used for evaluating the high temperature three-phase converter introduced in Chapter 7.

6.1 Introduction

IGBTs are widely used in a variety of industrial applications. In many applications such as aircraft and vehicles, the devices are required to operate at high junction temperatures due to the challenging thermal environment and the aggressive power density. Therefore the temperature control and thermal management become more of a concern.

An accurate junction temperature measurement is a valuable tool for prototype evaluation and avoids the unnecessary safety margin regarding device operating temperatures, which is significant especially for high temperature / high density converter applications.

The chapter introduces a method of junction temperature measurement using short circuit current. Short circuit current is negative temperature coefficient (NTC) and has adequate

temperature sensitivity. It is only determined by temperature and gate voltage, while the variance of gate voltage can be eliminated in the hard switching fault (HSF). Due to its good sensitivity and selectivity, short circuit current is suitable as TSEP for temperature measurement. A short circuit pulse is given under converter normal operation conditions and the short circuit current is measured for junction temperature estimation.

6.2 Calibration of Short Circuit Current vs. Temperature in an IGBT

6.2.1 Test Circuit and Hardware Setup for Calibration

The short circuit current of an IGBT decreases with temperature due to the dependence of electron mobility on temperature. To represent the relationship between short circuit current and device temperature, a calibration is conducted on an IGBT based phase-leg module.

Figure 6-1 (a) shows the test circuit schematic for calibration. The phase-leg module composed of two IGBT and diode cells is connected directly to the dc source. During the short circuit, the short circuit current is determined by DUT or its complementary IGBT, depending on which has higher junction temperature. To eliminate the effect of the complementary IGBT, a bypass IGBT is connected in parallel with the complementary IGBT. The bypass IGBT has larger current ratings than DUT. When the short circuit occurs, the short circuit current is limited by DUT, and the bypass IGBT and complementary IGBT still remain in the saturation region.

The switching sequences of the devices are shown in Figure 6-1 (b). At t_1, the bypass IGBT is turned on, and the dc bus voltage is applied across DUT. Then DUT is turned on into a short circuit at t_2. The current goes up quickly and reaches the peak. The DUT collector to emitter voltage V_{CE} remains at the value of input voltage after a small notch caused by the inductive parasitic elements of the circuit. Then the current gradually decreases with time because the short-circuit energy consumption increases the device temperature as well as MOS-channel

resistance. The short circuit current is recorded for junction temperature measurement of DUT. Then DUT is turned off at t_3 by the short circuit protection function of the gate driver or the gate control signal. Usually the short circuit period should be less than 10 µs to prevent the device destruction due to overheat. Finally the bypass IGBT is turned off at t_4.

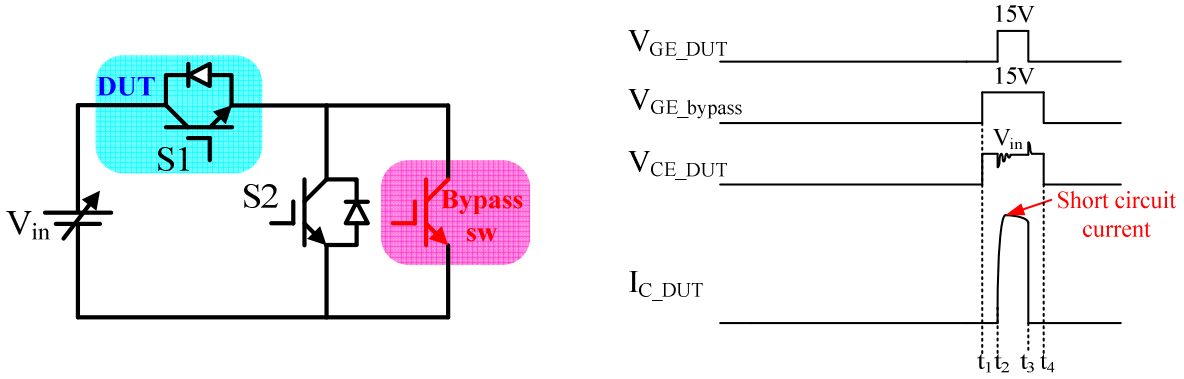

(a) Circuit schematic (b) IGBT waveforms

Figure 6-1. Calibration circuit schematic and device waveforms.

Fig. 2 shows the hardware setup for calibration. The phase-leg module under test is shown in Fig. 2 (a). It is composed of two IGBT chips (Infineon IGC50T120T6RL) and two anti-parallel diodes (Infineon IDC28D120T6M). The phase-leg module is driven by a gate drive board, on which there are two connectors connecting in parallel with the corresponding IGBTs, as shown in Fig. 2 (b). When the junction temperature of one IGBT needs to be measured or calibrated, the temperature measurement unit composed of the bypass IGBT and its gate drivers is inserted to the connector of the complementary IGBT. A hot plate is installed underneath to heat the module to various temperatures with the case temperature monitored by thermocouples. It is assumed that the junction temperature is the same with the case temperature before short circuit occurs.

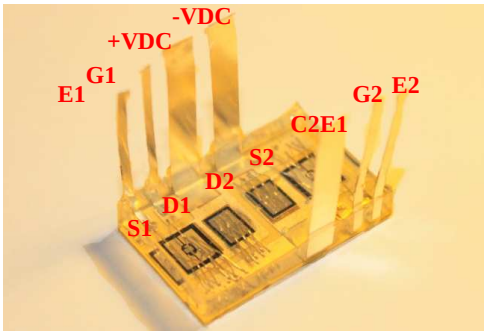

(a) Phase-leg power module under test

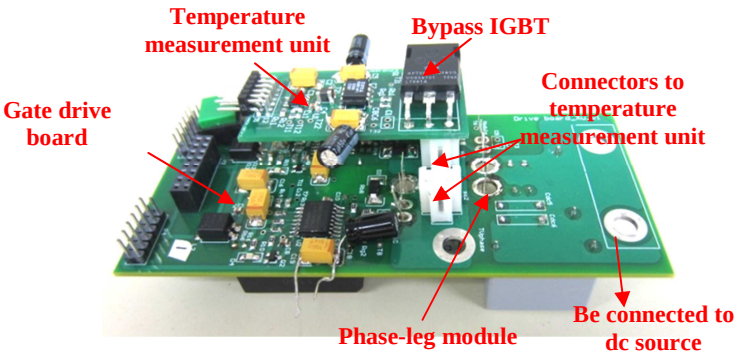

(b) Circuit board for temperature measurement of the phase-leg module

Figure 6-2. Hardware setup for calibration.

Figure 6-3 shows the gate drive circuit schematic for the IGBT module with short circuit protection. The module is driven by the driver IC 1ED020I12-F. The gate driver provides coreless transformer isolation, de-saturation protection and is suitable for high temperature operation up to 150 ˚C. The driver input and output sides are powered by 5 V and 15 V dc supplies respectively. Traco dc/dc converter (THB 3-2415) with a minimized input-output capacitance of 13 pF is used for supplying the driver output side. Four transient voltage suppressor diodes D3 to D6 are connected in series between IGBT collector and gate for active clamping. The de-saturation protection ensures the protection of the IGBT at short circuit. The output pin is driven low when the voltage on the DESAT pin exceeds 9 V, which is detected by desat diode D2. To prevent the false desat trips, the desat diode should have a fast reverse recovery. A 1200 V, 1 A ultrafast diode STTH112A with a reverse recovery time of 75 ns is used for D2. The desat diode is connected to the middle of the four clamping diodes instead of IGBT collector to further reduce the noise. To allow enough time for IGBT saturation during turn-on, a blanking time is set by the internal current source and an external capacitor. A 100 pF capacitor C1 is used for 4 µs blanking time. During short circuit, the IGBT gate can be pumped by a high dv/dt through miller capacitance. The driver provides the gate clamping function by connecting

the CLAMP pin to the gate. However, a current of maximum 500 mA for 10 µs could be fed back to the supply, which can cause the Traco output instable. The diode D1 is used to make sure the current is absorbed by the decoupling cap (or Zener diode) instead of the Traco power supply.

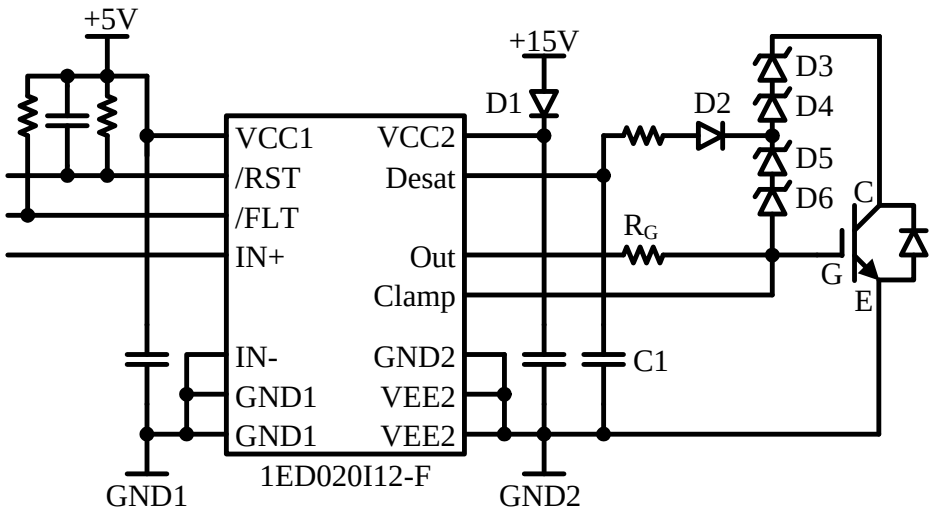

Figure 6-3. Gate drive circuit with de-saturation protection.

6.2.2 Experimental Results of Calibration

With the hardware setup, the short circuit is created at various temperatures and the corresponding short circuit current waveforms are recorded for calibration. The DUT gate voltage V_{GE} is 15 V, which is recommended in the device datasheet for continuous operation. The DUT collector to emitter voltage V_{CE} is 650 V. Figure 6-4 shows the experimental waveforms of the switches at 15 ˚C and 110 ˚C respectively. The short circuit current value at 3 µs after short circuit occurs is used for temperature indication both in calibration and measurement to eliminate the influence from electrical oscillations. The short circuit current at 3 µs after short circuit occurs is 207.4 A at 15 ˚C and 174.2 A at 110 ˚C. The short circuit current

values at various temperatures are then recorded and shown in Figure 6-5. The short circuit current has an adequate temperature sensitivity of 0.345 A/˚C and linearity. It is noted that the temperature in the curve is the device junction temperature before short circuit occurs, not at the time when the short circuit current is recorded. With the calibration curve, the IGBT junction temperature during converter operation can be derived from the short circuit current value.

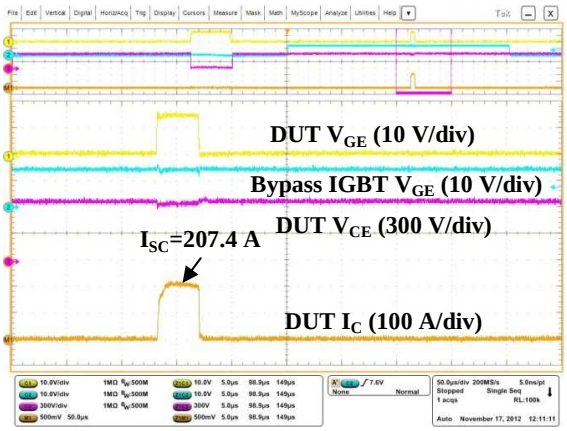

(a) IGBT short circuit current at 15 ˚C (5 µs/div)

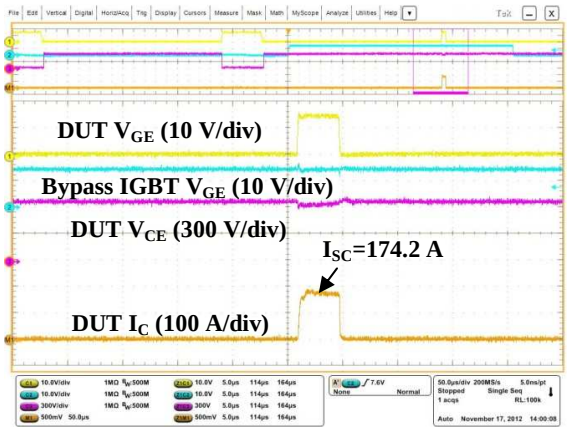

(b) IGBT short circuit current at 110 ˚C (5 µs/div)

Figure 6-4. Short circuit current at various temperatures in calibration.

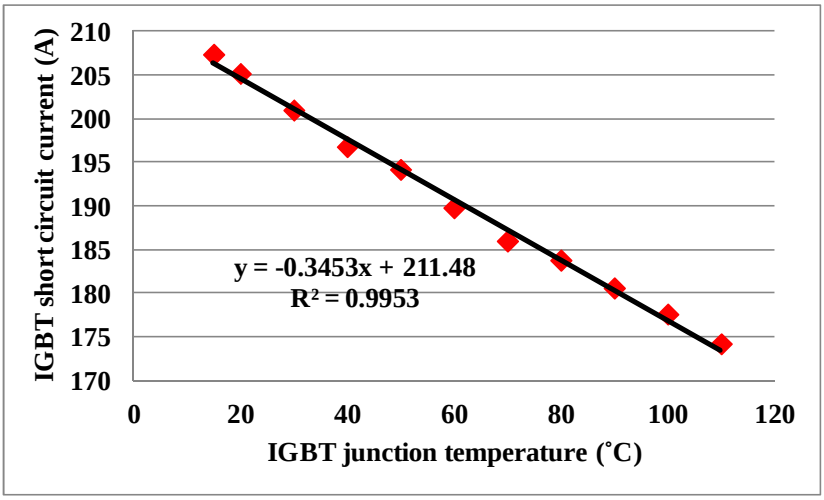

Figure 6-5. Short circuit current as a function of temperature (V_{GE}=15 V, V_{CE}=650 V).

6.3 Evaluation of Short Circuit Current as TSEP

6.3.1 Sensitivity of Short Circuit Current as TSEP

A method of comparing the accuracy of different TSEPs is proposed in [92] using the following ratio:

$$S = \frac{|s|}{|val_{\max}|} \tag{6-1}$$

where s is the temperature sensitivity of the TSEP while val_{max} is the maximum measured value of the parameters.

Based on I_{sc} vs. temperature calibration curve in Figure 6-5, the temperature sensitivity of short circuit current with V_{GE} of 15 V is 0.345 A/˚C. Considering the maximum short circuit current of 207 A, the sensitivity ratio is $1.66 \cdot 10^{-3}$ ˚C^{-1}. For voltage under high current, the ratio is from 0 ˚C^{-1} to $1 \cdot 10^{-3}$ ˚C^{-1} determined by the current value. These two parameters have adequate temperature sensitivities. For the saturation current under low gate voltage, the sensitivity is about 0.016 A/˚C in the temperature range from 110 ˚C to 150 ˚C. The sensitivity is much smaller in lower temperature range. Considering that the current sensor has to sustain the nominal current in normal operation of the power device, the ratio can be as small as $0.23 \cdot 10^{-3}$ ˚C^{-1} because the saturation current is much smaller than nominal current. The temperature sensitivity of switching time is around 2 ns/˚C. It is not compared with other TSEPs because the ratio cannot be applied to the parameter.

6.3.2 Linearity of Short Circuit Current as TSEP

A linear TSEP brings benefits to calibration step because it doesn't need a lot of measurement points. To better understand the linearity of the TSEP, the formula of the IGBT saturation current at different gate voltages is given in (5-2).

$$I_{sat} = (1+\beta_{PNP}\frac{\mu_{ns}C_{ox}Z_c}{2L_c})(V_{GS}-V_{TH})^2 \quad (6\text{-}2)$$

where I_{sat} is the saturation current. β_{PNP} is the current gain of the bipolar transistor in IGBT. μ_{ns} is the surface mobility of electrons in the channel. C_{ox} is the oxide capacitance. Z_c and L_c are channel width and channel length respectively. V_{GS} is the gate source voltage and V_{TH} is the gate threshold voltage. Among these parameters, the threshold voltage V_{TH} is negative temperature coefficient. The surface mobility of electrons μ_{ns} varies linearly with temperature.

For a low voltage V_{GS}, which is slightly larger than V_{TH} at room temperature, the influence of V_{TH} on the saturation current dominates and results in a nonlinear I_{sat} vs. temperature curve. The exponential curve leads to an increase of sensitivity with temperature and makes the measurement at low temperatures less precise.

In the proposed method in this chapter, V_{GS} is at the rated value of 15 V. The influence of µns dominates and the relationship between saturation current and temperature is approximately linear.

For the other two TSEPs, the switching times and V_{CE} under high current, they are also linear.

6.3.3 Selectivity of Short Circuit Current as TSEP

Selectivity represents the degree of TSEP influenced by other parameters than temperature. It is important to eliminate these effects due to the variation of the electrical parameters when using TSEP as an indicator of the junction temperature. The short circuit current is a function of collector to emitter voltage V_{CE} and gate voltage V_{GE} besides temperature.

The short circuit test is conducted by increasing the dc link voltage gradually from 100 V to 650 V. The curve of short circuit current I_{sc} as a function of V_{CE} is plotted in Figure 6-6. It is shown that the short circuit current doesn't depend a lot on V_{CE}. In comparison with the I_{sc} vs.

temperature curve in Figure 6-5, the measurement error of 1 V dc voltage results in the error of 0.096 ˚C in temperature measurement.

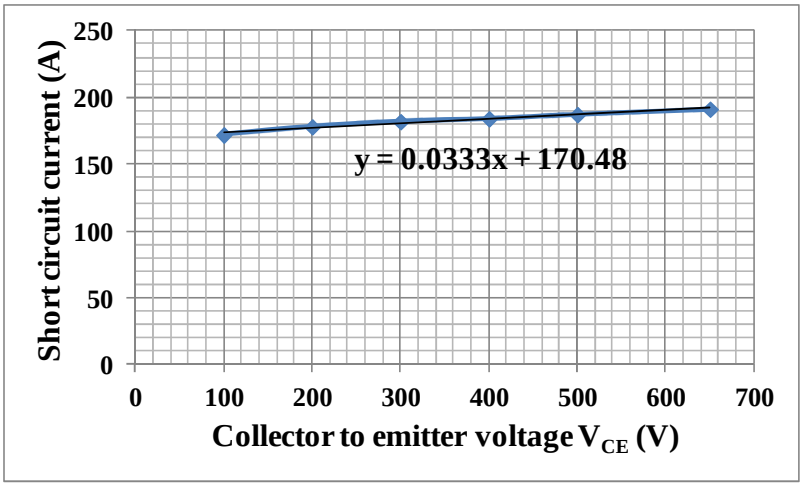

Figure 6-6. Curve of short circuit current I_{sc} vs. IGBT collector to emitter voltage V_{CE}.

From the transfer characteristics of IGBT, the short circuit current depends a lot on the gate voltage V_{GE}. Therefore, it is important to reduce the variance of gate voltage during the temperature measurement.

It is mentioned in Chapter 4 that there are two different types of short circuit. When IGBT turns on into a short circuit, it is called hard switching fault (HSF). When the short circuit is applied to an IGBT that is already on, it is called fault under load (FUL).

Figure 6-7 shows the waveforms of two short circuit conditions. In HSF, initially IGBT is off and dc bus voltage V_{DC} is supported across the device. Then the device is turned on to short circuit at t_1. The device enters the active region quickly and the voltage remains at V_{DC} after a notch. The gate voltage is little influenced if the devices are put close to dc bulk capacitors to minimize parasitic in the circuit loop. The device is turned off at t_2. In FUL, at t_1, IGBT is turned on and the voltage across the device V_{CE} is low. At t_2, a short circuit is applied to the device. The

current increases quickly and enters active region. The rise of V_{CE} charges the miller capacitor and thus pumps the gate voltage V_{GE} and increases the short circuit current correspondingly. The device is turned off at t_3.

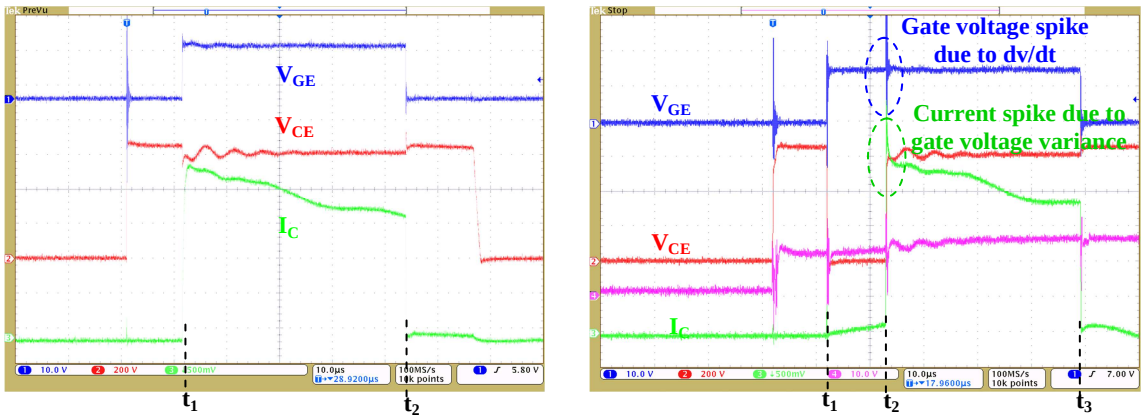

(a) Hard switching fault (b) Fault under load

Figure 6-7. Two types of short circuit fault conditions.

Comparing the two short circuit conditions, the gate voltage changes less during short circuit fault in HSF, while the gate voltage has spikes when short circuit happens in FUL. To reduce the effect of gate voltage variance on short circuit current, HSF is selected for temperature measurement.

In summary, the short circuit current doesn't depend much on voltage. It depends on the gate voltage, the variance of which could be greatly reduced by creating a HSF short circuit instead of FUL.

For the other TSEPs for online temperature measurements, the switching time can be influenced by numerous electrical parameters including gate voltage, gate resistor, load current, collector to emitter voltage, circuit parasitics, measurement probes, and etc. Thus it is important that the test circuits for calibration and continuous operation are kept the same for the accuracy of the measurement. The device voltage under a high current depends a lot on the resistance of

the electrical connection. Considering the difference of connection temperature during calibration and temperature, the measurement error can be caused by the variation of connection resistance. The saturation current of an IGBT under low gate voltage is little influenced by voltage and current value and only requires accurate gate voltage value, which is similar to the temperature measurement with short circuit current.

6.3.4 Genericity of short circuit current as TSEP

The temperature measurement using voltage under high current can be used with all power semiconductor chips including power transistors and diodes. The switching time can be used with transistors. The two TSEPs of saturation current at low gate voltage and short circuit current at nominal gate voltage are only suitable for IGBTs.

6.3.5 Ruggedness during Measurement

Under short circuit conditions, IGBT has to sustain both high voltage and high current at the same time, which can cause a significant increase in the local device temperature from the high power dissipation. High local temperature beyond a critical value prevents the ability to sustain the collector-emitter voltage and causes the destruction of the device. As a result, it is necessary to know the short circuit capability of the device before measuring the junction temperature using short circuit current.

IGBT manufacturers generally guarantee 10 µs of the short circuit withstand time (SCWT) below the rated junction temperature. For those IGBTs without SCWT defined in the datasheet or for the applications exceeding the rate temperature range, the short circuit capability can be evaluated with the SOA evaluation circuit board. The methods are described in details in Chapter

4. The IGBT should be turned off within SCWT in order to prevent the device from destruction during temperature measurement.

6.4 Temperature Measurement during Converter Operation

6.4.1 Temperature Measurement in Three-Phase Voltage Source Converters

Figure 6-8 shows the test schematic and switching sequences of the three-phase voltage source converter. All IGBTs are driven by the typical gate voltage of 15 V / 0 V. A bypass IGBT with larger current rating is connected in parallel with the complementary IGBT, and is activated only when DUT is in the off state. The three-phase converter is under normal operation condition and has reached the thermal equilibrium before t_0. Then the bypass IGBT is turned on at t_1, the current commutes from S4 to bypass IGBT to prevent S4 from de-saturation during short circuit. When the next turn on pulse of S1 comes at t_2, S1 turns on into a short circuit. The short circuit current is measured to derive the junction temperature. The de-saturation protection is activated and turns off the IGBTs at t_3.

The control signal of the short circuit pulse can be implemented with 555 timer connected for monostable operation. The pulse duration is set by R and C values. Figure 6-9 shows the short circuit pulse of the bypass IGBT and the PWM gate signals of DUT. The short circuit pulse starts when DUT is in the off state.

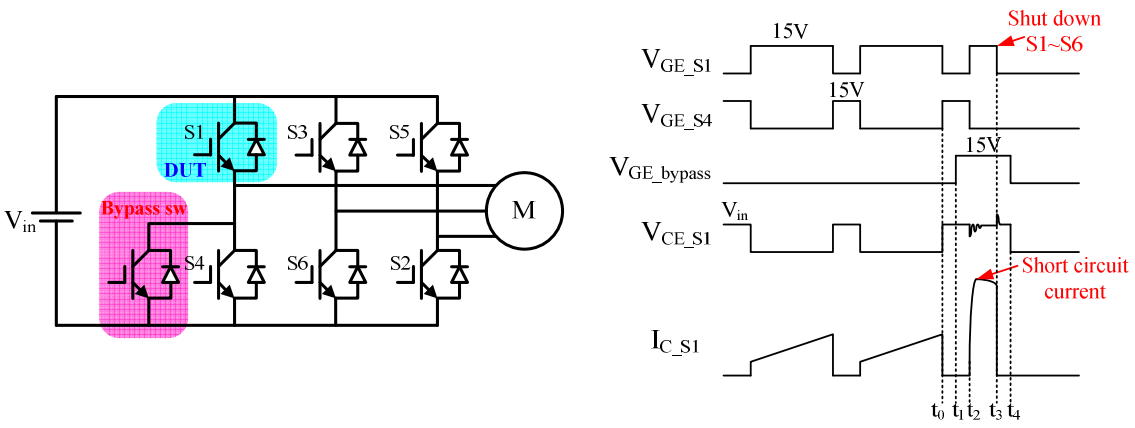

(a) Circuit schematic (b) IGBT waveforms

Figure 6-8. Calibration circuit schematic and device waveforms.

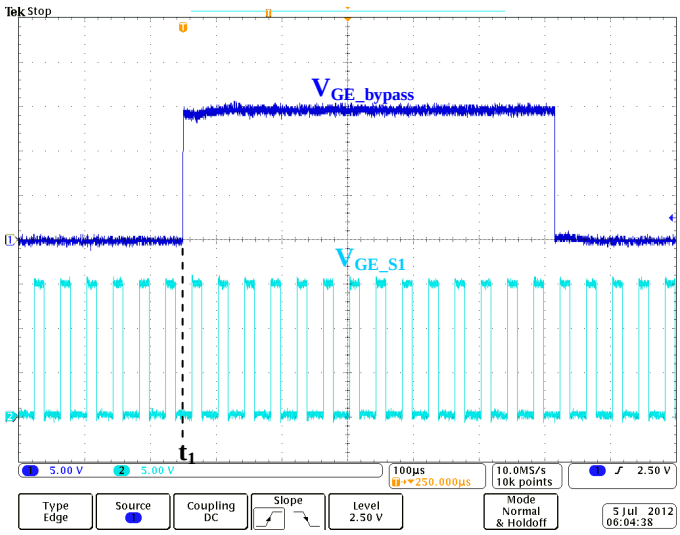

Figure 6-9. Short circuit pulse of bypass IGBT and PWM gate signal of DUT.

Figure 6-10 shows an example of junction temperature measurement in the three phase converter prototype. A temperature measurement unit composed of the bypass IGBT and its gate driver is designed. The three phase power module is driven by the gate drive board, on which there are six connectors connecting in parallel with its corresponding IGBT cell. When the junction temperature of one IGBT needs to be measured, the temperature measurement unit is inserted to the connectors of the complementary IGBT. Then by giving a short circuit pulse, the junction temperature can be derived from short circuit current by looking up the calibration table.

Figure 6-11 shows the experimental waveforms during the temperature measurement. The bypass IGBT is turned on when DUT is in the off state. A HSF short circuit is created when DUT is turned on. The protection is activated and DUT is turned off at 4 µs after the short circuit. The short circuit current is 180.8 A, indicating a junction temperature of 89 ˚C according to the calibration results.

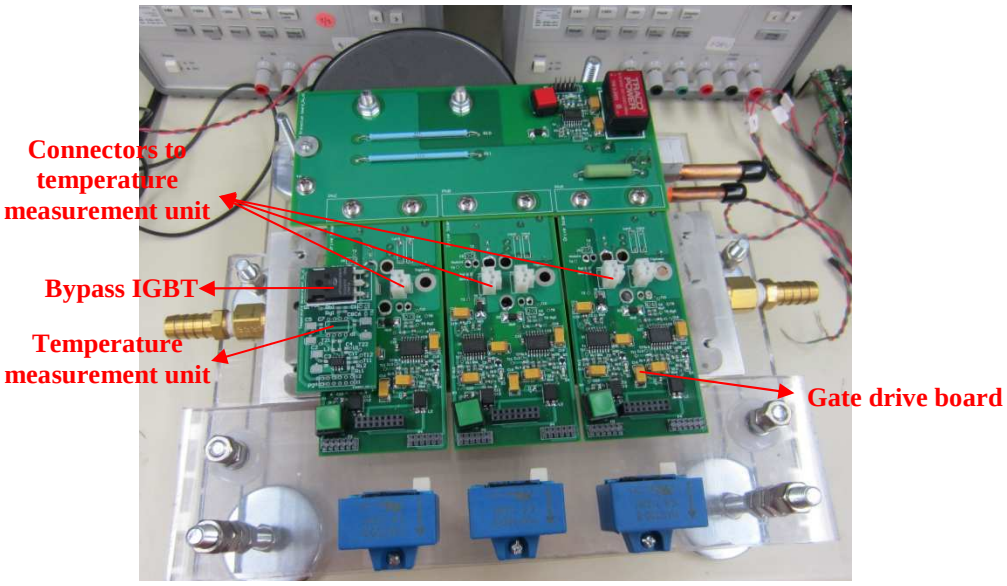

Figure 6-10. An example of junction temperature measurement in the three phase converter.

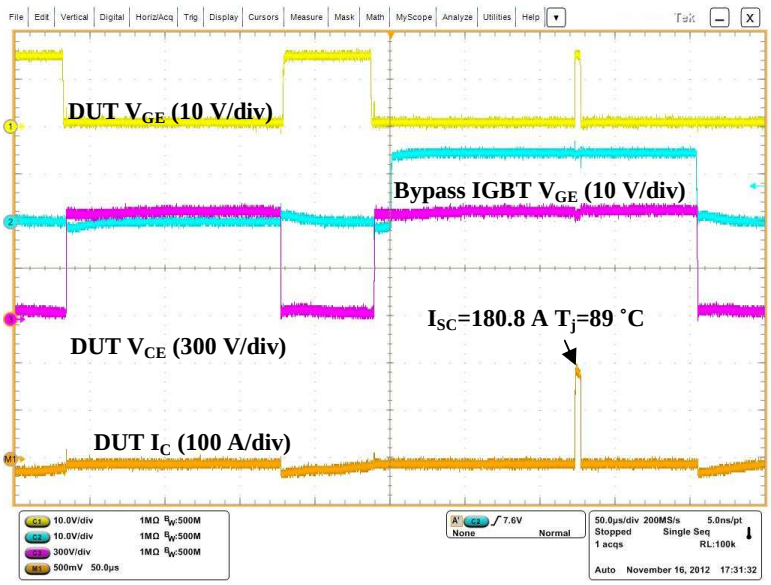

Figure 6-11. Short circuit waveforms during converter operation.

6.4.2 Temperature Measurement in the Other Circuit Topologies

The proposed method can be used in various power electronics circuit topologies. Figure 6-12 shows the measurement circuit in some dc-dc and ac-dc converters. By turning on the bypass IGBT, DUT are shorted to the dc source and the short circuit current is recorded at that time. The dc sources are different in different converters. For buck converter, DUT is shorted to input voltage source during measurement. For boost converter, DUT is shorted to output voltage source during measurement. For buck-boost converter, DUT is shorted to the serial connected input and output voltage source during measurement. For Cuk converter, DUT is shorted to the capacitor C_1. For three-phase current source converter, DUT is shorted to the phase to phase voltage source during measurement. It is noted that the value of the dc source voltage should be kept the same in the calibration and temperature measurement.

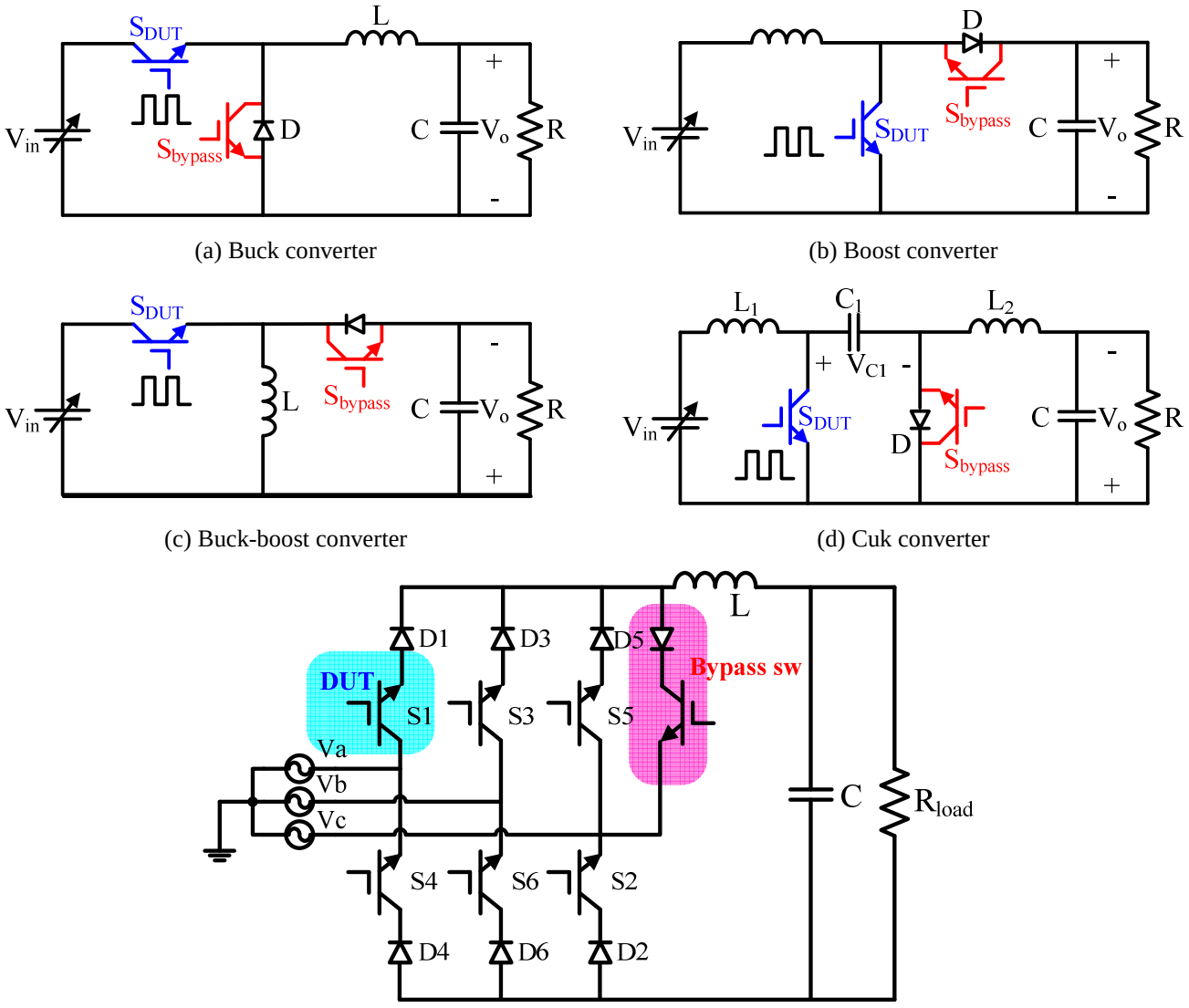

Figure 6-12. Temperature measurement circuits in dc-dc and ac-dc converters.

6.5 Summary

In this chapter, a method is proposed to measure the junction temperatures of IGBT discrete devices and modules using short circuit current I_{SC}. From the calibration between short circuit current and temperature, it is shown that I_{SC} has a good temperature sensitivity and linearity. I_{SC} is little influenced by voltage and current. By creating a short circuit in hard switching fault, the

effect of gate voltage variance on short circuit current is eliminated, so that the short circuit current is only determined by temperature. Due to these advantages, the short circuit current is suitable to be used for temperature measurement.

Test circuits are proposed for junction temperature measurement in various dc-dc and ac-dc converter topologies. By connecting a temperature measurement unit to the converter and giving a short circuit pulse, the IGBT junction temperature can be measured. The proposed method is validated in a three-phase voltage source converter prototype and will be used in Chapter 7.

Chapter 7. A 30 kW High Temperature Three Phase Converter with Reduced Cooling

In this chapter, a 30 kW Si IGBT based three-phase converter is developed for operating at 200 ˚C junction temperature with the 105 ˚C engine coolant in hybrid electric vehicles, leading to lower cost and higher power density. The chapter is organized as follows: Section 7.2 and section 7.3 presents the design and evaluation of the power module and the thermal management system. Section 7.4 shows the three phase converter design and implementation. The experimental results are given. Conclusions are drawn in Section 7.5.

7.1 Introduction

The challenging thermal environment in HEVs as well as the aggressive power density and cost targets established by industry and government makes the high temperature operation of power electronics devices desirable.

Today's HEVs use an additional low temperature (65 ˚C) cooling system for the power electronics traction systems. Although several researchers have built the converters that are capable of operating with 105 ˚C or 90 ˚C high temperature coolant [39]-[43], the tremendous rising cost is imposed by the newly developed techniques or larger semiconductor usage.

The objective of this chapter is to implement a 30 kW three phase converter prototype based on Si devices with 105 ˚C engine coolant. The high temperature capable power electronics module utilizing the technologies introduced in Chapter 5 is used for operation with 105 ˚C coolant, leading to a lower cost and higher power density. An integrated pin fin structured AlSiC baseplate is used for cooling design, which provides improved thermal performances and further increases the power density of the converter system. The short circuit current is employed as

TSEP for junction temperature measurement during converter operation, as introduced in Chapter 6. A 30 kW converter is then implemented and is compatible with the temperature measurement method. The experimental results demonstrate that the converter can operate successfully with the device junction temperature heated up to 200 ˚C with the high temperature engine coolant.

7.2 Power Module Design and Evaluation

Figure 7-1 shows the 10 kW phase-leg module designed for the three-phase converter. Compared to the modules developed in Chapter 5, the only difference is the layout is further improved for smaller volume and higher power density. The chips and packaging materials are the same with previous modules. The dimension and materials are listed in Table 7-1.

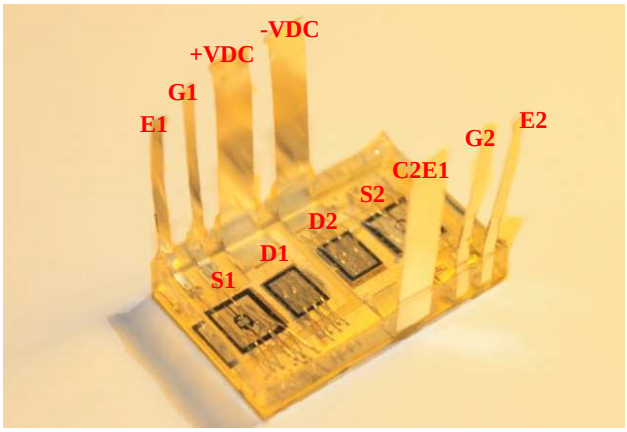

Figure 7-1. 10 kW fabricated power module for high temperature operation.

Table 7-1 Materials Selection and Dimension

Component	Dimension (mm)
IGBT chip (IGC50T120T6RL)	7.25 × 6.84 × 0.115
Emitter pad	5.37 × 5.74 × 0.004
Gate pad	1.31 × 0.81 × 0.004
Diode chip (IDC28D120T6M)	6.3 × 4.5 × 0.11
Anode pad	5.35×3.55×0.004
Substrate	33×21× (Cu: 0.203, Al_2O_3: 0.381)
Die attachment	Solder Au80Sn20, thickness: 0.2
Aluminum wires	10 mils × 6
Encapsulant	Silicone gel (Nusil R-2188)

The static characteristics of the module are tested with Tektronix 371B high power curve tracer at various temperatures. The parameters are shown in Table 7-2. The switching performance of the module is characterized with the standard double pulse test. The switching energies at various temperatures are shown in Table 7-3. The device characterization procedure is described in Chapter 5.

Table 7-2 Parameters of Static Characteristics at various Temperatures

Junction temperature (˚C)	V_t (V)	R_{CE} (mΩ)	V_f (V)	R_{AK} (mΩ)	Leakage current (mA)
25	0.9	33.5	1	31	N/A
175	0.7	53.5	0.8	48.5	0.86
200	0.6	57.3	0.7	53.5	3.98

Table 7-3 Switching Loss at Various Temperatures (650 V/70 A)

Junction temperature (˚C)	IGBT turn-on loss (mJ)	IGBT turn-off loss (mJ)	Diode reverse recovery loss (mJ)
25	3.9	3.2	1.2
175	6.7	6.1	2.8
200	7.2	6.5	3.2

The power losses dissipated on an IGBT in the 30 kW three phase converter operating at V_{dc}=650 V, f_s=12 kHz, M=1 and various temperatures are calculated according to equations from (2-5) to (2-8), and shown in Figure 7-2.

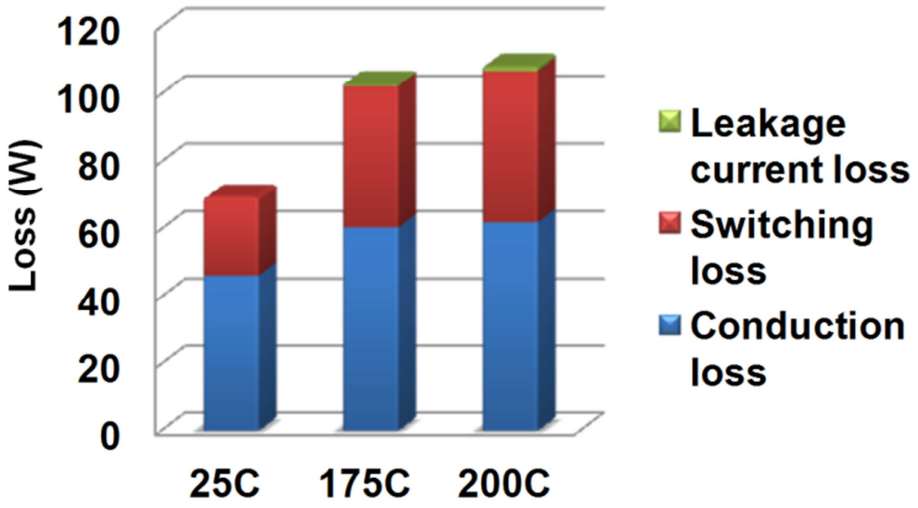

Figure 7-2. Power losses dissipated on an IGBT in the three phase converter at various temperatures.

7.3 Thermal Management System Design and Evaluation

7.3.1 Thermal management system design

Considering the power density and high temperature capability of the three phase converter, a thermal management system is developed with improved cooling performance by eliminating the thermal interface material and providing efficient heat spreading.

Figure 7-3 shows the thermal management system of the modules. The cross section of the module and cooling assemblies is shown in Figure 7-4. Three power modules are soldered to the AlSiC baseplate on its copper solderable surfaces. The AlSiC baseplate provides sufficient thermo-mechanical stability because the CTE of AlSiC is compatible with the module substrate (Al_2O_3). The baseplate is directly cooled by the liquid coolant due to its integrated pin fin structure, thus eliminates the thermal interface material (TIM) between the baseplate and cold plate in traditional baseplate technologies and improves the thermal performance. The water ethylene glycol (WEG) coolant is pumped to the cold plate with its inlet temperature regulated

by the liquid chiller. The coolant flow rate is 2.5 gallons per minute (GPM), which is the maximum value according to Department of Energy (DOE) specifications released in 2006.

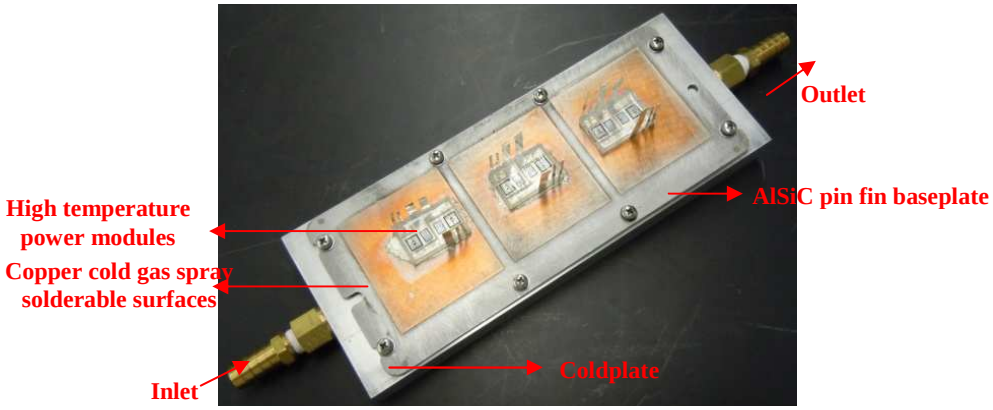

Figure 7-3. Thermal management of three-phase power modules.

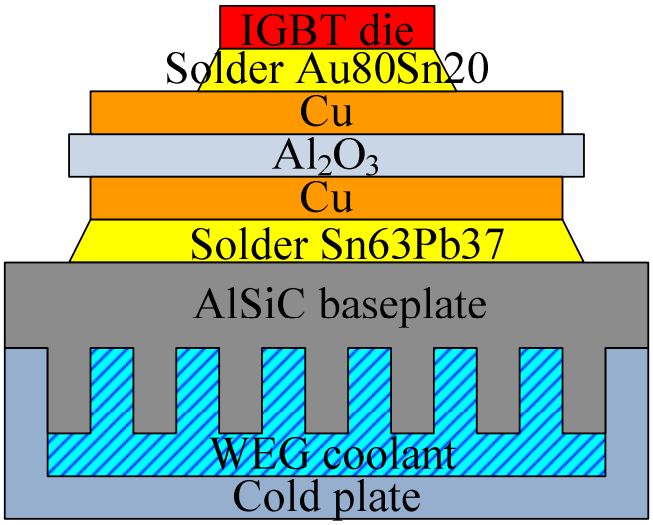

Figure 7-4. Cross section of power module and cooling assemblies.

7.3.2 Thermal performance evaluation through FEA simulation

A 3D model of the thermal management system is built in COMSOL Multiphysics for FEA simulation, as shown in Figure 7-5.

The simulation is then conducted to evaluate the thermal performance for each IGBT. As shown in Figure 7-6, the power loss of 100 W is dissipated averagely on one IGBT chip, and the temperature distribution over the device and cooling system is obtained through simulation. The maximum junction temperature achieves 188.5 ˚C. The thermal resistance of the top IGBT of module 1 from junction to inlet coolant is then given by (6-1).

$$R_{thj-a} = \frac{T_j - T_{amb}}{P} = \frac{188.5°C - 105°C}{100W} = 0.835°C/W \tag{7-1}$$

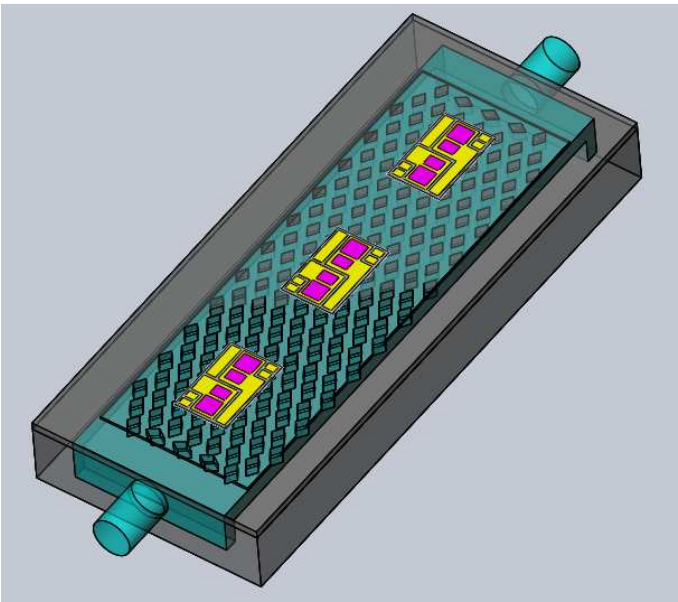

Figure 7-5. A 3D model of thermal management system for FEA simulation.

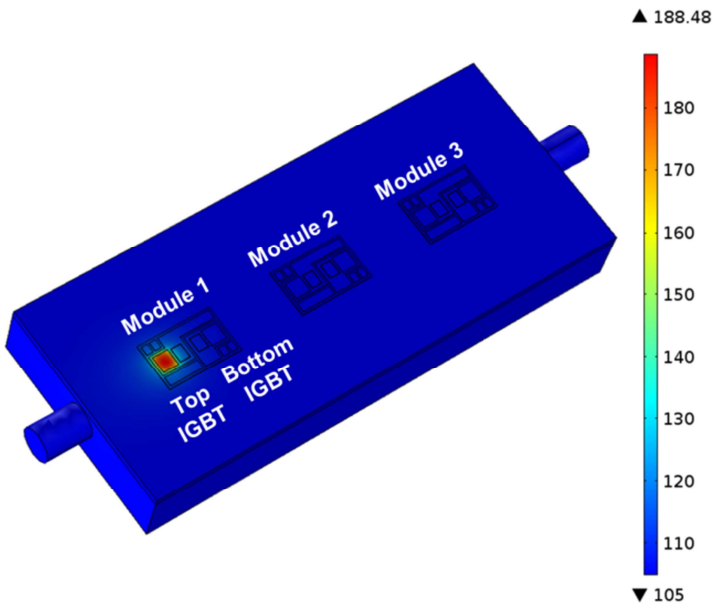

Figure 7-6. Temperature distribution with 100 W loss dissipated on top IGBT of module1 (Unit: ˚C).

The same method is applied to the other five IGBTs, and the thermal resistances of all IGBTs are shown in Figure 7-7. There are some small discrepancies between the thermal resistances of each IGBT due to the slightly different coolant velocities. The flowing velocity of the coolant is shown in Figure 7-8.

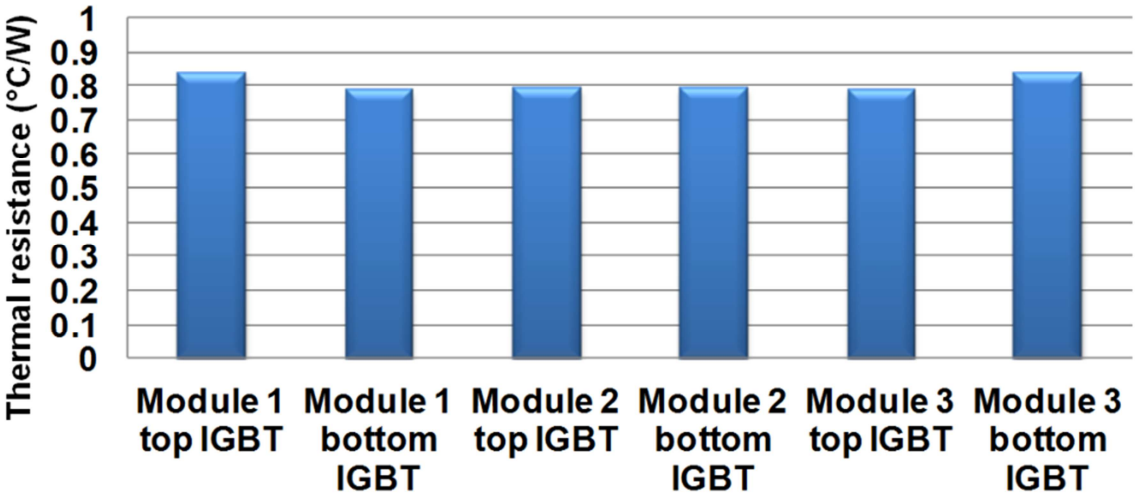

Figure 7-7. Simulation results of IGBT thermal resistances in three phase converter.

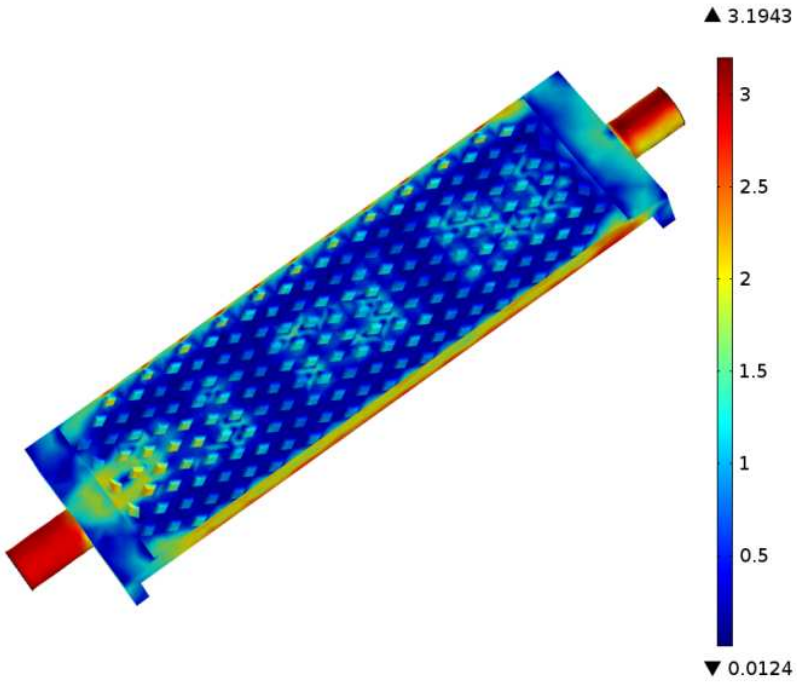

Figure 7-8. Velocity distribution of the liquid coolant (Unit: m/s).

With the losses obtained through device characterization and the FEA thermal model, the temperature distribution of the three phase converter operating under various conditions can be obtained through simulations. Figure 7-9 shows the temperature distribution of the converter when operating at the power rating of 30 kW, V_{dc}=650 V, f_s=12 kHz, M=1. The temperatures of six IGBTs and six diodes are shown in Figure 7-10. The IGBTs' temperatures are around 200 ˚C, and the diodes' temperatures are around 145 ˚C. The IGBT and diode which are close to the outlet of the cold plate represent the worst case, which are at the temperature of 203 ˚C and 148 ˚C, respectively.

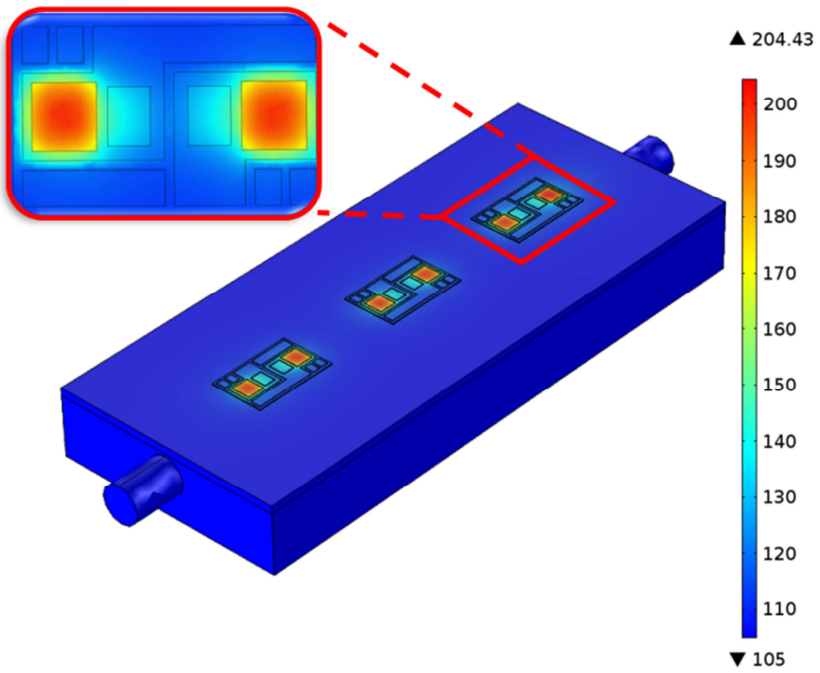

Figure 7-9. Temperature distribution of the 30 kW three phase converter (M=1) (Unit: ˚C).

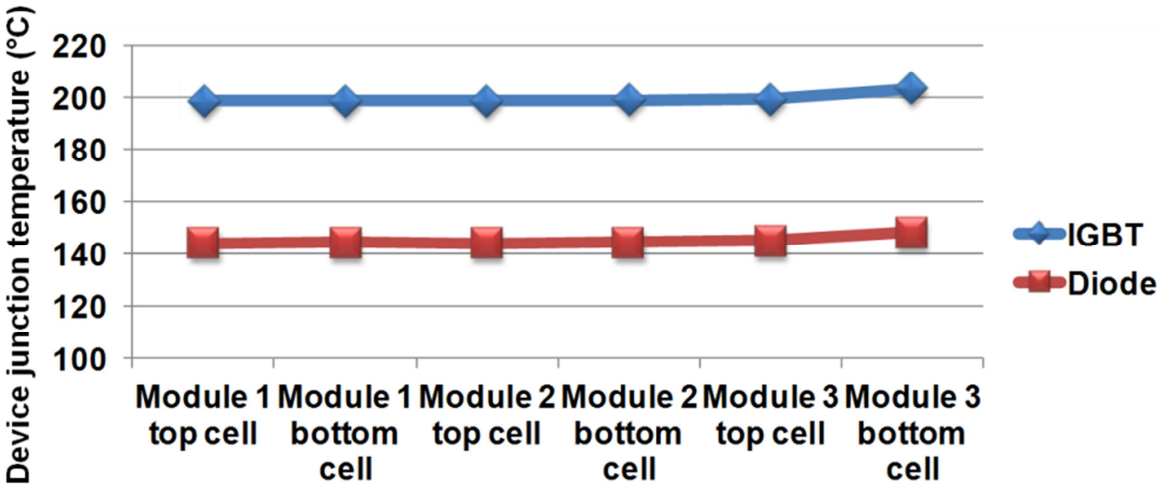

Figure 7-10. Temperatures of IGBTs and diodes of the three phase converter (M=1) in simulation.

A cross section of the simulation results is shown in Figure 7-11, which represents that the integrated pin fin baseplate provides a good heat spreading for the devices. The temperature distribution of the liquid coolant is shown in Figure 7-12.

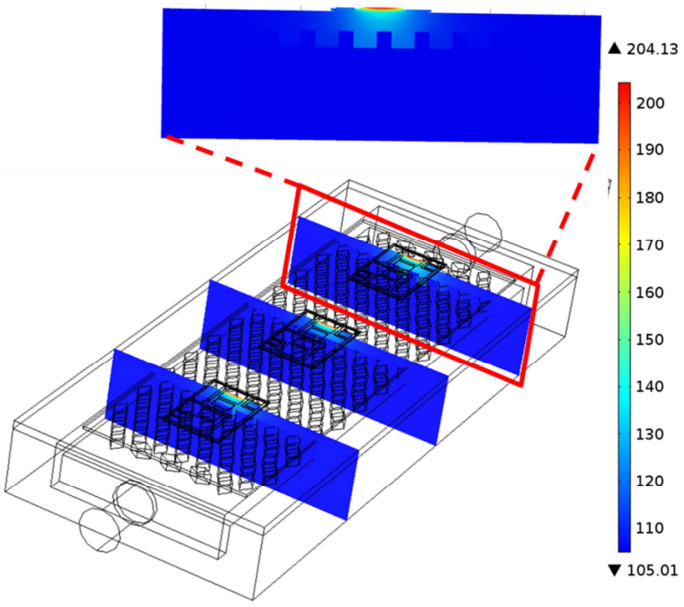

Figure 7-11. Cross section of thermal simulation results (Unit: ˚C).

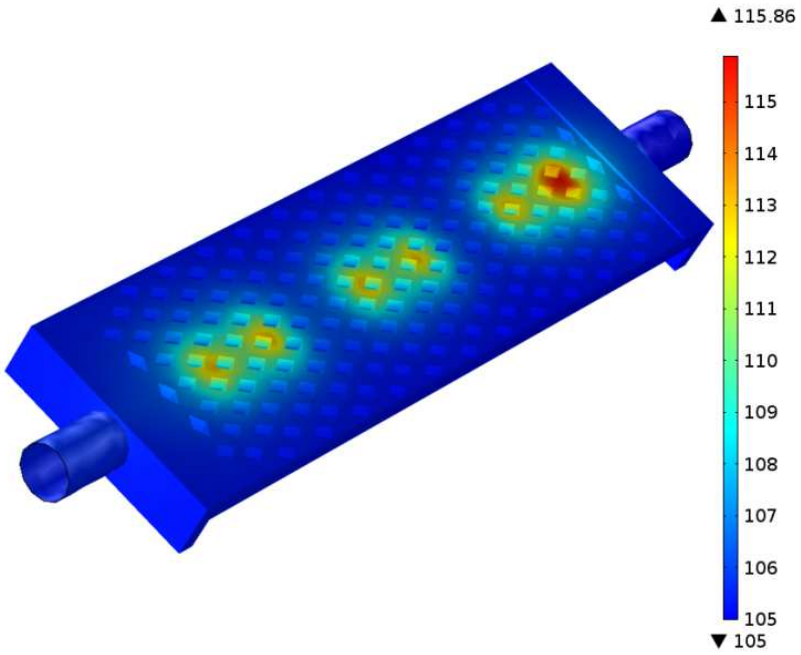

Figure 7-12. Temperature distribution of the liquid coolant (Unit: ˚C).

In a three phase traction inverter / motor drive, more current flows through the freewheeling diode with lower motor speed / modulation index, and causes the diode junction temperature to increase. The simulation is carried out for the operating condition with a low modulation index

(M=0.1). Figure 7-13 shows the temperature distribution of the three phase converter when operating at ten percent of the full speed and the rated torque. The device temperatures are shown in Figure 7-14. The diode temperatures are around 166 ˚C, and the IGBT temperatures are around 180 ˚C. Although the diode temperatures are higher in low speed conditions than full speed conditions, they still meet the temperature safety criterion.

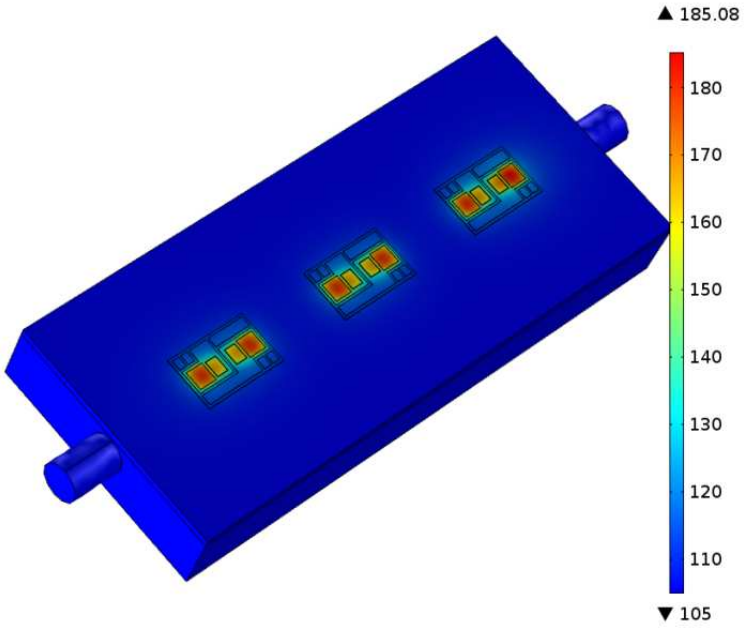

Figure 7-13. Temperature distribution of the three phase converter (M=0.1) (Unit: ˚C).

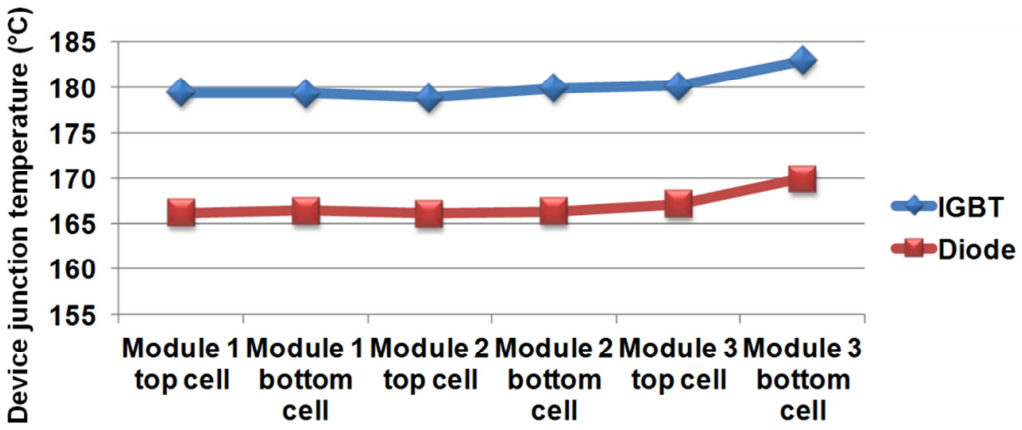

Figure 7-14. Temperatures of IGBTs and diodes of the three phase converter (M=0.1) in simulation.

7.3.3 Thermal performance evaluation through experiment

The thermal performance of the cooling system is characterized with an electro-thermal method utilizing device forward voltage drop $V_{CE(on)}$ as the temperature sensitive parameter. The method is introduced in Chapter 5 in details.

In the measurement, the thermal resistances of the six IGBTs from junction to inlet coolant temperature $R_{thj\text{-}a}$ vary from 0.78 ˚C/W to 0.86 ˚C/W, as shown in Figure 7-15. Small discrepancies between the simulation and experimental results are generated during the manufacturing process. The effectiveness of the FEA simulation is validated by the experimental results.

The corresponding specific thermal resistances vary from 0.387 cm^2•˚C/W to 0.427 cm^2•˚C/W, which are defined as the product of thermal resistance and die area. The experimental results show the integrated pin fin baseplate structure has better thermal performance than the cooling configurations including thermal grease, thermal pad, and direct bonding methods in today's commercial HEVs [93].

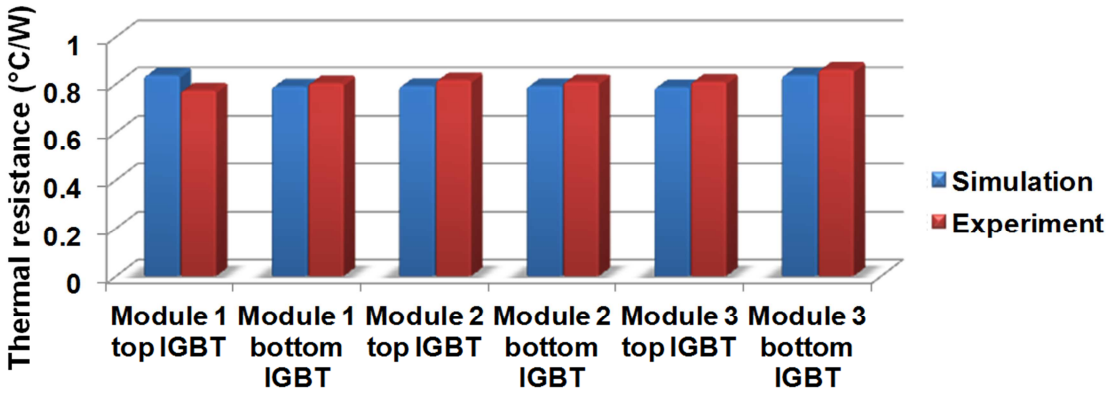

Figure 7-15. Thermal resistances of IGBTs in the three phase-leg power modules.

7.4 Three-Phase Converter Development and Experiments

7.4.1 Implementation of a 30 kW three-phase converter

The schematic of the designed three-phase converter is shown in Figure 7-16, including a dc link protection circuit and the IGBT junction temperature measurement circuit. Figure 7-17 shows the 30 kW three-phase converter built for operation at the junction temperature of 200 ˚C with 105 ˚C coolant. The converter has three phase-leg power modules. The modules are driven by the gate driver with de-saturation protection. There are two connectors connected in parallel with the corresponding IGBTs on the gate drive board. When the junction temperature of one IGBT needs to be measured or calibrated, the temperature measurement unit composed of the bypass IGBT and its gate drivers is inserted to the connector of the complementary IGBT. The cold plates are connected with the chiller for liquid circulation. The phase currents are sensed by three Hall effect current transducers HAS 100-S. The DSP TMS320F28335 from TI is used as the controller for AD sampling, closed-loop control implementation and PWM generation. The 1000 V/500 μF metalized polypropylene film capacitor from Electronic Concepts is used as the dc link filter capacitor. A bidirectional switch (1200 V/66 A IGBT and 1200 V/60 A anti-parallel diode) with de-saturation protection is embedded into the dc link capacitor. If a short circuit occurs, all the switches can be shut down within 5 μs and the dc link capacitor is disconnected.

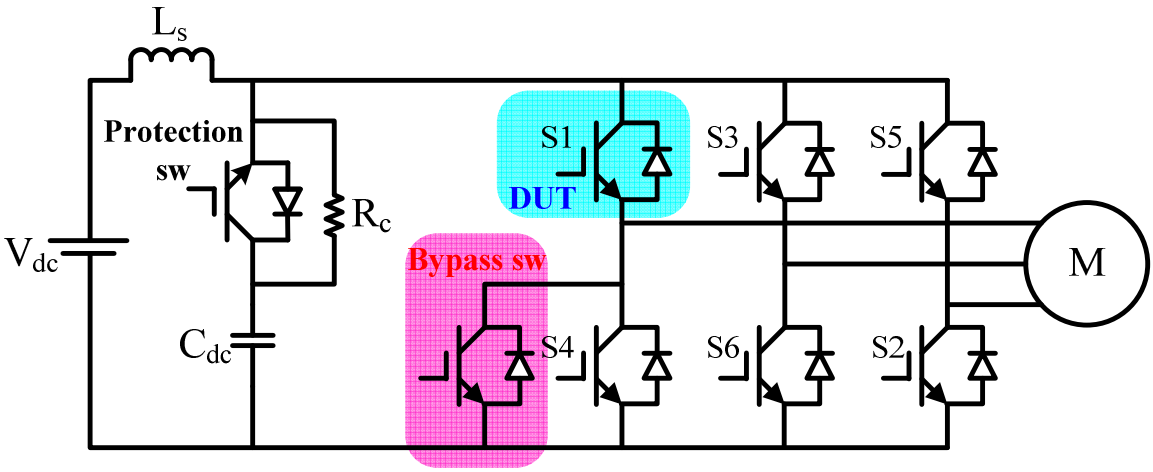

Figure 7-16. Schematic of the three-phase voltage source converter with dc link protection and temperature measurement circuit.

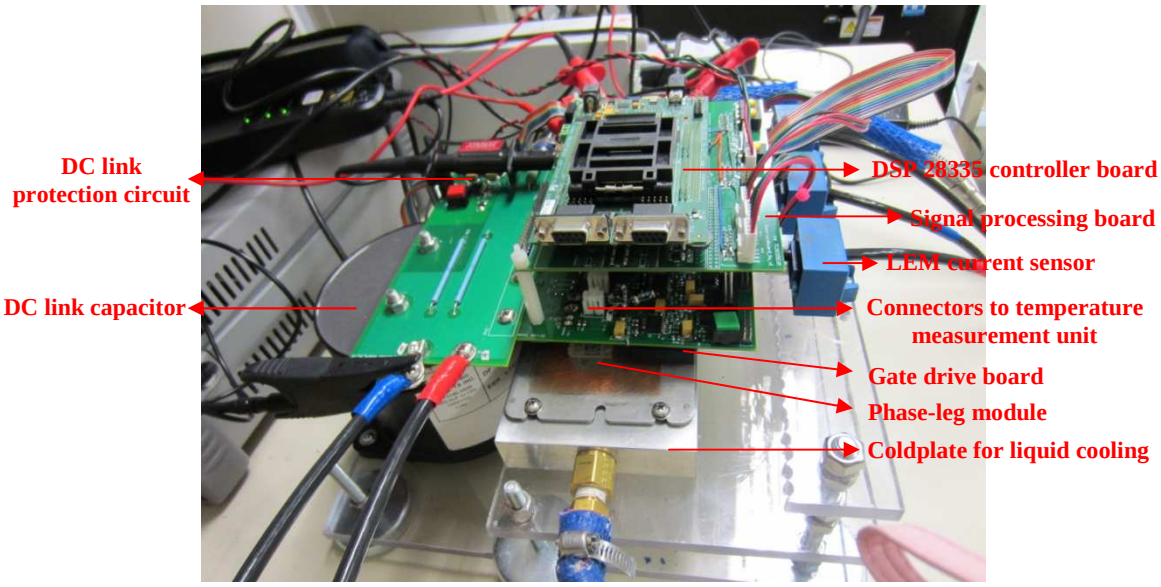

Figure 7-17. Hardware prototype of a 30 kW three-phase converter.

7.4.2 Experimental Results

The three-phase converter is operated with 650 V input voltage, the power rating of 30 kW, switching frequency from 5 kHz to 12 kHz, and the coolant temperature from 20 ˚C to 105 ˚C. Figure 7-18 shows the experimental results of the 30 kW three-phase converter with the gate voltage V_{GE}, dc link voltage V_{DC}, line-to-line voltage V_{CB}, and phase current I_C.

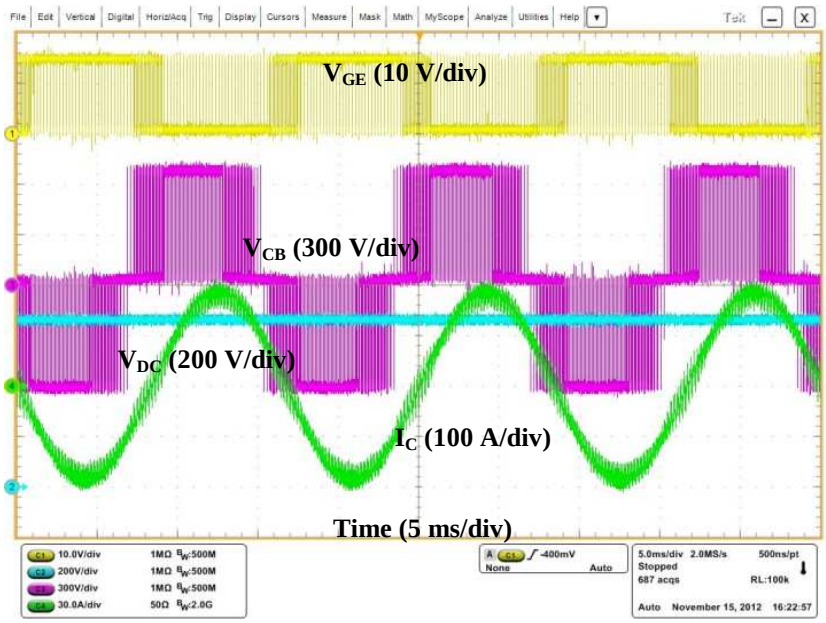

Figure 7-18. Experimental waveforms of three phase converter operating at 30 kW.

A short circuit pulse is given under each test conditions and the short circuit current is measured for junction temperature estimation. Figure 7-19 shows the short circuit waveforms when the converter operates at 30 kW output power, 5 kHz switching frequency and the coolant temperature at 20 ˚C and 105 ˚C. The short circuit current is 180.8 A and 150.6 A with different coolant temperatures, indicating a junction temperature of 89 ˚C and 176 ˚C respectively. The IGBT junction temperatures of the 30 kW converter at 5 kHz with different coolant temperatures are measured and shown in Figure 7-20.

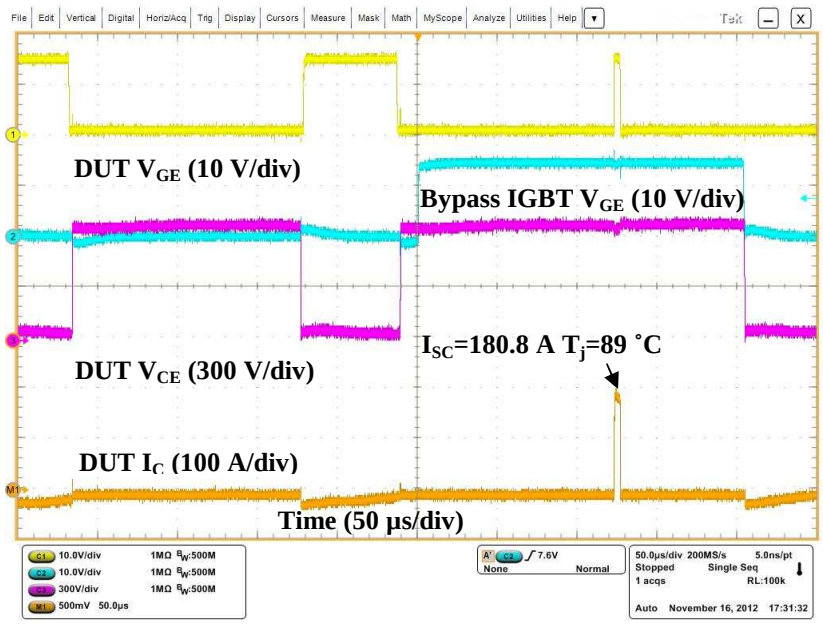

(a) Short circuit waveforms during converter operation with 20 ˚C coolant

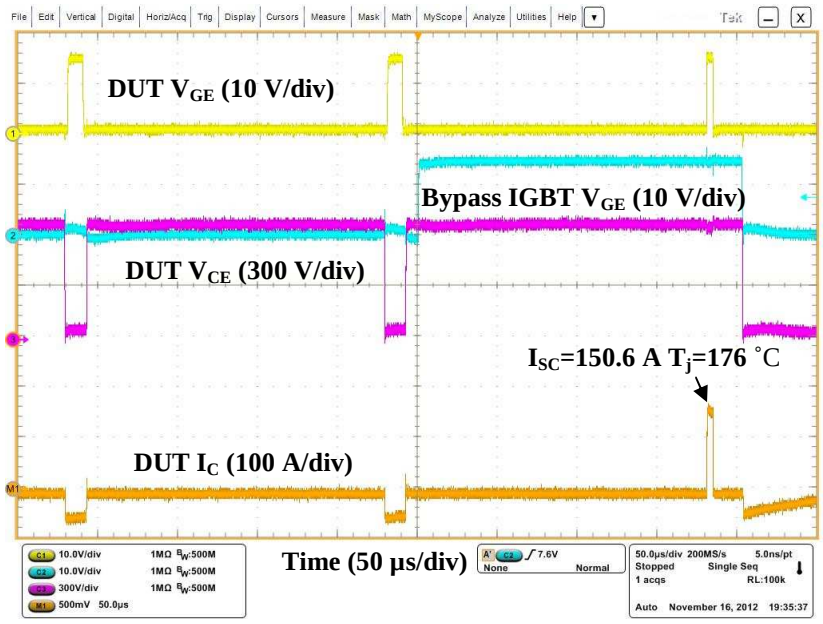

(b) Short circuit waveforms during converter operation with 105 ˚C coolant

Figure 7-19. IGBT junction temperature measurement of 30 kW converter with 20 ˚C and 105 ˚C coolant (f_s=5 kHz).

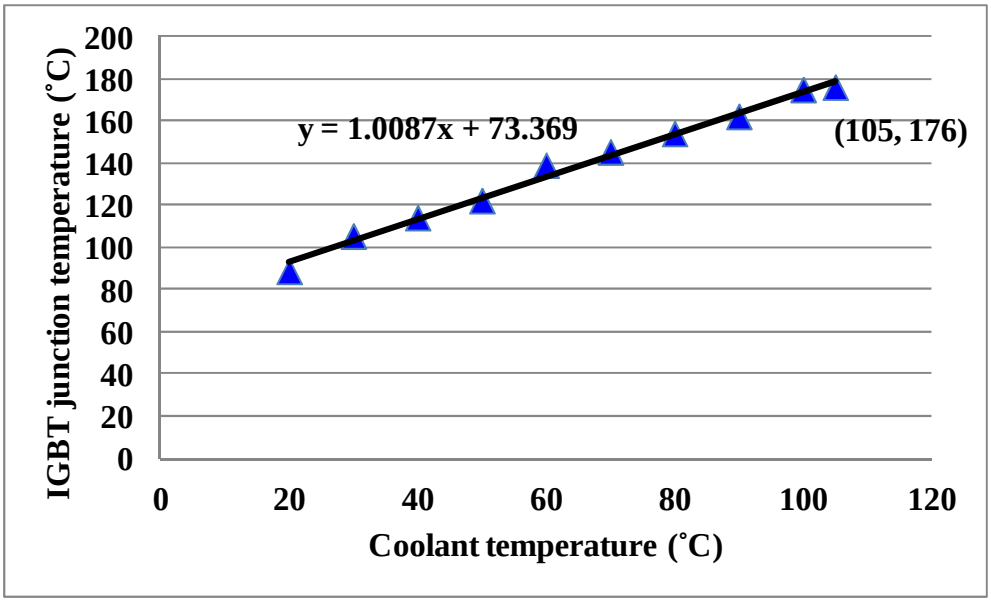

Figure 7-20. IGBT junction temperatures of 30 kW converter with different coolant temperatures (f_s=5 kHz).

The switching frequency is then increased from 5 kHz to 12 kHz to increase the IGBT junction temperature with 105 ˚C coolant and 30 kW output power. The short circuit waveforms at 12 kHz is shown in Figure 7-21. A short circuit current of 142.4 A indicates that the IGBT junction temperature reaches 200.1 ˚C. The junction temperatures of 30 kW three phase converter operating with 105 ˚C coolant at various temperatures are shown in Figure 7-22.

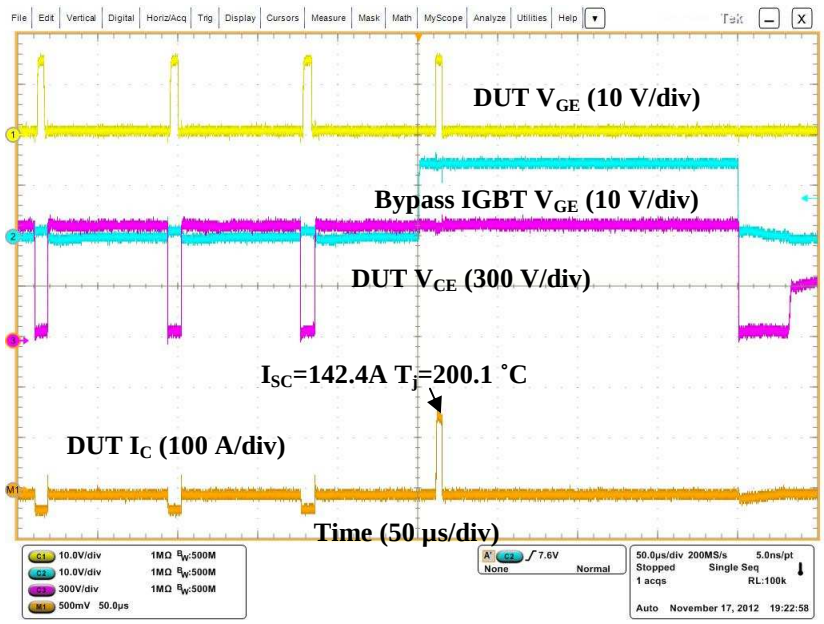

Figure 7-21. IGBT junction temperature measurement when the converter operates at 30 kW output power, 12 kHz switching frequency with 105 ˚C coolant.

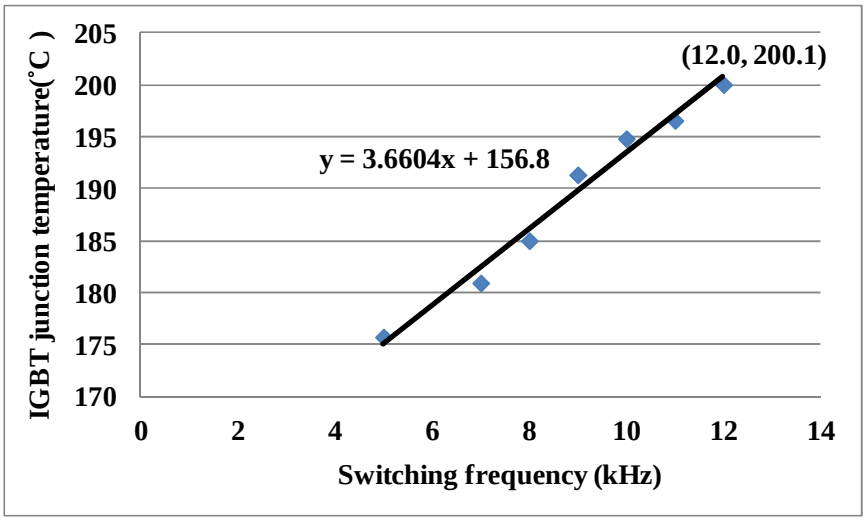

Figure 7-22. IGBT junction temperatures of the 30 kW converter operating with 105˚C coolant at various switching frequencies.

The experimental results demonstrate that the 30 kW three-phase converter can operate with the 105 ˚C coolant at the switching frequency up to 12 kHz, while the IGBT junction temperature is as high as 200 ˚C. The measured device junction temperature agrees with the FEA simulation results, which further validates the effectiveness of FEA simulation.

7.5 Guidelines of Operating Traction Inverter at 200 ˚C T_J with 105 ˚C Coolant

After investigating the feasibility of operating Si devices at 200 ˚C, this part provides the guidelines on how to operate the traction inverter at 200 ˚C junction temperature with 105 ˚C coolant.

(1) Thermal management system should be able to maintain the Si devices junction temperature below 200 ˚C during the converter operation.

In Chapter 3, it has been demonstrated that by extending the device junction temperature from 150 ˚C to 200 ˚C, the additional 65 ˚C cooling loop can be eliminated without compromising thermal performance. Therefore, the existing thermal management system in HEVs is adequate and can maintain the Si devices operating below 200 ˚C.

(2) Thermal performance should meet the criterion set by device leakage current to prevent thermal runaway.

In Chapter 3, it is claimed that the critical thermal conductance to allow thermal stability is the slope of the leakage current curve. Devices with smaller leakage current are more suitable for high temperature applications. Based on the test and calculation of the package module developed in this dissertation, the critical thermal resistance to allow stable operation at 200 ˚C is 6.5 ˚C/W. Most of the thermal management systems in today's HEVs (e.g. Toyota Prius 2010, Nissan LEAF, Hyundai Sonata, etc.) meet the requirement [93]. The existing thermal management system can support the Si devices operating at 200 ˚C without thermal runaway.

(3) The device ruggedness should be evaluated at 200 ˚C to ensure the safe operation.

For example, the short circuit capability of DUT is decreased when operating at elevated temperature of 200 ˚C, but it still meets the short circuit capability industry standard of 10 μs. The short circuit capability is adequate for converter protection.

(4) Conventional packaging materials should be replaced by high temperature packaging materials, including solder, encapsulant, etc.

For example, the commonly used solder for die attachment is Sn63Pb37, which has a melting point of 183 ˚C. Because Sn63Pb37 cannot support Si chips operating at 200 ˚C, it should be replaced by solders with higher melting point (e.g. Au80Sn20, Pb95Sn5, etc.) or sintering [17][18][48][97].

(5) Reliability of power semiconductor devices and packaging should meet the requirement for automobile applications. This part is not covered in this dissertation.

The reliability of the device operating at high temperatures can be tested using a combination of standard tests including high temperature reverse bias (HTRB), high temperature gate bias (HTGB), temperature humidity bias (THB) and so on.

The reliability of the packaging is another challenge for high temperature operation. High temperature cycling tests (thermal cycling and power cycling) should be used on the IGBT modules to evaluate the thermo-mechanical reliability under the harsh environmental conditions. The IGBT modules used in the application should have the thermal cycling capability from -40 ˚C to 200 ˚C with the increased ΔTc compared to the commercial HEVs nowadays, and the power cycling capability from 105 ˚C to 200 ˚C with ΔTj of 95 ˚C which does not change much.

Advanced packaging technologies aiming for high temperature capability and reliability have been studied and developed by universities and device manufactures in recent

years. For example, .XT technology by Infineon increases lifetime of IGBT modules and enables the operation at the junction temperature of 175 ˚C. SkiN technology from SEMIKRON increases the cycling capability with the solder free, pressure contact packaging concept. The packaging technologies are still under investigations to support the device operating at the junction temperature up to 200 ˚C.

7.6 Summary

In this chapter, a 30 kW Si IGBT based three-phase converter has been developed for operating at the junction temperature of 200 ˚C with the high temperature coolant in hybrid electric vehicle applications. The high temperature capable power electronics module utilizing the technologies introduced in Chapter 5 is used for operation with 105 ˚C coolant, leading to a lower cost and higher power density. An integrated pin fin structured AlSiC baseplate is used for cooling design, which provides improved thermal performances. Finally, a 30 kW three-phase converter is implemented. The experimental results demonstrate that the three-phase converter can operate at the junction temperature of 200 ˚C with 105 ˚C high temperature coolant, thus eliminating the need for the additional 65 ˚C coolant in HEVs. The guidelines are provided on how to operate the traction inverter at 200 ˚C junction temperature with 105 ˚C coolant.

Chapter 8. Investigation of Emerging 600 V GaN HEMT

In this chapter, the emerging 600 V GaN HEMT is investigated as a potential replacement of Si devices for future HEV applications. The fast switching characteristics and high temperature performance of the 600 V GaN HEMT is evaluated through experiments. In section 8.2, the inherent switching performance of the GaN HEMT is demonstrated in the double pulse test. In section 8.3, the limitation factors of the fast switching capability by the device packaging and application circuit are analyzed. In section 8.4, the high temperature static and switching characteristics up to 200 ˚C are tested and presented.

8.1 Introduction

Besides the high temperature capability, efficiency and power density are also critical for HEV applications. Although the wide bandgap devices are in development and costly, they could be potential replacements of conventional Si devices in future due to their many advantages such as fast switching speed, lower on state resistance and higher operating temperatures.

Theoretically, GaN devices have superior performances over Si and SiC devices, due to their high electron mobility, high breakdown field and high electron velocity. However, today's commercial GaN power electronics devices are still limited to low voltage applications, which usually have a blocking voltage below 200 V [32]-[33]. In the recent years, 600 V GaN devices have emerged, showing the advantages of fast switching and low on-state resistance [34]-[36]. However, the fast switching behavior could bring challenges and issues to the package and application circuit layout. The high temperature characteristics of the device remain unclear.

This chapter investigates the switching behavior and high temperature performance of the 600 V GaN HEMT. First, the inherent switching performance of the GaN HEMT is

demonstrated in the double pulse test. The GaN HEMT exhibits superior switching capability, with a di/dt reaching 9.6 A/ns and dv/dt reaching 140 V/ns. Then, the limitations of the fast switching capability by the device packaging and application circuit are analyzed. The interference between the current and gate through common source inductance limits the inherent switching speed. Packaging and circuit layout with small parasitics is critical in achieving fast switching. Finally, the high temperature static and switching characteristics up to 200 ˚C are also tested and given. The switching performance of the device is independent of temperature.

8.2 Evaluation of 600V GaN HEMT Switching Characteristics

A 600 V / 11 A GaN HEMT (TPH3006PS) from Transphorm is used for DUT. The device has a $R_{ds(on)}$ of 0.15 Ω and a low reverse recovery charge Q_{rr} of 54 nC. The cascode structure makes it normally off and compatible with standard Si drivers. Figure 8-1 shows the internal cascode structure of TPH3006PS. The fast switching speed makes it suitable for high efficiency and high density applications.

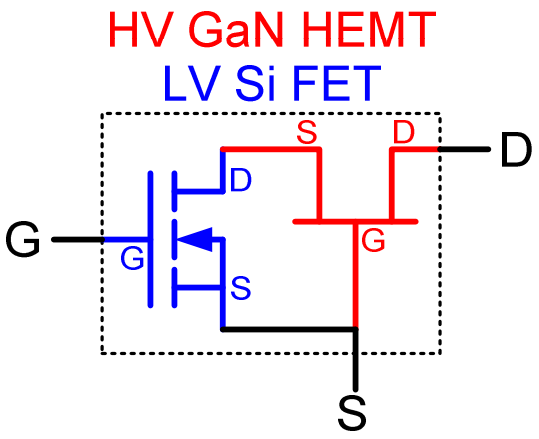

Figure 8-1. Cascode structure of TPH3006PS.

The switching performance of the DUT is evaluated with an inductive load double pulse test circuit. Figure 8-2 shows the circuit schematic and hardware of double pulse test (DPT). The inductive load is composed of three inductors, each of which has one layer of windings to minimize the equivalent parallel capacitance (EPC). The SiC Schottky diode is connected in parallel with the inductor as the freewheeling diode. The bottom switch is the DUT. The Kelvin source wiring is applied for the DUT instead of the conventional wiring in the test. The source-pin and source-tab are employed for gate and power loop respectively, which reduces the common source inductance dramatically, and thus, reduces the ringing on its gate. The Kelvin source wiring benefits the fast switching performance. However, it brings difficulty to thermal management since the tab is soldered to the PCB. The DUT is driven by a high speed, high current gate driver IXDN609 from IXYS. LDO LP2951 provides the flexibility of changing the turn on gate voltage. The decoupling capacitor is placed close to the DUT to minimize the parasitic inductance in the power loop. A 0.1 Ω shunt resistor with the bandwidth of 2 GHz is connected in series with the device source terminal to measure the collector current. V_{gs} and V_{ds} are measured using the Tektronix voltage probes P6139 and P5100 respectively.

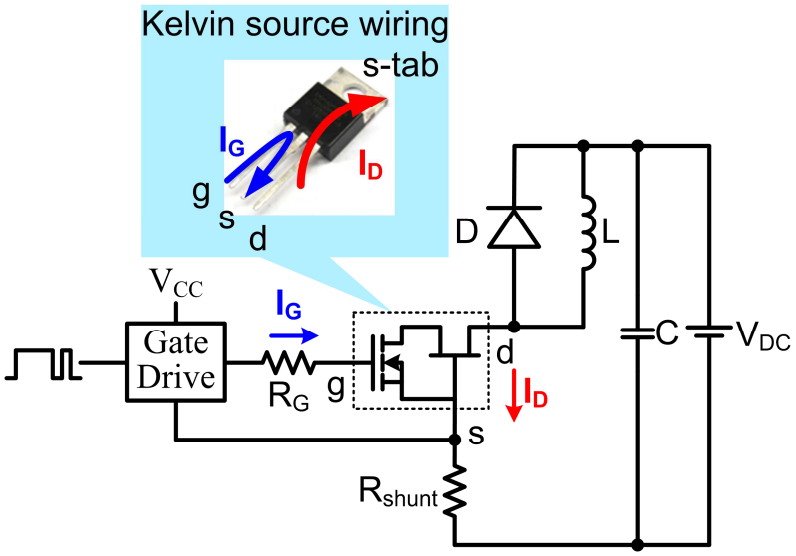

(a) Circuit schematic

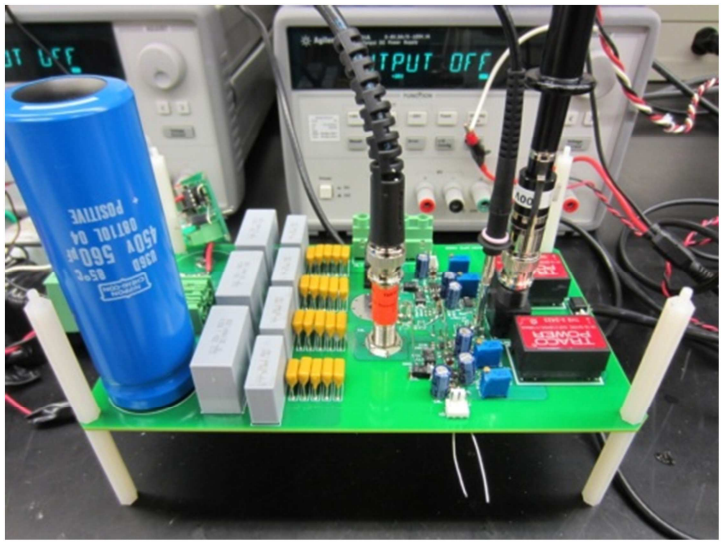

(b) Hardware

Figure 8-2. Double pulse test circuit.

The switching performance of the DUT is tested with a dc bus voltage of 400 V and a load current of 11 A. Figure 8-3 shows the switching transient using the gate voltage of 0 V / 13.5 V and the gate resistance of 0 Ω to push the switching speed. For the turn on transient, the dv/dt achieves 140 V/ns, and the di/dt achieves 9.6 A/ns. For the turn off transient, the dv/dt achieves

42 V/ns, and the di/dt achieves 2.4 A/ns. The turn off switching speed is smaller than turn on switching speed because the DUT junction capacitance needs to be charged by inductor current during turn off. The turn on switching energy is 4.3 µJ, and the turn off switching energy is 8.1µJ.

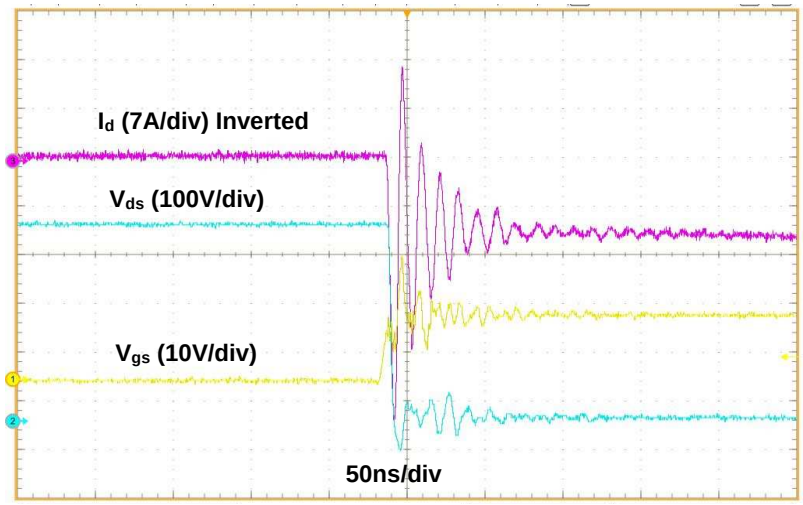

(a) Turn on

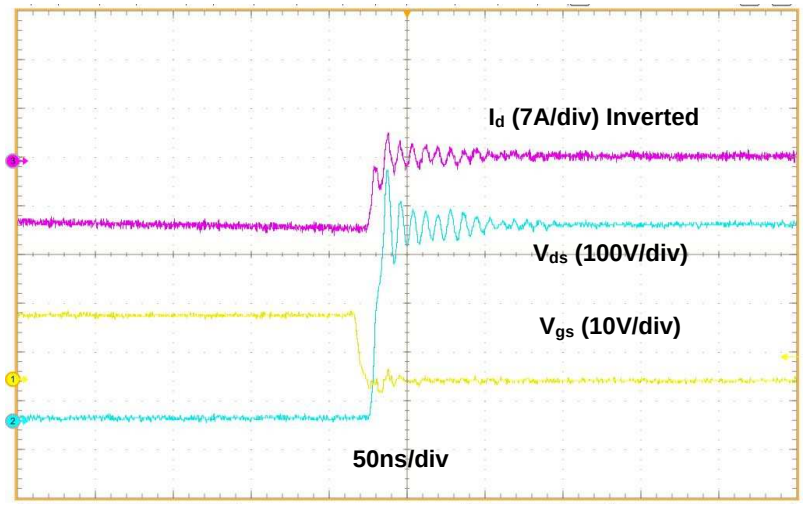

(b) Turn off

Figure 8-3. Switching waveforms of 600V GaN HEMT with 0 Ω R_g and 13.5 V V_{gs}.

The DUT is also tested with various gate voltage V_{gs} and gate resistance R_g under the same voltage and current conditions. Figure 8-4 shows the di/dt and dv/dt during turn on transient with various V_{gs} and R_g. Figure 8-5 show the turn on and turn off switching energy with various V_{gs} and R_g. The switching speed can be reduced with smaller V_{gs} or larger R_g to compromise for the circuit limitations (e.g. isolator dv/dt immunity in a phase leg configuration, gate ringing caused by di/dt on common source inductance), but the switching energy is increased accordingly.

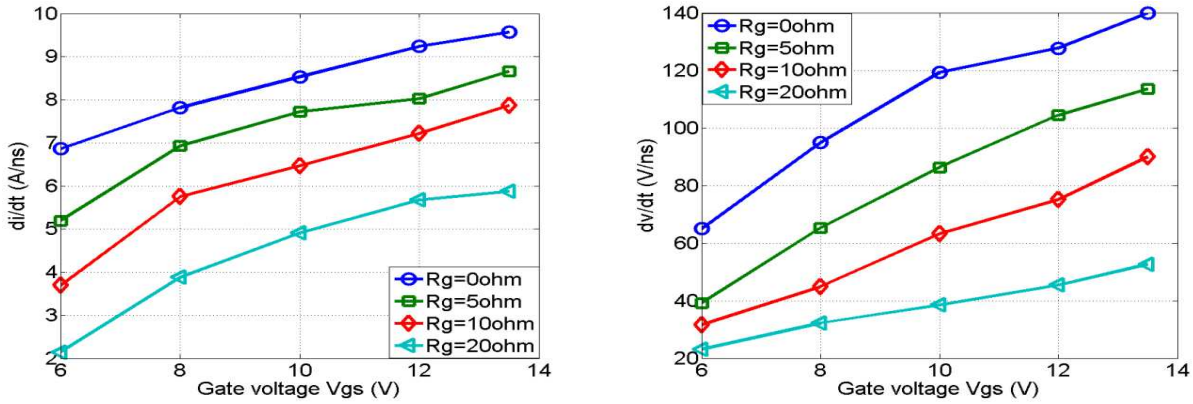

(a) di/dt (b) dv/dt

Figure 8-4. Turn on speed of 600V GaN HEMT with various R_g and V_{gs}.

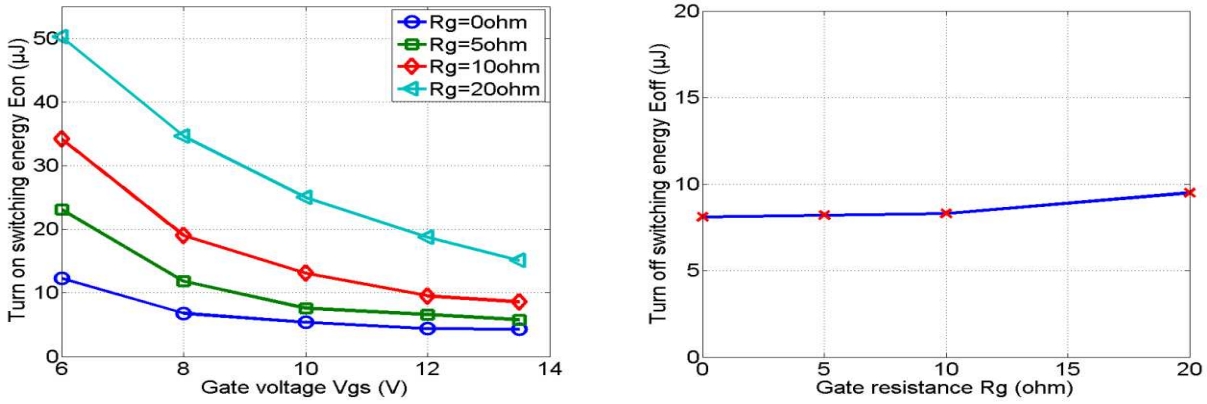

(a) Turn on switching energy (b) Turn off switching energy

Figure 8-5. Switching energy of 600V GaN HEMT with various R_g and V_{gs}.

8.3 Limitations of 600V GaN HEMT Switching Speed

Although the GaN HEMT has the inherent fast switching capability, it can be limited by circuit parasitics in practical applications.

The large di/dt can interfere with the gate voltage through common source inductance. Figure 8-6 shows the typical turn on waveforms of the DUT as the bottom switch. During t_1 and t_2, the rising current I_d causes a positive voltage drop on the common source inductance, and a dip on the gate voltage V_g is observed. If the gate voltage drops below the gate threshold voltage (1.8 V for TPH3006PS) at t_2, a false turn off can occur to the DUT during the turn on transient. During t_2 and t_3, the falling current can cause the rise on the gate voltage of the DUT. The top HEMT can be falsely turned on in a phase leg configuration.

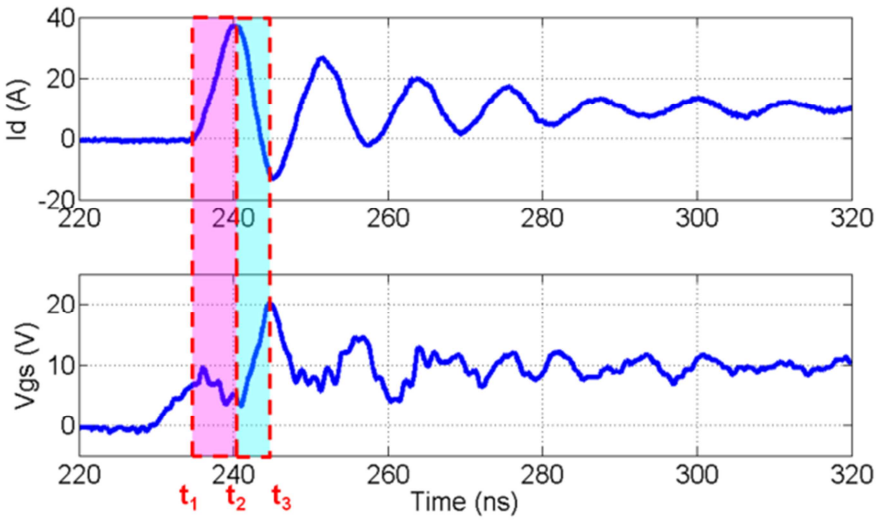

Figure 8-6. Influence of di/dt on gate voltage in a typical turn on transient.

Previous tests have shown that the DUT can be switched at the inherent speed using Kelvin source wiring without causing much ringing on gate. To investigate the influence of di/dt on the gate of the bottom switch, the DUT is switched with the conventional wiring to increase the

common source inductance, as shown in Figure 8-7 (a). The test results are shown in Figure 8-7 (b). With the gate voltage of 10 V and gate resistance of 0 Ω, the gate voltage drops below threshold voltage during the current rising and leads to a false turn off. The phenomenon can be mitigated by increasing the turn on gate voltage. With the gate voltage of 13.5 V and the same gate resistance, the gate voltage keeps above threshold voltage and not fault is observed. The di/dt achieves 9.1 A/ns.

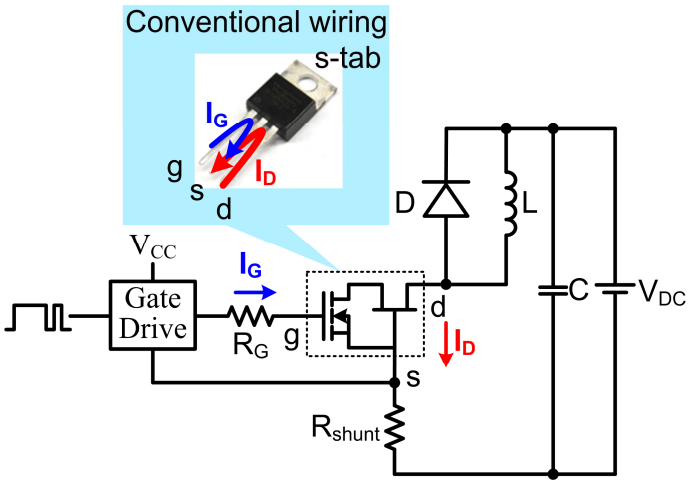

(a) Circuit schematic

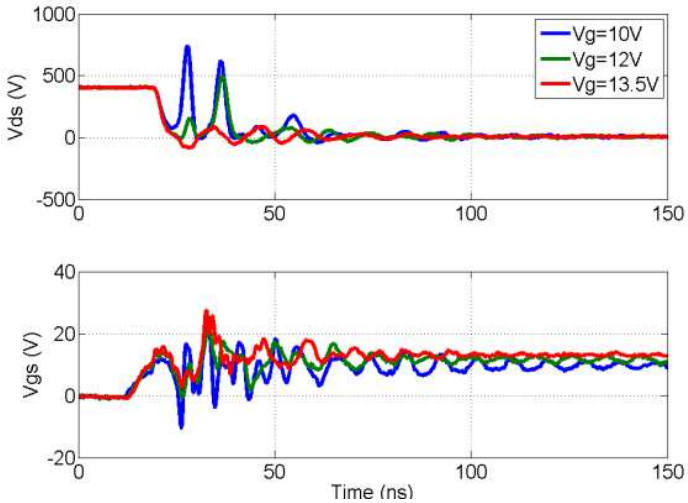

(b) Turn on waveforms with various V_{gs}

Figure 8-7. False turn off of bottom GaN HEMT with conventional wiring.

A phase leg configuration composed of two GaN HEMT as both top diode and bottom switch is built, as shown in Figure 8-8 (a). To investigate the influence of di/dt on the gate of top HEMT, the conventional wiring is applied for top HEMT and Kelvin source wiring is applied for bottom HEMT. With the gate voltage of 0 V applied on the top device, a severe ringing is observed after the bottom HEMT is turned on, as shown in Figure 8-8 (b). The phenomenon is caused by the false turn on of the top device and can be mitigated by negative biasing the gate voltage. Figure 8-8 (c) shows the turn on transient of the bottom HEMT with the negative voltage applied to the gate of the top HEMT. No fault turn on is observed when the gate voltage of -5 V is applied for the top HEMT with a conventional wiring or 0 V V_{gs} is applied for top HEMT with Kelvin source connection. The di/dt of falling current achieves 18.7 A/ns.

In summary, the limitation of GaN HEMT's inherent large di/dt is the inference between the current and gate voltage. The solutions include reducing the common source inductance with better packaging and circuit layout, increasing the turn on voltage, and negative biasing the turn off voltage.

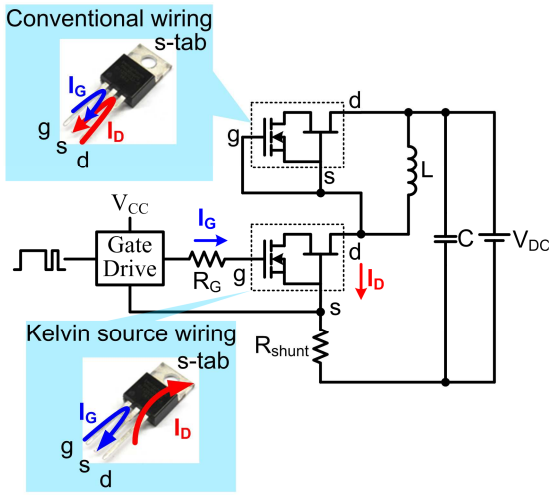

(a) Circuit schematic

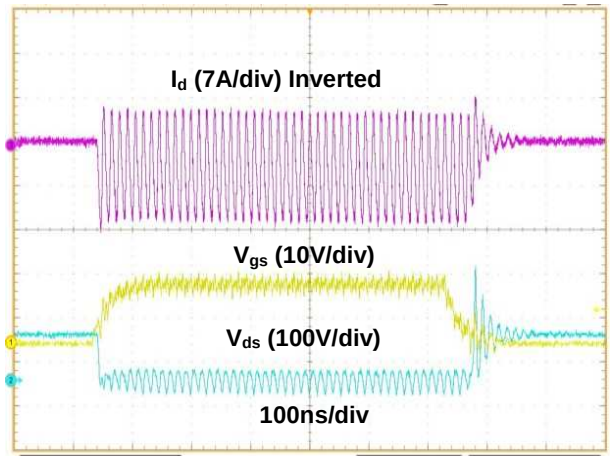

(b) Ringing caused by top GaN HEMT with 0 V gate voltage

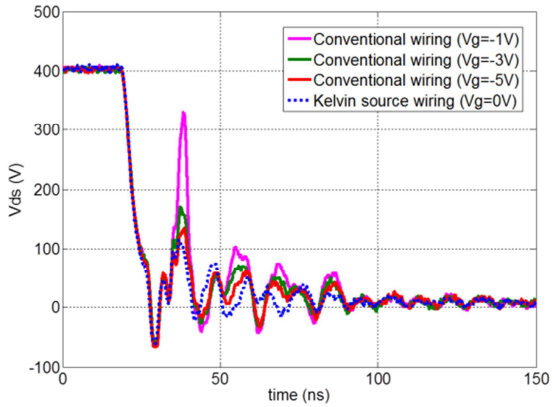

(c) Negative gate voltage applied to top GaN HEMT

Figure 8-8. False turn on of top GaN HEMT with conventional wiring.

8.4 High Temperature Characteristics of 600V GaN HEMT

The GaN HEMT is tested at various temperatures up to 200 ˚C. The circuit schematic for switching characterization is shown in Figure 8-7 (a). The conventional wiring is employed for the DUT since the s-tab is attached to a hot plate for heating the device. The device case temperatures are monitored by thermocouples. Since the switching loss caused by two pulses is negligible, the DUT junction temperature can be regarded as the same as the case temperature. The test conditions are: dc bus voltage V_{dc} is 400 V, load current is 11 A, gate voltage V_{gs} is 0 V / 13.5 V, and gate resistance R_g is 0 Ω.

Figure 8-9 shows the switching performance of GaN HEMT at 25˚C, 100 ˚C, and 200 ˚C. The switching speed and switching energy does not change with the temperatures.

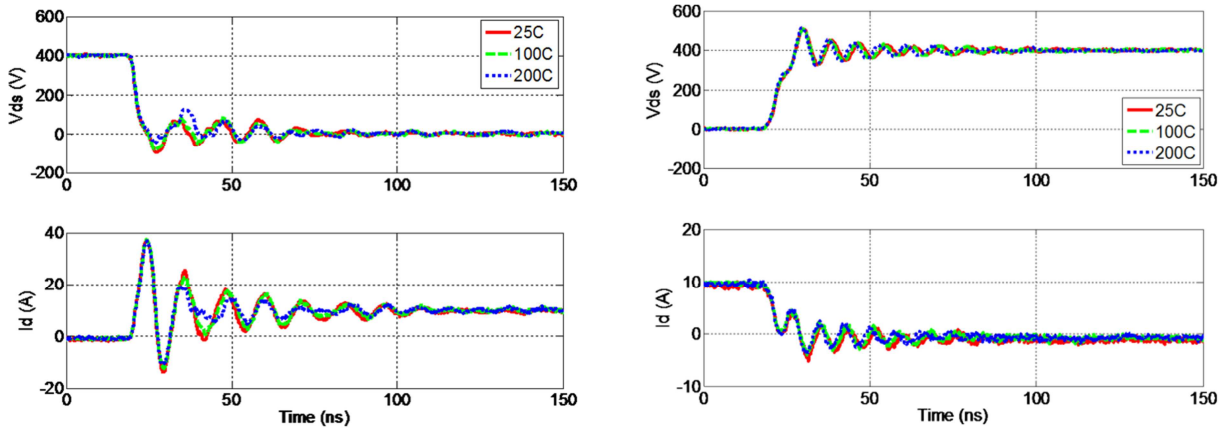

(a) Turn on (b) Turn off

Figure 8-9. Switching characterization of GaN HEMT at various temperatures.

The static characterization of the GaN HEMT is carried out with a high power curve tracer at various temperatures. The output characteristics and leakage current at 400 V are shown in Fig. 10 and Fig. 11 respectively. The on-state resistance Rds(on) and leakage current increase with temperatures.

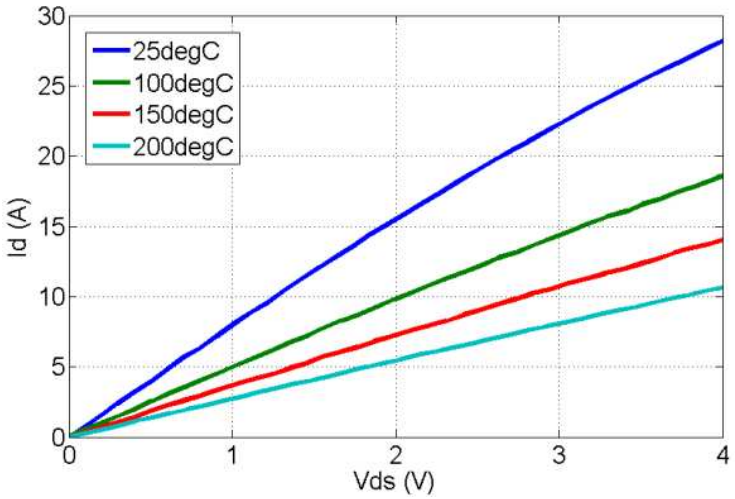

Figure 8-10. Output characteristics of GaN HEMT.

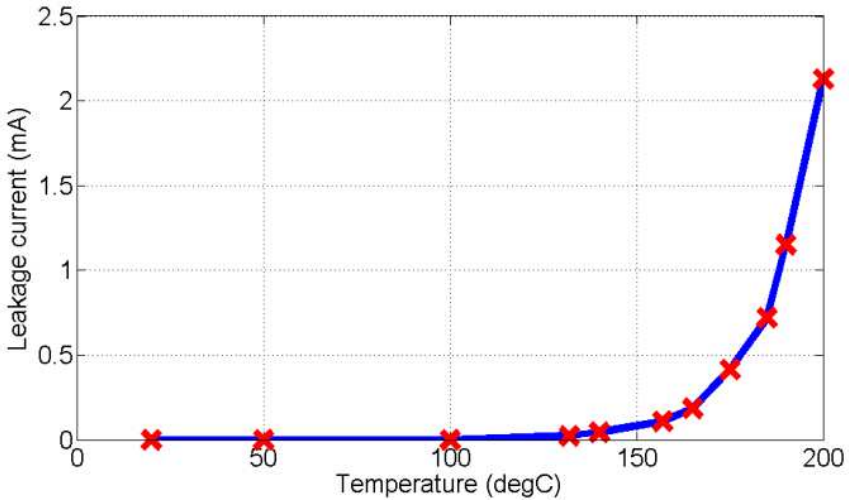

Figure 8-11. Leakage current of GaN HEMT at 400 V.

8.5 Summary

The 600 V GaN HEMT is investigated through experiment in terms of fast switching and high temperature capabilities. The GaN HEMT exhibits superior switching capability, with a di/dt reaching 9.6 A/ns and dv/dt reaching 140 V/ns. However, the inherent fast switching can be limited by many factors in practical application circuits. Experiments demonstrate the

interference between the current and gate thorough common source inductance limits the inherent switching speed. Packaging and circuit layout with small parasitic is critical in achieving fast switching. Negative biasing turn-off gate voltage and increasing turn-on gate voltage help mitigate the effect. Finally, the high temperature static and switching characteristics up to 200 ˚C are also tested and given. The switching performance of the device is independent of temperatures.

Chapter 9. Conclusions and Future Work

This chapter summarizes this dissertation and gives some suggestions for future work in this research area.

9.1 Conclusions

This dissertation investigates the feasibility of operating Si devices at 200 ˚C and provides the guidelines for the development of a high temperature Si converter for operating with 105 ˚C high temperature coolant. The main conclusions are summarized below.

First, the device characterization shows that the commercial 175 ˚C Si IGBT under test can be successfully switched at an elevated junction temperature of 200 ˚C with increased but acceptable losses. Comparing with the power semiconductor operation in commercial HEVs, by extending the junction temperature to 200 ˚C without compromising power density and thermal management design, the additional 65 ˚C cooling loop can be eliminated with the trade-off of the decreased efficiency by 0.2 percent.

Second, the IGBT shows very good latch-up immunity even at very high temperatures. The short circuit capability is decreased at 200 ˚C, but it is still adequate for protection. The IGBT can be turned off safely in the wide temperature range from 25˚C to 200 ˚C as long as it does not exceed the rated voltage. However, it has limited avalanche capability and cannot be subjected to over voltage stress. The important criteria considering latch-up immunity, short circuit capability and avalanche capability are given to ensure the safe and reliable operation of Si IGBTs at 200 ˚C.

Third, to support the Si devices operating continuously at the junction temperature of 200 ˚C, a Si IGBT phase-leg module is packaged utilizing high temperature packaging technologies

and appropriate thermal management. The thermal performance of the module and cooling system should be within the device limit to allow thermal stability of Si IGBTs. A 10 kW buck converter composed of a phase-leg module is operated successfully with the device junction temperature heated up to 200 ˚C, which demonstrates the high temperature capability of the designed package module.

Fourth, a method is proposed to measure the junction temperatures of IGBT discrete devices and modules using short circuit current I_{SC}. The calibration between short circuit current and temperature shows that I_{SC} has a good temperature sensitivity and linearity. I_{SC} is little influenced by the voltage across the device (0.096 ˚C/V). By creating a short circuit in hard switching fault, the effect of gate voltage variance on short circuit current is eliminated, so that the short circuit current is only determined by temperature. Due to these advantages, the short circuit current is suitable to be used for temperature measurement. By connecting a temperature measurement unit to the converter and giving a short circuit pulse, the IGBT junction temperature can be measured.

Fifth, a 30 kW Si IGBT based three-phase converter has been developed for operating at the junction temperature of 200 ˚C with the high temperature coolant in hybrid electric vehicle applications. An integrated pin fin structured AlSiC baseplate is used for cooling design, which provides improved thermal performances compared to a two-tube cold plate. The experimental results demonstrate that the three-phase converter can operate at the junction temperature of 200 ˚C with the 105 ˚C high temperature coolant, thus eliminating the need for the additional 65 ˚C coolant in HEV.

Additionally, the emerging 600 V GaN HEMT is investigated as a potential replacement of Si devices for high efficiency and high temperature in future HEV applications. The GaN HEMT exhibits superior switching capability, with a di/dt reaching 9.6 A/ns and dv/dt reaching 140 V/ns.

However, the inherent fast switching can be limited by many factors in practical application circuits. Experiments demonstrate the interference between the current and gate thorough common source inductance limits the inherent switching speed. Packaging and circuit layout with small parasitic is critical in achieving fast switching. Negative biasing turn-off gate voltage and increasing turn-on gate voltage help mitigate the effect. The high temperature static and switching characteristics up to 200 ˚C are also tested and given. The switching performance of the device is temperature insensitive.

9.2 Future Work

Based on the above conclusions, the following aspects can be considered for future research.

(1) Reliability of Si IGBT device and packaging for operation at 200 ˚C

For the reliability of the device itself, degradation and breakdown of oxides and electro-migration are the main issues. Besides, high temperature operation can give rise to thermal instabilities due to the easier current filament formation at higher temperatures. Thus, the reliability of the device should be further studied under the harsh environmental conditions using a combination of standard tests including high temperature reverse bias (HTRB), high temperature gate bias (HTGB), temperature humidity bias (THB) and so on.

The reliability of the packaging is another key challenge for high temperature operation. High temperature cycling tests (thermal cycling and power cycling) will be used on the IGBT modules to evaluate the thermo-mechanical reliability under the harsh environmental conditions. The power cycling lifetime is mainly limited by the bonding wire joints and the solder layer under the chip. The thermal cycling lifetime is mainly limited by the solder joints between the substrate and the baseplate. In the HEVs with high temperature coolant as described in the dissertation, the coolant temperature range is from -40 ˚C up to 105 ˚C and the ambient

temperature is -40 ˚C to 140 ˚C. The IGBT modules used in the application should have the thermal cycling capability from -40 ˚C to 200 ˚C with the increased ΔTc compared to the commercial HEVs nowadays, and the power cycling capability from 105 ˚C to 200 ˚C with ΔTj of 95 ˚C which does not change much.

(2) Health condition monitoring of power modules using short circuit current

A method of IGBT junction temperature measurement is proposed in this dissertation using short circuit current as a TSEP. The method is used for converter prototype evaluation to help determine the safe operating region and avoid the unnecessary safety margin regarding device temperatures.

Furthermore, the junction temperature measurement method could be applied in the periodic check to monitor for a health condition monitoring and a lifetime prediction of the power conversion stage, which should be further explored [94]-[95]. For example, during the converter self check before the converter is started, a short circuit pulse can be generated to monitor the wear-out status of the power semiconductor devices and packaging.

It should be noted that repetitive short circuits could have a cumulative degradation effect and finally cause the device failure. In [96], it is claimed that the IGBT reaches failure after some 10^4 short circuits. Therefore, the degradation effect caused by measurement should be taken into consideration, and the measurement times through the whole device lifetime should be much less than that causes failure. For the same reason, the short circuit current is not suitable to be used for online measurement for over temperature protection, which requires repetitive measurement during the converter operation.

(3) Emerging 600V GaN HEMT switching performance improvement with packaging

The dissertation reveals that the inherent fast switching of the GaN HEMT can be limited by many factors in practical application circuits. The interference between the current and gate through common source inductance limits the inherent switching speed. For the discrete device with standard TO-220 package, the Kelvin source wiring helps reduce the common source inductance dramatically, but it brings difficulty to thermal management since the tab is soldered to the PCB. A packaged module could be developed for the GaN HEMT to improve both of the switching performance and thermal performance.

REFERENCES

[1] C. Buttay, D. Planson, B. Allard, D. Bergogne, P. Bevilacqua, C. Joubert, M. Lazar, C. Martin, H. Morel, D. Tournier, and C. Raynaud, "State of the art of high temperature power electronics," *Materials Science and Engineering*: B, vol. 176, no. 4, pp. 283 – 288, Mar. 2011.

[2] R. W. Johnson, C. Wang, Y. Liu, and J. D. Scofield, "Power device packaging technologies for extreme environments," *IEEE Transactions on Electronics Packaging Manufacturing*, vol. 30, no. 3, pp. 182 – 193, Jul. 2007.

[3] P. G. Neudeck, R. S. Okojie, and L. Chen, "High-temperature electronics - a role for wide bandgap semiconductors?," *Proceedings of the IEEE*, vol. 90, no. 6, pp. 1065 – 1076, Jun. 2002.

[4] R. W. Johnson, J. L. Evans, P. Jacobsen, J. R. Thompson, and M. Christopher, "The changing automotive environment: high-temperature electronics," *IEEE Transactions on Electronics Packaging Manufacturing*, vol. 27, no. 3, pp. 164 – 176, Jul. 2004.

[5] C. C. Chan, "The state of the art of electric, hybrid, and fuel cell vehicles," *Proceedings of the IEEE*, vol. 95, no. 4, pp.704 – 718, Apr. 2007.

[6] L. Chen, "Practical design and challenges of traction inverter for electrified vehicles," *Tutorial presentation slides in IEEE Energy Conversion Congress and Expo (ECCE)*, 2011.

[7] *Evaluation of the 2010 Toyota Prius hybrid synergy drive system*, ORNL/TM-2010/253, Oak Ridge National Laboratory, March 2011.

[8] N. R. Brown, T. M. Jahns, and R. D. Lorenz, "Power converter design for an integrated modular motor drive," in *Proc. IEEE Industry Applications Conference (IAS)*, pp. 1322 – 1328, Sept. 2007.

[9] R. John, O. Vermesan, and R. Bayerer, "High temperature power electronics IGBT modules for electrical and hybrid vehicles," in *Proc. IMAPS High Temperature Electronics Network (HiTEN)*, 2009, pp. 199 – 204.

[10] R. Bayerer, "Higher junction temperature in power modules - a demand from hybrid cars, a potential for the next step increase in power density for various variable speed drives," in *PCIM Europe Conference*, 2008.

[11] B. Wrzecionko, J. Biela, and J. W. Kolar, "SiC power semiconductors in HEVs: Influence of junction temperature on power density, chip utilization and efficiency," in *Proc. IECON*, 2009, pp. 3834 – 3841.

[12] T. Laska, G. Miller, M. Pfaffenlehner, P. Turkes, D. Berger, B. Gutsmann, P. Kanschat, and M. Munzer, "Short circuit properties of Trench-/Field-Stop-IGBTs-design aspects for a superior robustness," in *IEEE Proc. Power Semiconductor Devices and ICs (ISPSD)*, 2003, pp. 152 – 155.

[13] H. Ruething, F. Umbach, O. Hellmund, P. Kanschat, and G. Schmidt, "600V-IGBT3: trench field stop technology in 70 μm ultra thin wafer technology," in *IEEE Proc. Power Semiconductor Devices and ICs (ISPSD)*, 2003, pp. 63 – 66.

[14] M. Babler, P. Kanschat, F. Umbach, and C. Schaeffer, "1200V IGBT4–high power–a new technology generation with optimized characteristics for high current modules," in *PCIM Europe Conference*, 2006.

[15] Z. Liang, "Status and trend of automotive power packaging," in *Proc. ISPSD*, 2012, pp. 325 – 331.

[16] *Evaluation of 2008 Lexus LS 600H hybrid synergy drive system*, ORNL/TM-2008/185, Oak Ridge National Laboratory, January 2009.

[17] A. Ciliox, J. Gorlich, K. Guth, F. Hille, S. Krasel, D. Siepe, P. Szcupak, and F. Umbach, "New module generation for higher life-time", in *Proc. PCIM*, 2010.

[18] K. Guth, D. Siepe, J. Gorlich, H. Torwesten, R. Roth, F. Hille, and F. Umbach, "New assembly and interconnects beyond sintering methods," in *Proc. PCIM*, 2010.

[19] T. Stockmeier, "From packaging to "un"-packaging - trends in power semiconductor modules," in *Proc. ISPSD*, 2008, pp. 12 – 19.

[20] SKiM IGBT modules technical explanations, Semikron, 2011. [Online]. Available: http://www.semikron.com/skcompub/en/skim_6393_technical_explanations-1087.htm

[21] P. Beckedahl, T. Grasshoff, and M. Lederer, "A new power module concept for automotive applications," in *Proc. PCIM*, 2007.

[22] T. Stockmeier, P. Beckedahl, C. Gobl, and T. Malzer, "SKiN: Double side sintering technology for new packages," in *Proc. ISPSD*, 2011, pp. 324 – 327.

[23] N. Pluschke, and P. Beckedahl, "Novel packaging technology for power modules," in *Proc. ISIE*, 2012, pp. 420 – 424.

[24] T. Sasaki, H. Takao, T. Shikano, S. Fujita, D. Nakajima, and T. Shinohara, "Development of high current transfer-mold type power module with high heat-cycle durability," in *Proc. ISPSD*, 2004, pp. 293 – 296.

[25] N. Kaminski, "State of the art and the future of wide band-gap devices," in *Proc. European Conference on Power Electronics and Applications (EPE)*, 2009, pp. 1 – 9.

[26] Infineon, [Online] Available: http://www.infineon.com/.

[27] Cree, [Online] Available: http://www.cree.com/.

[28] SemiSouth, [Online] Available: http://www.semisouth.com/.

[29] W. Bergner, F. Bjoerk, D. Domes, and G. Deboy, “Infineon’s 1200 V SiC JFET - the new way of efficient and reliable high voltages switching,” [Online] Available: http://http://www.infineon.com/dgdl/Infineon+-+Article+-+CoolSiC_SiCJFET.pdf.

[30] K. Sheng, Y. Zhang, M. Su, J. H. Zhao, X. Li, P. Alexandrov, and L. Fursin, “Demonstration of the first SiC power integrated circuit,” *Solid State Electronics*, vol. 52, no. 10, pp. 1636 – 1646, Oct. 2008.

[31] M. Gurfinkel, H. D. Xiong, K. P. Cheung, J. S. Suehle, J. B. Bernstein, Y. Shapira, A. J. Lelis, D. Habersat, and N. Goldsman, “Characterization of transient gate oxide trapping in SiC MOSFETs using fast I-V techniques,” *IEEE Transactions on Electron Devices*, vol. 55, no. 8, pp. 2004 – 2012, Aug. 2008.

[32] D. Reusch, D. Gilham, Y. Su, and F.C. Lee, “Gallium Nitride based 3D integrated non-isolated point of load module,” in Proc. Applied Power Electronics Conference and Exposition (APEC), 2012, pp. 38 – 45.

[33] W. Zhang, Y. Long, Z. Zhang, F. Wang, L. M. Tolbert, B. J. Blalock, S. Henning, C. Wilson, and R. Dean, “Evaluation and comparison of silicon and gallium nitride power transistors in LLC resonant converter,” in *Proc. Energy Conversion Congress and Exposition (ECCE)*, 2012, pp.1362 – 1366.

[34] Y. Wu, M. Jacob-Mitos, M. L. Moore, and S. Heikman, “A 97.8% efficient GaN HEMT boost converter with 300-W output power at 1 MHz,” *IEEE Electron Device Letters*, vol. 29, no. 8, pp. 824 – 826, Aug. 2008.

[35] X. Huang, Z. Liu, Q. Li, and F. C. Lee, “Evaluation and application of 600V GaN HEMT in cascode structure,” in *Proc. Applied Power Electronics Conference and Exposition (APEC)*, 2013, pp. 1279 – 1286.

[36] H. Nakao, Y. Yonezawa, T. Sugawara, Y. Nakashima, T. Horie, T. Kikkawa, and K. Watanabe, “2.5-kW power supply unit with semi-bridgeless PFC designed for GaN-HEMT,” in *Proc. Applied Power Electronics Conference and Exposition (APEC)*, 2013, pp. 3232 – 3235.

[37] *FreedomCAR and fuel partnership electrical and electronics technical team roadmap*, U.S. Department of Energy, Nov. 2006.

[38] M. Helsper, and B. Brendel, “Challenges for IGBT modules in hybrid buses,” in *Proc. European Conference on Power Electronics and Applications (EPE)*, 2009, pp. 1 – 8.

[39] P. Sun, J.S. Lai, H. Qian, W. Yu, C. Smith, J. Bates, B. Arnet, A. Litvinov, and S. Leslie, “Efficiency evaluation of a 55kW soft-switching module based inverter for high temperature hybrid electric vehicle drives

application," in *Proc. IEEE Applied Power Electronics Conference and Exposition (APEC)*, 2010, pp. 474 – 479.

[40] T.E. Salem, D.P. Urciuoli, R. Green, and G.K. Ovrebo, "High-temperature high-power operation of a 100 A SiC DMOSFET module," in *Proc. IEEE Applied Power Electronics Conference and Exposition (APEC)*, 2009, pp. 653 – 657.

[41] T.J. Han, J. Nagashima, S.J. Kim, S. Kulkarni, and F. Barlow, "Implementation of a fully integrated high density 50 kW inverter using a SiC JFET based six-pack power module," in *Proc. IEEE Energy Conversion Congress and Expo (ECCE)*, 2011, pp. 3144 – 3150.

[42] F. Xu, D. Jiang, J. Wang, F. Wang, L. M. Tolbert, T. J. Han, and S. J. Kim, "Characterization of a high temperature multichip SiC JFET-based module," in *Proc. IEEE Energy Conversion Congress and Expo (ECCE)*, 2011, pp. 2405 – 2412.

[43] S. K. Mazumder, and P. Jedraszczak, "Evaluation of a SiC dc/dc converter for plug-in hybrid-electric-vehicle at high inlet-coolant temperature," *IET Power Electronics*, vol. 4, no. 6, pp. 708 – 714, July 2011.

[44] E. R. Motto, and J. F. Donlon, "New compact IGBT modules with integrated current and temperature sensors," *Powerex technical library*, 2005.

[45] H. Ichikawa, T. Ichimura, and S. Soyano, "IGBT modules for hybrid vehicle motor driving," *Fuji electric review*, vol. 55, no. 2, pp. 46 – 50, 2009.

[46] R. Schmidt, and U. Scheuermann, "Using the chip as a temperature sensor – the influence of steep lateral temperature gradients on the Vce(T)-measurement," in *Proc. of European Conference on Power Electronics and applications (EPE)*, 2009, pp.1 – 9.

[47] S. Feng, X. Xie, C. Lu, G. Shen, G, Gao, and X. Zhang, "The thermal characterization of packaged semiconductor device," in *Proc. IEEE Semiconductor Thermal Measurement and Management Symposium*, 2000, pp. 220 – 226.

[48] X. Cao, T. Wang, K.D.T. Ngo, and G. Lu, "Characterization of lead-free solder and sintered nano-silver die-attach layers using thermal impedance," *IEEE Transactions on Components, Packaging and Manufacturing Technology*, vol. 1, no. 4, pp. 495 – 501, Apr. 2011.

[49] H. Kuhn, and A. Mertens, "On-line junction temperature measurement of IGBTs based on temperature sensitive electrical parameters," in *Proc. of European Conference on Power Electronics and Applications (EPE)*, 2009, pp. 1 – 10.

[50] D. Bergogne, B. Allard, and H. Morel, "An estimation method of the channel temperature of power MOS devices," in *Proc. IEEE Power Electronics Specialists Conference (PESC)*, 2000, pp.1594 – 1599.

[51] Y. S. Kim, and S. K. Sul, "On-line estimation of IGBT junction temperature using on-state voltage drop," in *Proc. IEEE Industry Applications Conference (IAS)*, 1998, pp. 853 – 859.

[52] P. Ning, R. Lai, F. Wang, K.D.T. Ngo, V.D. Immanuel, and K.J. Karimi, "SiC wirebond multichip phase-leg module packaging design and testing for harsh environment," *IEEE Transactions on Power Electronics*, vol. 25, no. 1, pp. 16 – 23, Jan. 2010.

[53] P. Ning, F. Wang, and K.D.T. Ngo, "250 °C SiC high density power module development," in *Proc. IEEE Applied Power Electronics Conference and Exposition (APEC)*, 2011, pp. 1275 – 1281.

[54] J. M. Hornberger, E. Cilio, B. McPherson, R. M. Schupbach, and A. B. Lostetter, "A fully integrated 300°C, 4 kW, 3-phase, SiC motor drive module," in *Proc. IEEE Power Electronics Specialists Conference (PESC)*, 2007, pp. 1048 – 1053.

[55] E. Cilio, J. Hornberger, B. McPherson, R. Schupbach, A. Lostetter, and J. Garrett, "A novel high density 100 kW three-phase silicon carbide (SIC) multichip power module (MCPM) inverter," in *Proc. IEEE Applied Power Electronics Conference and Exposition (APEC)*, 2007, pp. 666 – 672.

[56] J. Hornberger, S. Mounce, R. Schupbach, B. McPherson, H. Mustain, A. Mantooth, W. Brown, and A.B. Lostetter, "High-temperature integration of silicon carbide (SiC) and silicon-on-insulator (SOI) electronics in multichip power modules (MCPMs)," in *Proc. European Conference on Power Electronics and Applications (EPE)*, 2005, pp. 1 – 10.

[57] T. Funaki, J.C. Balda, J. Junghans, A.S. Kashyap, H.A. Mantooth, F. Barlow, T. Kimoto, and T. Hikihara, "Power conversion with SiC devices at extremely high ambient temperatures," *IEEE Transactions on Power Electronics*, vol. 22, no. 4, pp. 1321 – 1329, July 2007.

[58] S. Mounce, B. McPherson, R. Schupbach, and A. B. Lostetter, "Ultralightweight, high efficiency SiC based power electronic converters for extreme environments," in *Proc. 2006 IEEE Aerosp. Conf.*, 2006, pp. 1 – 19.

[59] M.J. Palmer, R.W. Johnson, T. Autry, R. Aguirre, V. Lee, and J.D. Scofield, "Silicon carbide power modules for high-temperature applications," *IEEE Transactions on Components, Packaging and Manufacturing Technology*, vol. 2, no. 2, pp. 208 – 216, Feb. 2012.

[60] R.A. Wood, and T.E. Salem, "Evaluation of a 1200-V, 800-A all-SiC dual module," *IEEE Transactions on Power Electronics*, vol. 26, no. 9, pp. 2504 – 2511, Sept. 2011.

[61] H. Wang, F. Wang, A. Q. Huang, and C. W. Tipton, "Investigation of power MOSFETs for high temperature operation," in *Conf. Rec. IEEE-IAS Annu. Meeting*, 2005, pp. 388 – 392.

[62] U. Schlapbach, M. Rahimo, C. von Arx, A. Mukhitdinov, and S. Linder, "1200V IGBTs operating at 200°C? An investigation on the potentials and the design constraints," in *Proc. IEEE ISPSD*, 2007, pp. 9 – 12.

[63] *Evaluation of 2004 Toyota Prius hybrid electric drive system*, ORNL/TM-2006/423, Oak Ridge National Laboratory, May 2005.

[64] *Evaluation of 2005 Honda Accord hybrid electric drive system*, ORNL/TM-2006/535, Oak Ridge National Laboratory, September 2006.

[65] *Evaluation of 2007 Toyota Camry hybrid electric drive system*, ORNL/TM-2007/190, Oak Ridge National Laboratory, January 2008.

[66] D. Jiang, R. Burgos, F. Wang, and D. Boroyevich, "Temperature-dependent characteristics of SiC devices: performance evaluation and loss calculation," *IEEE Transactions on Power Electronics*, vol. 27, no. 2, pp. 1013 – 1024, Feb. 2012.

[67] S. Bellone, F.G.D. Corte, L.D. Benedetto, and G.D. Licciardo, "An analytical model of the switching behavior of 4H-SiC p+-n-n+ diodes from arbitrary injection conditions," *IEEE Transactions on Power Electronics*, vol. 27, no. 3, pp. 1641 – 1652, Mar. 2012.

[68] A.M. Trzynadlowski, and S. Legowski, "Minimum-loss vector PWM strategy for three-phase inverters," *IEEE Trans. on Power Electronics*, vol. 9, no. 1, pp. 26 – 34, Aug. 2002.

[69] M. H. Bierhoff, F. W. Fuchs, "Semiconductor losses in voltage source and current source IGBT converters based on analytical derivation," in *Proc. IEEE PESC*, 2004, pp. 2836 – 2842.

[70] K.H. Oh, Y.C. Kim, K.H. Lee, and C.M. Yun, "Investigation of short-circuit failure limited by dynamic-avalanche capability in 600-V punchthrough IGBTs," *IEEE Trans. on Device and Materials Reliability*, vol. 6, no. 1, pp. 2 – 8, Mar. 2006.

[71] M. Otsuki, Y. Onozawa, H. Kanemaru, Y. Seki, and T. Matsumoto, "A study on the short circuit capability of field stop IGBTs," IEEE Transactions on Electron Devices, vol. 50, no. 6, pp. 1525 – 1531, Jun. 2003.

[72] A. Benmansour, S. Azzopardia, J. C. Martina and E. Woirgarda, "Failure mechanism of trench IGBT under short-circuit after turn-off," *Microelectronics and Reliability*, vol. 46, no. 9 – 11, pp. 1778–1783, Sept. – Nov. 2006.

[73] F. Hille, F. Umbach, T. Raker, and R. Roth, "Failure mechanism and improvement potential of IGBT's short circuit operation," in *Proc. IEEE ISPSD*, 2010, pp. 33 – 36.

[74] M. Otsuki, Y. Onozawa, M. Kirisawa, H. Kanemaru, K. Yoshihara, and Y. Seki, "Investigation on the short-circuit capability of 1200V trench gate field-stop IGBTs," in *Proc. IEEE ISPSD*, 2002, pp. 281 – 284.

[75] V. Bolloju, and J. Yang, "Influence of short circuit conditions on IGBT short circuit current in motor drives," in *Proc. IEEE APEC*, 2011, pp. 1675 – 1679.

[76] M. Trivedi, and K. Shenai, "Failure mechanisms of IGBTs under short-circuit and clamped inductive switching stress," *IEEE Trans. on Power Electronics*, vol. 14, no. 1, pp. 108 – 116, Jan. 1999.

[77] A. Bhalla, S. Shekhawat, J. Gladish, J. Yedinak, and G. Dolny, "IGBT behavior during desat detection and short circuit fault protection," in *Proc. IEEE ISPSD*, 1998, pp. 245 – 248.

[78] A. Muller, F. Pfirsch, and D. Silber, "Trench IGBT behaviour near to latch-up conditions," in *Proc. IEEE ISPSD*, 2005, pp. 255 – 258.

[79] D. W. Brown, M. Abbas, A. Ginart, I. N. Ali, P. W. Kalgren, and G. J. Vachtsevanos, "Turn-Off time as an early indicator of insulated gate bipolar transistor latch-up," *IEEE Transactions on Power Electronics*, vol. 27, no. 2, pp. 479 – 489, Feb. 2012.

[80] C. Abbate, G. Busatto, F. Iannuzzo, "IGBT RBSOA non-destructive testing methods: analysis and discussion," *Microelectronics Reliability*, vol. 50, no. 9-11, pp. 1731 – 1737, Sept. –Nov. 2010.

[81] M. Otsuki, Y. Onozawa, S. Yoshiwatari, and Y. Seki, "1200V FS-IGBT module with enhanced dynamic clamping capability," in *Proc. of IEEE ISPSD*, 2004, pp. 339 – 342.

[82] A. Castellazzi, J. Saiz, and M. Mermet-Guyennet, "Experimental characterization and modeling of high-voltage IGBT modules off-state thermal instability," in *conf. EPE*, 2009, pp. 1 – 9.

[83] C.C. Shen, A.R. Hefner, D.W. Berning, and J.B. Bernstein, "Failure dynamics of the IGBT during turn-off for unclamped inductive loading conditions," *IEEE Trans. on Industry Applications*, vol. 36, no. 2, pp. 614 – 624, Mar./Apr. 2000.

[84] P. Lefranc, D. Planson, H. Morel, and D. Bergogne, "Analysis of the dynamic avalanche of punch through Insulated Gate Bipolar Transistor (PT-IGBT)," *Solid-State Electronics*, vol. 53, no. 9, pp. 944 – 954, Sept. 2009.

[85] X. Perpina, J.F. Serviere, J. Urresti-Ibanez, I. Cortes, X. Jorda, S. Hidalgo, J. Rebollo, and M. Mermet-Guyennet, "Analysis of clamped inductive turnoff failure in railway traction IGBT power modules under overload conditions," *IEEE Trans. on Industry Electronics*, vol. 58, no. 7, pp. 2706 – 2714, Jul. 2011.

[86] Fuji IGBT modules application manual, Fuji Electric Device Technology Co., Ltd., 2004. [Online]. Available: www.fujielectric.com

[87] W. W. Sheng, and R. P. Colino, *Power electronic modules: design and manufacture*, CRC press, Boca Raton, 2005.

[88] Y. Avenas, L. Dupont, Z. Khatir, "Temperature measurement of power semiconductor devices by thermo-sensitive electrical parameters—a review," *IEEE Transactions on Power Electronics*, vol. 27, no. 6, pp. 3081 – 3092, June 2012.

[89] D. Graovac, A. Christmann, and M. Miinzer, "Power semiconductors for hybrid and electric vehicles," in *Proc. IEEE Power Electronics and ECCE Asia (ICPE & ECCE)*, 2011, pp. 1666 – 1673.

[90] Advanced Thermal Management of Power Electronics, Mikros Thermal Systems, Claremont, NH. [Online]. Available: http://www.mikrostechnologies.com/webdocs/CoolingPowerElectronicsWhitePaper.pdf

[91] X. Yu, L. Zhang, E. Zhou, and Q. Feng, "Heat transfer of an IGBT module integrated with a vapor chamber," *Journal of Electronic Packaging*, vol. 133, no. 1, pp. 011008, Mar. 2011

[92] Y. Avenas, L. Dupont, and Z. Khatir, "Temperature measurement of power semiconductor devices by thermo-sensitive electrical parameters—a review," *IEEE Transactions on Power Electronics*, vol. 27, no. 6, pp. 3081 – 3092, Jun. 2012.

[93] P. Ning, Z. Liang, F. Wang, and L. Marlino, "Power module and cooling system thermal performance evaluation for HEV application," in *Proc. IEEE Applied Power Electronics Conference and Exposition (APEC)*, 2012, pp. 2134 – 2139.

[94] S. Yang, D. Xiang, A. Bryant, P. Mawby, L. Ran, and P. Tavner, "Condition monitoring for device reliability in power electronic converters: a review," *IEEE Transactions on Power Electronics*, vol. 25, no. 11, pp. 2734 – 2752, Nov. 2010.

[95] A. Morozumi, K. Yamada, T. Miyasaka, S. Sumi, and Y. Seki, "Reliability of power cycling for IGBT power semiconductor modules," *IEEE Transactions on Industry Applications*, vol. 39, no. 3, pp. 665 – 671, May-Jun. 2003.

[96] M. Arab, S. Lefebvre, Z. Khatir, and S. Bontemps, "Experimental investigations of trench field stop IGBT under repetitive short-circuits operations," in *Proc. IEEE Power Electronics Specialists Conference (PESC)*, 2008, pp. 4355 – 4360.

[97] H. Zheng, D. Berry, J. N. Calata, K. D. T. Ngo, S. Luo, and G.-Q. Lu, "Low-pressure joining of large-area devices on copper using nanosilver paste," *IEEE Transactions on Components, Packaging and Manufacturing Technology*, vol. 3, no. 6, pp. 915 – 922, June 2013.

VITA

Zhuxian Xu was born in Nantong, China on January 9, 1986. She received her B.S. degree in Zhejiang University, Hangzhou, China, in 2008. She received her M.S. degree in Virginia Tech, Blacksburg, VA, in 2010. And She received her Ph.D. degree in the University of Tennessee, Knoxville, in 2013. She will start to work in Ford Motor Company after graduation.